Branching shear zones in the Arabian-Nubian Shield

Dissertation zur Erlangung des Grades
"Doktor der Naturwissenschaften" im Promotionsfach Geologie

am Fachbereich Chemie, Pharmazie und Geowissenschaften
der Johannes Gutenberg-Universität Mainz

Sven Erik Meyer
geb. in Mainz

Mainz, Oktober 2015

Erklärung

Hiermit versichere ich, die vorgelegte Arbeit selbstständig und unter Verwendung der angegebenen Quellen und Hilfsmittel verfasst zu haben.

Mainz, Oktober 2015

Everything has a natural explanation. The moon is not a god, but a great rock, and the sun a hot rock

Anaxagoras (510 – 428 BC)

Look deep into nature, and then you will understand everything better

Albert Einstein (1879 – 1955)

I. Abstract

Ductile strike-slip shear zones show a wide variation in their characteristics (length, width and strain-rate). These structures can form large branching or anastomosing shear zone networks and play an essential role in the geodynamic processes of continental collision zones. This thesis reports the nucleation and interconnection of strike-slip shear zones with associated kinematic adjustments. The research is based on detailed structural field mapping on two interacting strike-slip shear zones in contact with a metamorphic core complex, and on paired nucleated shear zones in the Arabian-Nubian Shield. To analyse the rheological effect of the material on the evolution of the shear zone networks and to gain insight into the kinematics during the interaction of the shear strands, two-dimensional numerical models were developed.

Microstructural analysis was performed on thin-sections of the shear zones and the core complex of the Qazaz Core Complex in Saudi Arabia to reconstruct the metamorphic condition of the deformation. The analysis of the structural data together with mineral exchange geothermobarometers provides comprehension of the mechanics of two interacting strike-slip shear zones linked to a detachment structure. The simultaneously operating vertical and lateral shear components is an efficient way to exhume a lower crust, accommodated by a crustal shortening. This structure may be an explanation for isolated core complexes along crustal-scale strike-slip fault systems.

Numerical two-dimensional experiments were performed by MILAMIN_VEP with a visco-elastic-plastic code to reproduce complex anastomosing or branched shear zone networks, improving our understanding of the rheology of the material during shear zone evolution. The simulations represent a large-scale model on a geological time-scale with constant strain-rate boundary conditions, initiating shear localization under Mohr Coulomb plasticity or power-law rheology. Systematic changes to the material's rheological parameters show that the progression of strain-softening during deformation has an important effect on the geometries of shear zone networks. The context of the strain-softening and its consequences to the development of the shear zones is presented via numerical models. Furthermore, the interaction of anti- and synthetic shear faults in brittle as well as ductile regimes and the simultaneous activity of the shear strands led to a more complex internal kinematic pattern. The more complex shear zone geometry caused by the

interconnection of the shear strands locally changed the orientation of the maximum compressive stress (σ_1). This is shown by the varying orientation of the new localized shear zones towards the bulk stress. In addition, the numerical experiments indicate that shear zones nucleate along a heterogeneous contrast of the material, induced in the simulations by a difference in the rheology of the material.

To expand the current knowledge of possible types of nucleation of shear zones, parallel propagated shear zones in Jordan were studied by structural and microstructural analysis (Fabric Analyser). The investigation shows an association of the development of paired shear zones with a lithological effect of the material by reactivation and overprinting. Differences in grain-size lead to a strict limitation of the deformed zone by high strain, exhibiting a sharp boundary with the undeformed surrounding rocks at the millimeter-scale. This leads to the conclusion that the nucleation and interaction of shear strands can form complex geodynamic structures in the crust, which lead locally to a change in the kinematic pattern. The similarity of the results of numerical experiments with natural examples adds support to the proposed explanations discussed in this thesis for variations in the orientation of shear zones in networks, and the evolution of the kinematics within the shear zone.

II. Zusammenfassung

In dieser Studie liegt der Fokus auf einer Geländearbeit-basierenden Untersuchung zweier interagierender Scherzonen in Saudi Arabien. Des Weiteren wird ein neuer Typ einer Scherzonenbildung in Verbindung mit einer prä-existierenden Struktur beschrieben. Zudem werden 2-dimensionale numerische Modelle erstellt, um den Einfluss der rheologischen Eigenschaften des Materials auf die Entwicklung von Scherzonen zu untersuchen. Duktile Scherzonen sind Deformationsflächen, die sich in ihrer Breite, Länge oder Verformungsrate unterscheiden. Solche Strukturen können groß-maßstäbliche komplexe, anastomosierte, vernetzte Störungsflächen aufbauen, die in Verbindung zu geodynamischen Prozessen an kontinentalen Kollisionszonen stehen. Solche Scherzonen durchziehen die gesamte Erdkruste und sind ein entscheidender Faktor bei der krusteninternen Bewegung des Gesteins. Das Vernetzen solcher krustenmaßstäblicher Blattverschiebungszonen führt zu einer Interaktion, die die Kinematik des Gesteins intern verändert.

Die interagierenden Scherzonen und die hochgradig metamorphen Gesteine (Gneiss) wurden mikrostrukturell und geothermobarometrisch untersucht und mit Hilfe einer Temperatur-Druckrekonstruktion der unteren Kruste zugeordnet. Die Kombination aus einer Blattverschiebungsstörung mit einer Abscherungsstörung bildet eine neue Mechanik aus einer horizontalen und vertikalen Scherkomponente. Die in dieser Studie neu beschriebene Struktur stellt ein neu entwickeltes Modell dar, um Krustengesteine aus größerer Tiefe an die Erdoberfläche zu exhumieren. Durch die kontinentale Kollision entwickeln sich Scherzonen, die miteinander interagieren. Sie stellen die treibende Kraft für die Aufwärtsbewegung der unteren Kruste dar und liefern eine neue Erklärung für diese geodynamischen Prozesse.

Simulationen mit 2-dimensionalen numerischen Modellen wurden durchgeführt, um die Entwicklung von vernetzten, groß-maßstäbliche anastomosierenden Scherzonen in der oberen und unteren Kruste in geologischen Zeitaltern zu verdeutlichen. Die Resultate zeigten, dass das weicher werdende Verhalten des Materials während der Verformung den größten Einfluss auf die Entwicklung der verschiedenen Geometrien von Scherzonen ausübt. Duktile Scherzonen können innerhalb einer schmalen Zone oder verteilt in einem Bereich von mehreren Kilometern Breite lokalisieren. Durch eine Testreihe wurden diese verschiedenen Charakteristika klassifiziert und dargestellt. Neu entwickelte Visualisie-

rungsskripte halfen, die Interaktion von Scherzonen genauer zu studieren. Die Auswertungen zeigen, verbinden sich zwei Scherzonen im spröden oder im duktilen Regime, bleiben beide Scherzonen in den meisten Fällen simultan aktiv. Die Interaktion einzelner Scherzonen zu einem komplexeren Netzwerk führt zu einer Veränderung der Bewegungsrichtung des zwischen den Scherzonen liegenden Gesteins. Zudem übt die zusammenlaufende Scherzonengeometrie eine interne Verschiebung der maximalen prinzipalen Spannung innerhalb des Materials aus. Die neu entstehenden Scherzonen zeigen aufgrund dieser Veränderung eine unterschiedliche Orientierung zur festgelegten Hauptspannung. Dieser interessante Einblick in die Verteilung der internen Spannung ist eine mögliche Erklärung für die größeren Variationen von Scherflächenorientierungen der im Gelände vorgefundenen Strukturen.

Geländearbeiten und numerische Modelle verdeutlichen die wichtige Rolle von Heterogenitäten innerhalb des Materials zur Erzeugung von Scherzonen. Bekannt ist, dass sich Scherzonen entlang von Bereichen lokalisieren, die sich weicher verhalten als das umliegende Gestein. Untersuchungen der parallel wachsenden Scherzonen in Jordanien bestätigten diese Studie und lieferten einen detaillierten Einblick in die Entstehungsprozesse.

Schlussfolgernd, führen die Interaktion von verschiedenen Scherzonen und die gleichzeitige Aktivität der Scherkomponente zu Veränderungen der Kinematik des Gesteins. Zudem ergeben die numerischen Modelle mögliche Erklärungen für die unterschiedlichen Entwicklungen von Scherzonen und deren interne Strukturen.

III. Table of Contents

I. Abstract I

II. Zusammenfassung III

III. Table of Contents V

IV. Nomenclature VII

1. Introduction 1
   1.1 Previous work and background on branching ductile shear zones 1
   1.2 Aim of the study and methods 5
   1.3 Organization 8
   1.4 Contributions 10
   1.5 References 10

2. A strike-slip core complex from the Najd fault system, Arabian Shield 17
   2.1 Introduction 17
   2.2 The Najd shear zones system 19
   2.3 Qazaz metamorphic complex 20
   2.4 Depth of Emplacement 23
   2.5 Discussion 26
   2.6 Conclusions 28
   2.7 References 29

3. Numerical models of branching brittle and ductile shear zones 33
   3.1 Introduction 34
   3.2 Modeling approach (Methology) 35
   3.3 Model setup 37
   3.4 Results 39
      3.4.1 Brittle strain localization 39
      3.4.1.1 Influence of heterogeneities and material properties on shear localization 41
      3.4.1.2 Effect of crustal depth on shear zone patterns 43
      3.4.1.3 Effect of initial viscosity on rheology 44
      3.4.1.4 Effect of strain softening 45
      3.4.2 Ductile shear zone localization 48
      3.4.2.1 Effect of heterogeneous material (number of anomalies) 49
      3.4.2.2 Internal and External influence of material behavior 50
      3.4.2.3 Effect of strain weakening 52
   3.5 Discussion and applications to field examples 56
   3.6 Conclusion 62
   3.7 References 63

4. Lithology-driven shear zone nucleation: an example from the Wadi Filk (Jordan) and Hafafit (Egypt) 74
4.1 Introduction 74
4.2 Geological overview 76
4.3 Wadi Filk mylonite - Jordan 77
4.3.1 Wadi Filk microstructure 79
4.3.2 Quartz crystallographic preferred orientation (CPO) of Wadi Filk 83
4.4 Hafafit mylonite shear zone - an example from Egypt 85
4.4.1 Microscale observations 86
4.4.2 Quartz crystallographic preferred orientation in Wadi Hafafit . 88
4.5 Discussion 89
4.5.1 Lithology driven shear zones - Wadi Filk 89
4.5.2 A new setting to nucleate paired shear zones 93
4.6 Conclusions 95
4.7 References 95

5. Conclusion 101
5.1 Interaction of crustal-scale strike-slip shear zones and their effect on the kinematics 101
5.2 Effect of rheological parameters on the development of shear zone networks (Chapter 3) 102
5.3 Lithology constitutes an important factor in shear zone nucleation (Chapter 4) 103
5.4 Suggestions for future research 105
5.5 References 107

6. Appendix 110
6.1 Appendix A: 110
6.2 Appendix B: DVD-ROM 111

Acknowledgement .....**Fehler! Textmarke nicht definiert.**

IV. Nomenclature

τ	shear stress
C	cohesion
μ	coefficient of internal friction
σ_n	normal stress
ϕ	angle of internal friction
σ_{II}	second invariant total stress tensor
σ_{xx}	normal stress in x-direction
σ_{yy}	normal stress in y-direction
σ_{xy}	shear stress
σ_y	yield stress
F	yield function
$\dot{\varepsilon}_{ij}$	deviatoric strain-rate
G	elastic shear modulus
τ_{ij}	deviatoric stress
$\dot{\lambda}$	plastic multiplier
Q	associated plastic flow potential
η_{eff}	effective viscosity
η_0	specified material viscosity at the initial stage for T_0
n	stress exponent
e_0	a reference strain-rate
k	Arrhenius type temperature dependency of viscosity
A	factor to reduce the effective viscosity

T	temperature
T_0	a reference temperature
$\dot{\varepsilon}_{BG}$	overall strain-rate
T_s	shear heating
χ	efficiency of shear heating
γ	critical strain
σ_1	maximum compressive stress
σ_3	minimum principal stress

1. Introduction

The subject of this thesis is the study of complex geometries of ductile strike-slip shear zones. The aim of the introduction is to give a general overview of previous field- and numerical-based research into the development of ductile shear zones, with a focus on their geometries and characteristics (more detailed introductions can be found in chapters 2, 3 and 4). The aim of the study and associated methods are explained in the second part of this introduction. In a third part, an overview of the organization of this thesis is presented. Since the chapters are organized in independent sections, this part is a guideline to link individual parts within the framework of the study.

1.1 Previous work and background on branching ductile shear zones

Ductile strike-slip shear zones are deformation structures characterized by a steeply oriented plane of high strain surrounded by less deformed rocks. Ductile strike-slip shear zones have been the subject of numerous studies (e.g. Hull, 1988; Lamouroux et al., 1994; Means, 1995; Passchier & Trouw, 2005; Platt & Behr, 2011; Schrank et al., 2008). The ideal shear zone as would be present in fairly isotropic rock and with a simple shear flow regime, shows an increase in strain towards the highest strain zone from development of a foliation at an angle of 45 ° in zones of lowest strain (Ramsay, 1980; Ramsay and Huber, 1983). Such shear zones with approximately simple shear regimes are most commonly described, but there are also operating systems where high-strain zones develop in transtension, transpression, stretching or shortening regimes (e.g. Harland, 1971; Sanderson and Marchini, 1984; Kligfield and Crespi, 1989; Paterson and Wainger, 1991; Fossen and Tikoff, 1993; Krantz, 1995, Jones and Tanner, 1995; Jiang and White, 1995; Tikoff and Greene, 1997; Jones et al., 1997). As for typical shear zones, they similarly involve displacement along a high-strain zone, whereas the lowest strain foliation orientation, and the orientation of lineations may be different. Ductile shear zones can form isolated single structures (Fig. 1.1a), e.g. those in plutonic rocks described by Ramsay and Graham (1970); Burg and Laurent (1978); Simpson (1983); Vauchez (1987); Selverstone et al. (1991); Dutruge et al. (1995); Christiansen and Pollard (1997); Arbaret and Burg (2003)

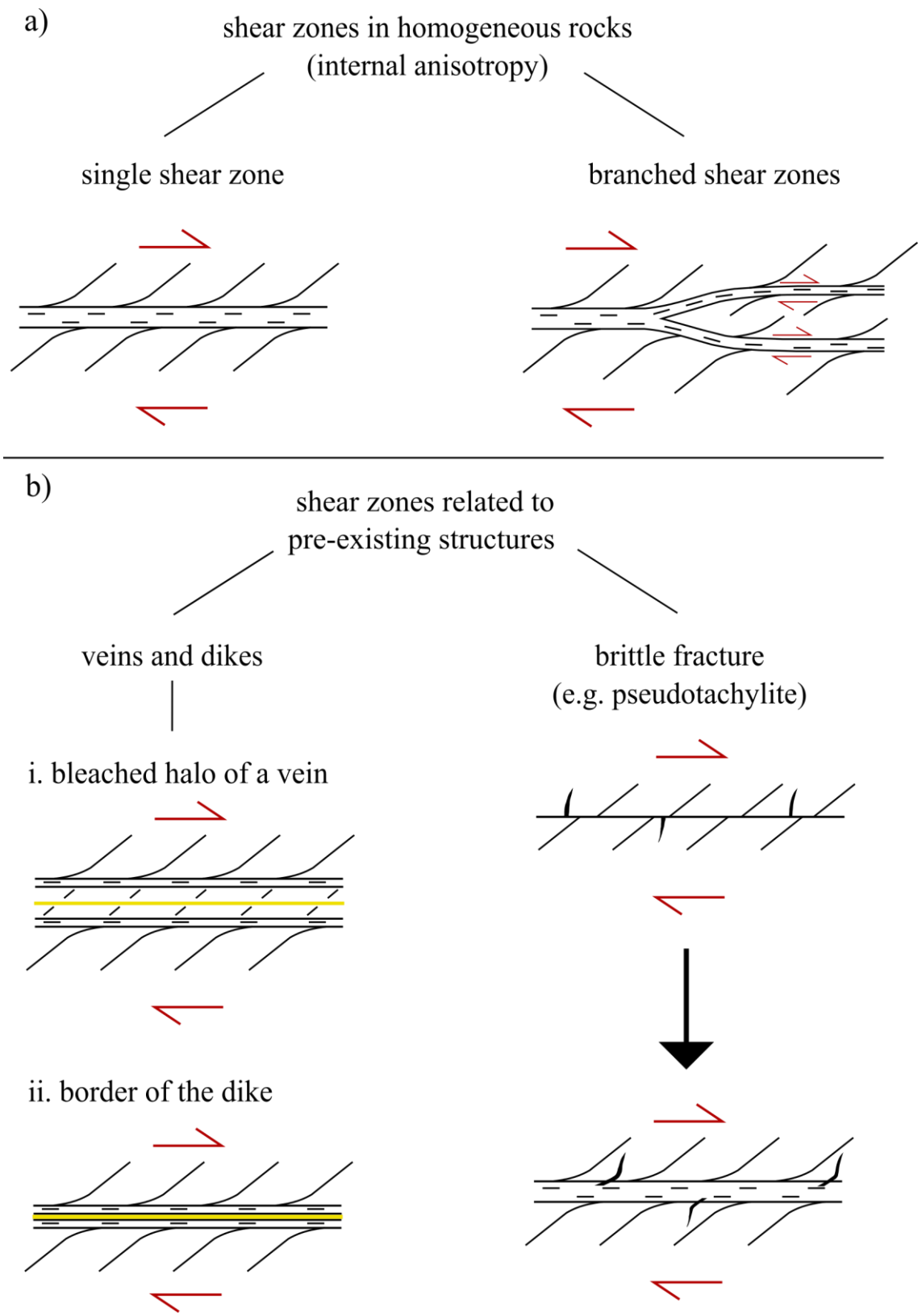

Figure 1.1 Types of nucleation of ductile shear zone - diagonal lines represent the foliation, the horizontal lines the high-strain zones; a) Single and branched shear zone nucleation in a homogeneous plutonic rock; b) Reactivations of pre-existing structures by overprinting of ductile shearing; Illustration of paired ductile shear zones in association to a border of a bleached halo (i.) or a dike (ii.) (Mancktelow and Pennacchioni, 2005), and the single development of a shear zone related to a brittle fracture (e.g. Passchier et al., 1990)

and Rolland et al. (2003), but can also be more complex: subparallel, anastomosing or branching structures commonly occur (Fig. 1.1a) and are the main subject of this thesis.

The nucleation and interconnection of shear zones influences the geometry. In most cases shear zones localize along zones of weakness. Strain-softening is a further process of weakening of the material during the deformation, and is associated with a decrease in grain-size, a change in mineral composition, or the presence of fluids. A further influence on the nucleation of shear zones is the existence of pre-existing structures, e.g. brittle faults, veins or dikes (Fig. 1.1b). These fabrics represent a weakness of the material in comparison to the surrounding rocks, and in a later stage the pre-existing structures can be reactivated and overprinted by a brittle or ductile shear zone (e.g. Passchier et al., 1990; Christiansen and Pollard, 1997; Pennacchioni and Mancktelow, 2007). According to the work of Mancktelow and Pennacchioni (2005), the aforementioned structures form simple geometries - either single or paired, depending on the pre-existing rock structure. Field studies of small- and large-scale shear zones give examples of a more complex patterns, which can form a networks of shear zones (e.g. Mitra, 1978; Bell, 1981; Choukrone and Gapais, 1983; Gapais et al., 1987; LaFrance et al., 1998; Imber et al., 2001; Arbaret and Burg, 2003; Fusseis et al., 2006; Pennacchioni and Mancktelow, 2007; Carreras et al., 2010). Such a system of different shear zone strands can form an anastomosing pattern (Fig. 1.2a, b).

Anastomosing shear zone patterns can develop in different ways. Relatively sub-parallel shear strands may connect to each other by a small variation in the orientation determined by a pre-existing structure (Carreras, 2001). Alternatively different shear sets may develop, which start to join and form a more complex anastomosing pattern (e.g. Marquer et al., 1996; Martínez et al., 1996; Arbaret et al., 2000; Brum da Silveira et al., 2009). Experimental studies of shear zone networks have focused on kinematics and strain distribution (e.g. Cobbold et al., 1971; Harris and Cobbold, 1985; Dennis and Secor, 1987; Williams and Price, 1990; Herwegh and Handy, 1996; Huddleston, 1999), whereas numerical modeling studies have presented the effects of rheology on the development and nucleation of shear zones (e.g. Huisemans and Beaumont, 2003; Regenauer-Lieb and Yuen, 2003; Montési, 2013; Guyedan et al., 2014; Jammes et al., 2015).

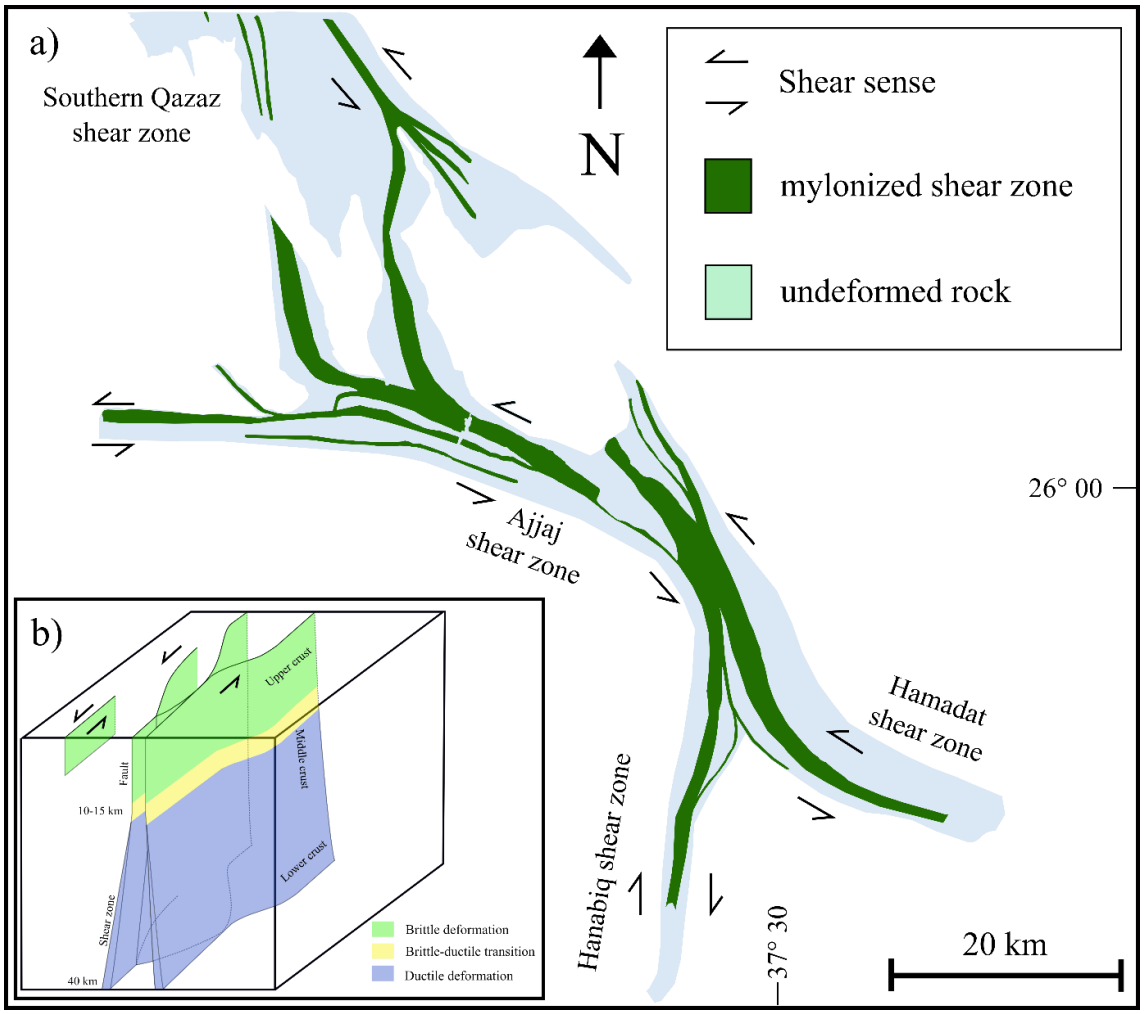

Figure 1.2 a) Example of the anastomosing pattern of a shear zone network, showing the Ajjaj, Hamadat and Hanabiq shear zones in the Arabian Shield (Saudi Arabia); b) Illustration of the 3-dimensional complex geometry of branched crustal-scale strike-slip shear zones

The interaction and evolution of different shear zone sets are still an active area of study. Field observations have given us an insight into the evolution of shear zone networks (Carreras, 2001; Fusseis et al., 2006), and results indicate that the development of complex shear zone geometries is greatly influenced by pre-existing structures. A recent publication on anastomosing shear zone networks (Carreras et al., 2010) shows that sinistral and dextral shear strands can occur in a single deformation event in a non-coaxial regime. Generally, anastomosing shear zone networks exhibit shear plane orientations relative to the bulk stress, and these variations are explained in the described examples as being due to either the influence of pre-existing structures or a change in the ratio of the shortening and the strike-slip component in a transpression regime. An additional theory, proposed by Bell (1986) and Ham and Bell (2004) is that multiple deformation events exist, during which the stress field changes.

1.2 Aim of the study and methods

Strike-slip shear zones form some of the largest structures on Earth, especially in collision zones, and play an essential role in plate tectonics. Previous studies (e.g. Mitra, 1978; Ramsay, 1980; Ramsay and Huber, 1983; Simpson, 1983; Arbaret and Burg, 2003; Baird and Hudleston, 2007) have focused on the development and the classification of shear zones to define their structure and to characterize their typical features. The interpretation of such strike-slip shear zones is important for the reconstruction of the local geological history, and subsequent identification of conditions at the initial stage. In most cases, detailed and quantitative studies have focused on straight shear zones since these are easier to remodel with numerical finite element or practical experimental methods. Satellite observations of large-scale strike-slip shear zone systems on earth, however, show them to be more complex: the shear zones can form anastomosing geometries.

A previous study into anastomosing shear zones (Carerras et al., 2010) has indicated that antithetic and synthetic shear zones can develop in a single deformation event, where single shear strands grow at different stages. The described example displays a complex pattern of geometry by reactivation of pre-existing structures and by an overprinting of new localized shear zones. This study was focused on the evolution of shear zones, to explain how these structures developed and to reconstruct single deformation events. The simultaneous activity of differently- or parallel-oriented shear strands in a network has a significant influence on the kinematics of the material, and therefore on the geodynamics of the crust. Furthermore the interaction of strike-slip shear zone strands and their effect on the surrounding rocks, especially at the junction zone, is not well known. It is also not clear how the activity of the shear strands are impaired by the interconnection (Fig. 1.3). Therefore this study is mostly focused on the interaction of branching to anastomosing shear zones, with a special focus on the junction zone.

In order to increase our understanding of branching shear zones, it is necessary to consider both natural shear zones, and numerical shear zone models. Three fundamental questions are addressed:

1) How do crustal-scale strike-slip shear zones interact, and how does this affect their kinematics?
2) Which rheological parameters control the development of shear zone networks?
3) What role does lithology play on shear zone nucleation?

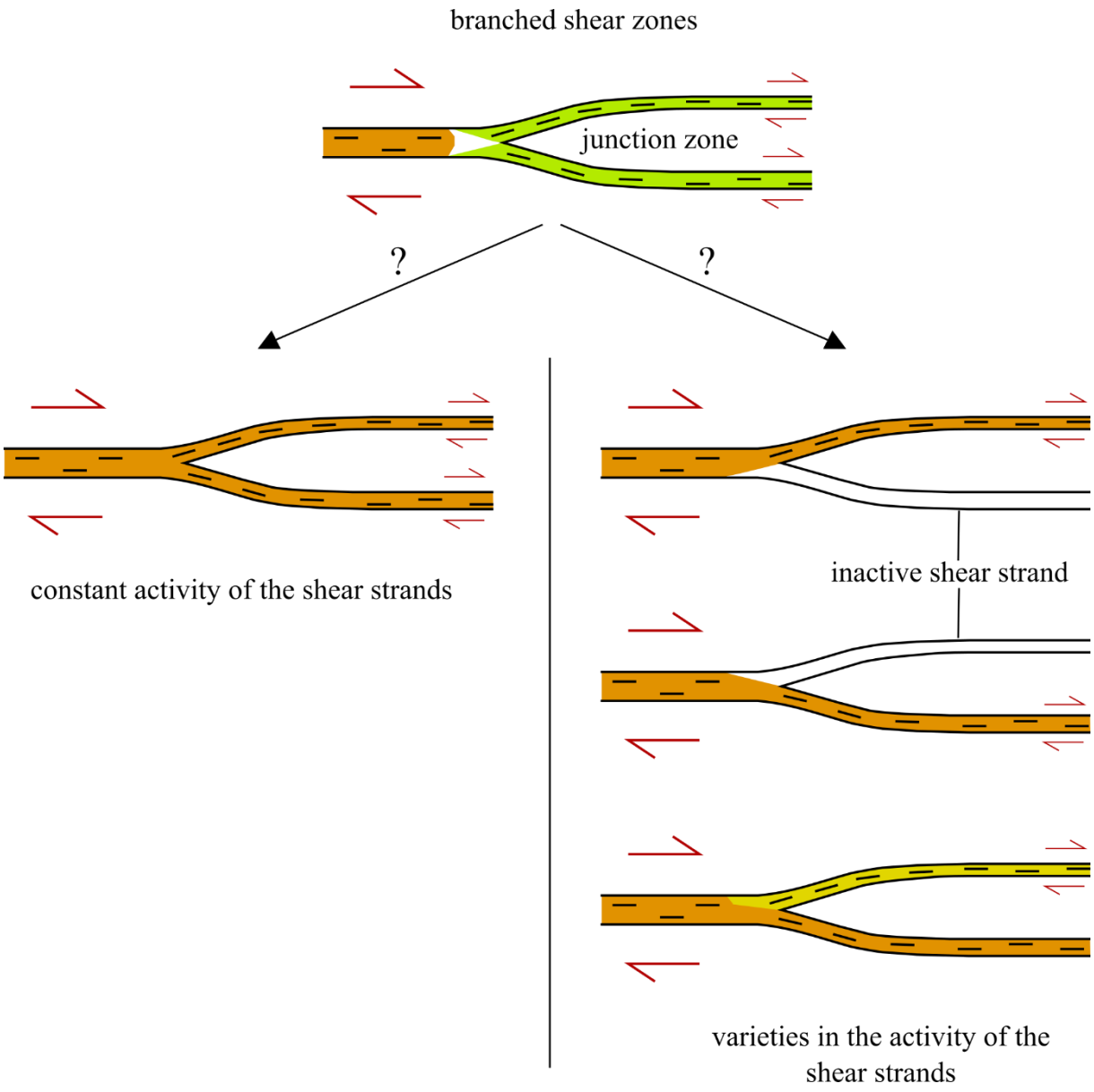

Figure 1.3 Illustration of the interconnection of shear strands with a dextral shear sense, showing possible variations in the activity (strain-rate) of the shear strands

For field examples, a study was made of shear zones in the Arabian Nubian Shield. Detailed observation of the Najd shear zone in the Arabian-Nubian Shield (Johnson and Woldehaimanot, 2003; Stern and Johnson, 2010) indicates a complex geology where isolated gneissic domes (metamorphic core complexes) are present along a NW-SE trending network of anastomosing shear zones. In that context, the study focuses on the strike-slip shear zones in the Arabian-Nubian Shield, where one structure stands out: the Qazaz Dome complex. This structure consists of two strike-slip shear zones with a metamorphic high-grade gneissic rock in the center and a detachment structure to the South, described

in Chapter 2. In addition, theoretical and experimental studies have shown that strain localizations are related to pre-existing anisotropies, e.g. foliations, veins or dikes (e.g. Carreras, 2001; Mancktelow and Pennacchioni, 2005), or by mechanical properties e.g. viscosity contrast (Biot, 1964). We present a field example of a new type of ductile shear zone nucleation, which develops through reactivation of a pre-existing structure, shown in Chapter 4.

The second direction in this study was the use of numerical modeling to improve understanding of rheology in the evolution of complex branched or anastomosed strike-slip shear zones. Previous publications regarding numerical simulation of shear zones have shown that strain-weakening during deformation has a strong effect on the localization of shear zones, and that shear planes can rotate during bulk deformation (e.g. Mancktelow, 2002; Huismans and Beaumont, 2003; Mancktelow, 2006). A recently published paper shows the influence of polymineralic rock composition, in relation to temperature, on the development of anastomosing shear zones (Jammes et al., 2015). Following question (2), our study utilizes simulations of complex networks of branched or anastomosed strike-slip shear zones to systematically test the influence of certain rheological material properties on the development of strike-slip networks, reported in Chapter 3. The interaction of shear strands and the effects on the junction zones between two shear zones were studied with specific visualization scripts, to compare the results with natural examples.

Methods used

The fieldwork-based study used Discover Mobile, a portable geographic information system (GIS) on a Trimble microcomputer, and subsequently a special GIS related mapping program (MapInfo) to create the structural and geological maps. The microstructural analysis performed to classify the temperature of the deformation was based on the work of Stipp et al., (2002) and Passchier & Trouw, (2005). The calculation of the peak metamorphic condition was realized with the Al-in-hornblende barometer (Johnson and Rutherford, 1989) together with mineral exchange thermobarometers of garnet-biotite (Hodges and Crowley, 1985), muscovite-plagioclase (Green and Usdansky, 1986) and hornblende-plagioclase (Holland and Bundy, 1994).

The numerical modeling of branched shear zones in a brittle and ductile regime was contributed to by a MATLAB-based finite element method (FEM), which solves millions of unknown dimensional problems, called MILAMIN_VEP (Crameri and Kaus, 2010; Kaus, 2010). This code applies a range of plastic deformation laws to simulations of shear

zones in brittle (Drucker-Prager or Mohr-Coulomb plasticity) or ductile regimes (power-law rheology) by using equations described by Kaus (2010). The program enables the simulation of 2-dimensional structures on a geological timescale, providing both an insight into and a visualization of the localized shear zones. Furthermore, the codes were modified to be applicable to a horizontal model to obtain some perspective on the development of strike-slip motioned shear zones, with a focus on the geometries of the shear strands. However, the most importance equations are shown in Chapter 3.

The analysis of the c-axis contributions in quartz was realized by a Microfabric Analyser. The analytical method is described in detail in Wilson et al., (2007). The instrument uses eight white light emitting diodes (LED) which are polyaxial with a vertical axis, to focus the light arrays on the thin section. With the aid of the data set from the polarized light images, the c-axis of each quartz grain can be presented with an axial distribution diagram (AVA-"Achsenverteilungsanalyse") with a resolution of 5µm/pixel. The preparation of the data sets was realized by the software INVESTIGATOR (Peternell et al., 2010).

1.3 Organization

This work, based on a research project at the Johannes Gutenberg University in Mainz, was funded for one years by Geocycles (scholarship) and for two years by the Center for Computational Sciences (SRFN). The project was funded for a further year by DFG Grant PA578/16-1.

The thesis itself is organized in five chapters. These chapters are self-contained studies, each one subdivided into abstract, introduction, geology / results, discussion and conclusion.

Chapter 1 is the introduction;

Chapter 2 shows an example of the interaction of strike-slip shear zones in the Arabian Nubian Shield. A new structure was found, related to two sinistral strike-slip shear zones linked to a detachment which form a new mechanism to exhume deeper crustal rocks. This new model represents an effective way in which small metamorphic core complexes can develop linked to a crustal-scale strike-slip system. This chapter is published in Terra Nova (Meyer et al., 2014).

Chapter 3 describes 2-dimensional numerical simulations on the development of a network of brittle and ductile shear zones. The numerical experiments contains also simulations in the brittle regime, to understand how the geometries of shear zone networks are influenced by different plastic regimes related to crustal-scale structures described in Chapter 2. The focus of this study was the influence of rheology on the development of branched or anastomosing shear zones over a geological timescale. The application of new visualization scripts helped to show the effect of different rheological parameters on the development of shear zones. Furthermore, the simulation indicated that strain-weakening strongly affects the geometry of shear zone networks and the interaction of shear strands. The interaction of the shear strands - and therefore the development of a more complex geometry - leads to a change in the kinematic patterns of the junction zone and exerts an influence on the nucleation of new shear zones. Finally, the results give new insight into the development of branched or anastomosing shear zones in comparison to natural field examples. This Chapter was in review to Geochemistry, Geophysics, Geosystems.

Chapter 4 presents two examples of a localization of ductile shear zones through the reactivation of a pre-existing structure, in Jordan and Egypt. In the Wadi Filk (Jordan), paired ductile shear zones have developed along the chilled margins of a rhyolite dyke, with a steep strain-gradient to the wall rock and with no evidence of deformation. The trend of the dike is favorably oriented for a stress field associated with simple shear related to the active phase of the East-West Gondwana collision. This is an example of a lithology-driven shear zone, where a grain-size gradient leads to a weaker zone by anisotropic behavior and therefore to localization of a ductile shear zone. The development of the Wadi Filk mylonites show the influence of pre-existing structures on the nucleation and propagation of shear zones, and suggest our numerical observations that a change of the rheology initiate shear zones. This chapter is in preparation for publication in the near future.

Chapter 5 presents the final conclusion of the work and a short outlook on future research.

1.4 Contributions

My contribution for Chapter 2 was in field work, including the collection of structural-geological field data, satellite imaging, the sampling and processing of the data with GIS mapping software (MapInfo) and thin section studies. Fieldwork was carried out together with colleagues from the Saudi geological Survey, and Prof. Cees Passchier. The preparation and the interpretation of geothermobarometry data was realized by Dr. Tamer Abu-Alam and Prof. Kurt Stüwe.

The work for Chapter 3 was realized with a MATLAB-based finite element program of the Geophysics group under the supervision of Prof. Boris Kaus, at the University of Mainz. My contributions were to modify the codes for the simulation of strike-slip shear zones and the creation of a new setup. All experimental runs were implemented by myself, as were the compilation of codes for the visualization of the results.

To the work for Chapter 4 was the preparation of the samples for thin section, microstructural analysis and the determination of the c-axis distribution of the quartz grains using a Fabric Analyser. Dr. Mark Peternell supported the work with the Fabric Analyser. The field work was carried out by Prof. Cees Passchier and Prof. Ghaleb Jarrar from the University of Amman (Jordan), who also helped organize the samples. The field study in Egypt was carried out in cooperation with Prof. Cees Passchier, whereas the collection of the field data and samples was my work.
My overall contribution to this thesis is 90%.

1.5 References

Arbaret, L., Hussain, S., Dawood, H., Burg, J. -P., Zeilinger, G., and Chaudhry, N., 2000. Pre-collisional anastomosing shear zones in the Kohistan arc, NW Pakistan. In: Khan, M. A., Treloar, P. J., Searle, M.P., Jan, M. Q. (Eds.), Tectonics of the Nanga Parbat Syntaxis and the Western Himalaya. Geological Society, London, Special Publications, vol. 170, pp. 295-311.

Arbaret, L., and Burg, J. P., 2003. Complex flow in lowest crustal, anastomosing mylonites: strain gradients in a Kohistan gabbro, northern Pakistan. Journal of Geophysical Research-Solid Earth 108, art. no. 2467.

Baird, G. B., and Hudleston, P. J., 2007. Modeling the influence of tectonic extrusion and volume loss on the geometry, displacement, vorticity, and strain compatibility of ductile shear zones. Journal of Structural Geology, 29 (10), 1665-1678.

Bell, T. H., 1981. Foliation development: the contribution, geometry and significance of progressive, bulk, inhomogeneous shortening. Tectonophysics 75, 273-296.

Bell, T.H., 1986. Foliation development and refraction in metamorphic rocks: reactivation of earlier foliations and decrenulation due to shifting patterns of deformation partitioning. Journal of Metamorphic Geology 4, 421-444.

Biot, M. A., 1964, Theory of viscous buckling of multilayered fluids undergoing finite, strain, in the physics of fluids: Am. Inst. Physics Mag., v. 7, no. 6, p. 855-859.

Brum da Silveira, A., Cabral, J., Perea, H., and Ribeiro, A., 2009. Evidence for coupled reverse and normal active faulting in W Iberia: The Vidigueira-Moura and Alqueva faults (SE Portugal). Tectonophysics 474, 184-199.

Burg, J. P., and Laurent, P., 1978. Strain analysis of a shear-zone in a granodiorite. Tectonophysics 47, 15-42.

Carreras, J., 2001. Zooming on northern Cap de Creus shear zones. Journal of Structural Geology 23, 1457-1486.

Carreras, J., Czeck, D. M., Druguet, E., and Hudleston, P. J., 2010. Structure and development of ananastomosing network of ductile shear zones. Journal of Structural Geology, 32 (5), 656-666.

Christiansen, P. P., and Pollard, D. D., 1997. Nucleation, growth and structural development of mylonitic shear zones in granitic rock. Journal of Structural Geology 19, 1159–1172.

Choukroune, P., Gapais, D., 1983. Strain pattern in the Aar granite (Central Alps): orthogneiss developed by bulk inhomogeneous flattening. Journal of Structural Geology 5, 411-418.

Cobbold, P. R., Cosgrove, J. W., and Summers, J. M., 1971. The development of internal structures in deformed anisotropic rocks. Tectonophysics 12, 23-53.

Dennis, A. J., and Secor, D. T., 1987. A model for the development of crenulations in shear zones with applications from the Southern Appalachian Piedmont. Journal of Structural Geology 9 (7), 809-817.

Dutruge, G., Burg, J. P., Lapierre, J., and Vigneresse, J. L., 1995. Shear strain analysis and periodicity within shear gradients of metagranite shear zones. Journal of Structural Geology 17, 819–830.

Fossen, H., and Tikoff, B., 1993. The deformation matrix for simultaneous simple shearing, pure shearing and volume change, and its application to transpression - transtension tectonics. Journal of Structural Geology 15, 413-422.

Fusseis, F., Handy, M. R., and Schrank, C., 2006. Networking of shear zones at the brittle- to-viscous transition (Cap de Creus, NE Spain). Journal of Structural Geology 28, 1228-1243.

Gapais, D., Bale, P., Choukroune, P., Cobbold, P. R., Mahjoub, Y., and Marquer, D., 1987. Bulk kinematics from shear zone patterns: some field examples. Journal of Structural Geology 9, 635-646.

Gueydan, F., Précigout, J., and Montési, L. G. J., 2014. Strain weakening enables continental plate tectonics, Tectonophysics, Volume 631, p. 189-196.

Green, N., and Usdansky, S., 1986. Ternary-feldspar mixing relations and thermobarometry: American Mineralogist, 71, 1109-1117.

Ham, A.P., and Bell, T. H., 2004. Recycling of foliations during folding. Journal of Structural Geology 26, 1989-2009.

Harland, W. B., 1971. Tectonic transpression in Caledonian Spitsbergen. Geological Magazine 108, 27-42.

Harris, L. B., and Cobbold, P. R., 1985. Development of conjugate shear bands during bulk simple shearing. Journal of Structural Geology 7 (1), 37-44.

Herwegh, M., and Handy, M. R., 1996. The evolution of high-temperature mylonitic microfabrics: evidence from simple shearing of a quartz analogue (norcamphor). Journal of Structural Geology 18 (5), 689-710.

Hodges, K., and Crowley, P., 1985. Error estimation and empirical geothermobarometry for pelitic systems: American Mineralogist, 70, 702-709.

Holland, T., and Bundy, J., 1994. Non-ideal interactions in calcic amphiboles and their bearing on amphibole-plagioclase thermometry: Contributions to Mineralogy and Petrology, 116, 433-447.

Huddleston, P., 1999. Strain compatibility and shear zones: is there a problem? Journal of Structural Geology 21, 923-932.

Hull, J., 1988. Thickness-displacement relationships for deformation zones. Journal of Structural Geology 10, 431-435.

Huismans, R. S., and Beaumont, C., 2003. Symmetric and asymmetric lithospheric extension: Relative effects of frictional-plastic and viscous strain softening, J. Geophys. Res., 108(B10), 2496, doi:10.1029/2002JB002026.

Imber, J., Holdsworth, R. E., and Butler, C. A., 2001. A reappraisal of the Sibson-Scholz fault zone model: the nature of the frictional to viscous ("brittle-ductile") transition along a long-lived, crustal scale fault, Outer Hebrides, Scotland. Tectonics 20 (5), 604–624.

Jammes, S., Lavier, L. L., and Reber, J. E., 2015. Localization and delocalization of deformation in a bimineralic material, J. Geophys. Res. Solid Earth, 120, doi: 10.1002/2015JB011890.

Jiang, D., and White, J. C., 1995. Kinematics of rock flow and the interpretation of geological structures, with particular reference to shear zones. Journal of Structural Geology 20, 1105-1120.

Johnson, M. and Rutherford, M., 1989. Experimental calibration of the aluminum-in-hornblende geobarometer with application to Long Valley caldera (California) volcanic rocks: Geology, 17, 837-841.

Johnson, P. R., and Woldehaimanot, B., 2003. Development of the Arabian -Nubian Shield: Perspectives on accretion and deformation in the northern East African Orogen and the assembly of Gondwana: Geology Society London. Special Publication 206, 289-325.

Jones, R. R., and Tanner, P. W. G., 1995. Strain partitioning in transpression zones. Journal of Structural Geology 19, 1201-1217.

Jones, R. R., Holdsworth, R. E., and Bailey, W., 1997. Lateral extrusion in transpression zones: The importance of boundary conditions. Journal of Structural Geology 19, 1201-1217.

Kaus, B., 2010. Factors that control the angle of shear bands in geodynamic numerical models of brittle deformation Tectonophysics 484, 36-4.

Kligfield, R., and Crespi, J., 1984. Displacement and strain patterns of extensional orogens. Tectonics 3, 577-609.

Krantz, R. W., 1995. The transpressional strain model applied to strike-slip, oblique-convergent and oblique-divergent deformation. Journal of Structural Geology 17, 1125-1137.

Lafrance, B., John, B. E., and Frost, B. R., 1998. Ultra high-temperature and subsolidus shear zones: examples from the Poe Mountain anorthosite, Wyoming. Journal of Structural Geology 20 (7), 945–955.

Lamouroux, C., Debat, P., Ingles, J., Guerrero, N., Sirieys, P., and Soula, J.C., 1994. Rheological properties of rock inferred from the geometry and microstructure in two natural shear zones.Mechanics of Materials 18, 79-87.

Mancktelow, N. S., 2002. Finite-element modelling of shear zone development in visco-elastic materials and its implications for localization of partial melts. Journal of Structural Geology 24, 1045-1053.

Mancktelow, N.S., 2006. How ductile are ductile shear zones? Geology 34, 345-348.

Mancktelow, N. S., and Pennacchioni, G., 2005. The control of precursor brittle fracture and fluid-rock interaction on the development of single and paired ductile shear zones. Journal of Structural Geology, 27 (4), 645-661.

Marquer, D., Challandes, N., and Baudin, T., 1996. Shear zone patterns and strain distribution at the scale of a Penninic nappe: the Suretta nappe (Eastern Swiss Alps). Journal of Structural Geology 18, 753-764.

Martínez, F. J., Carreras, J., Arboleya, M. L., and Ditsch, C., 1996. Structural and metamorphic evidence of local extension along the Vivero fault coeval with bulk crustal shortening in the Variscan chain (NW Spain). Journal of Structural Geology 18, 61-73.

Means, W.D., 1995. Shear zones and rock history. Tectonophysics 247, 157-160.

Meyer, S. E., Passchier, C., Abu-Alam, T., and Stüwe, K., 2014. A strike-slip core complex from the Najd fault system, Arabian shield. Terra Nova, 26 (5), 387-394.

Mitra. G. 1978. Ductile deformation zones and mylonites: the Nature. Load. 280, 222-223. Mechanical processes involved in the deformation of crystalline White, S. 1979c. Sub-grain and grain size variations across a shear basement rocks. Am. J. Sci. 278, 1057-1084.

Montési, L. G. J., 2013. Fabric development as the key for forming ductile shear zones and enabling plate tectonics. Journal of Structural Geology 50, 254-266, doi: 10.1016/j.jsg. 2012.12.011.

Passchier, C. W., Hoek, J. D., Bekendam, R. F., and De Boorder, H., 1990. Ductile reactivation of Proterozoic brittle fault rocks; an example from the Vestfold Hills, East Antarctica. Precambrian research, 47 (1), 3-16.

Passchier, C. W. and Trouw, R. A. J., 2005. Microtectonics. Second Edition.

Paterson, S. R., and Wainger, L. 1991. Strains and structures associated with a terrane bounding stretching fault: the Melones fault zone, central Sierra Nevada, California. Tectonophysics 94, 69-90.

Pennacchioni, G., and Mancktelow, N. S., 2007. Nucleation and initial growth of a shear zone network within compositionally and structurally heterogeneous granitoids under amphibolite facies conditions. Journal of Structural Geology, 29 (11), 1757-1780.

Platt, J. P., and Behr, W. M., 2011. Deep structure of lithospheric fault zones. Geophysical Research Letters, Vol. 38, Issue 24.

Ramsay, J. G., 1980. Shear zone geometry: a review. Journal of Structural Geology 2, 83-99.

Ramsay, J. G., and Graham, R. H., 1970. Strain variations in shear belts. Canadian Journal of Earth Sciences7, 786-813.

Ramsay, J. G., and Huber, M. I., 1983. The Techniques of Modern Structural Geology. Volume 1: Strain Analysis. Academic Press, London.

Regenauer-Lieb, K., and Yuen, D. A., 2003. Modeling shear zones in geological and planetary sciences: solid- and fluid-thermal-mechanical approaches. Earth-Science Reviews 63 (3-4), 295-349.

Rolland, Y., Cox, S. F., Boullier, A. M., Pennacchioni, G., and Mancktelow, N., 2003. Rare Earth and trace element mobility in mid-crustal shear zones: insights from the Mont Blanc Massif (Western Alps). Earth and Planetary Science Letters 214, 203–219.

Sanderson, D. and Marchini, R. O., 1984. Transpression. Journal of Structural Geology, 6, 449-458.

Schrank, C. E., Handy, M. R. and Fusseis, F., 2008. Multiscaling of shear zones and the evolution of the brittle-to-viscous transition in continental crust. Journal of Geophysical Research 113, B01407,doi: 10.1029/2006JB004833.

Selverstone, J., Morteani, G., and Staude, J. -M., 1991. Fluid channelling during ductile shearing: transformation of granodiorite into aluminous schist in the Tauern Window, Eastern Alps. Journal of Metamorphic Geology 9, 419-431.

Simpson, C., 1983. Strain and shape-fabric variations associated with ductile shear zones. Journal of Structural Geology 5, 61-72.

Stern, R.J., and Johnson, P., 2010. Continental lithosphere of the Arabian Plate: A geologic, petrologic, and geophysical synthesis: Earth Science Reviews, 101, 29-67.

Stipp, M., Holger, S., Heilbronner, R., and Schmid, S. F., 2002. Dynamic recrystallization of quartz: correlation between natural and experimental conditions: Geological Society London Special Publications 200: 171-190.

Tikoff, B., and Greene, D. 1997. Stretching lineations in transpressional shear zones: an example from the Sierra Nevada Batholith, California. Journal of Structural Geology 19, 29-41.

Vauchez, A., 1987. The development of discrete shear-zones in a granite: stress, strain and changes in deformation mechanisms. Tectonophysics 133, 137-156.

Williams, P. F., and Price, G. P., 1990. Origin of kink bands and shear-band cleavage in shear zones-an experimental study. Journal of Structural Geology 12 (2), 145-164.

Wilson, C. J. L., Russell-Head, D. S., Kunze, K., and Viola, G., 2007. The analysis of quartz caxis fabrics using a modified optical microscope. J. Microsc. 227, 30-41.

2. A strike-slip core complex from the Najd fault system, Arabian Shield

Abstract

Metamorphic core complexes are usually thought to be associated with regional crustal extension and crustal thinning, where deep crustal material is exhumed along gently dipping normal shear zones oblique to the regional extension direction. We present a new mechanism to exhume metamorphic core complexes along crustal-scale strike-slip fault systems that accommodated crustal shortening. The Qazaz metamorphic dome in Saudi-Arabia was exhumed along a gently dipping jog in a crustal-scale vertical strike-slip fault zone that caused more than 25 km of exhumation of lower crustal rocks by 30 km of lateral motion. Subsequently, the complex was transected by a branch of the strike-slip fault zone, and the segments were separated by another 30 km of lateral motion. Strike-slip core complexes like the Qazaz Dome may be common, may have an important local effect on crustal strength.

This chapter was published as:

Meyer, S. E., Passchier, C., Abu-Alam, T., and Stüwe, K., 2014. A strike-slip core complex from the Najd fault system, Arabian shield. Terra Nova, 26 (5), 387-394.

2.1 Introduction

Metamorphic domes surrounded by low-grade metamorphic rocks are commonly formed by the exhumation of medium to high-grade metamorphic rocks from lower crustal levels (Davis and Coney, 1979; Crittenden et al., 1980). The most common mechanisms of exhumation is thought to be regional-scale extension (Davis et al., 1986; Wernicke, 1981) and crustal thinning, where higher grade rocks are brought up in the footwall of gently dipping shear zone systems oblique to the regional extension direction (often termed “low angle detachments”) forming so-called core complexes (Lister et al., 1984;

Tirel et al., 2008; Huet et al., 2010; Fig. 2.1a). Here, we present evidence that core complexes can also be locally exhumed along major vertical strike-slip shear zones in areas of crustal shortening without regional scale crustal thinning, using an example from the Najd shear zone system in Saudi Arabia (Abdelsalam and Stern, 1996; Fig. 1b).

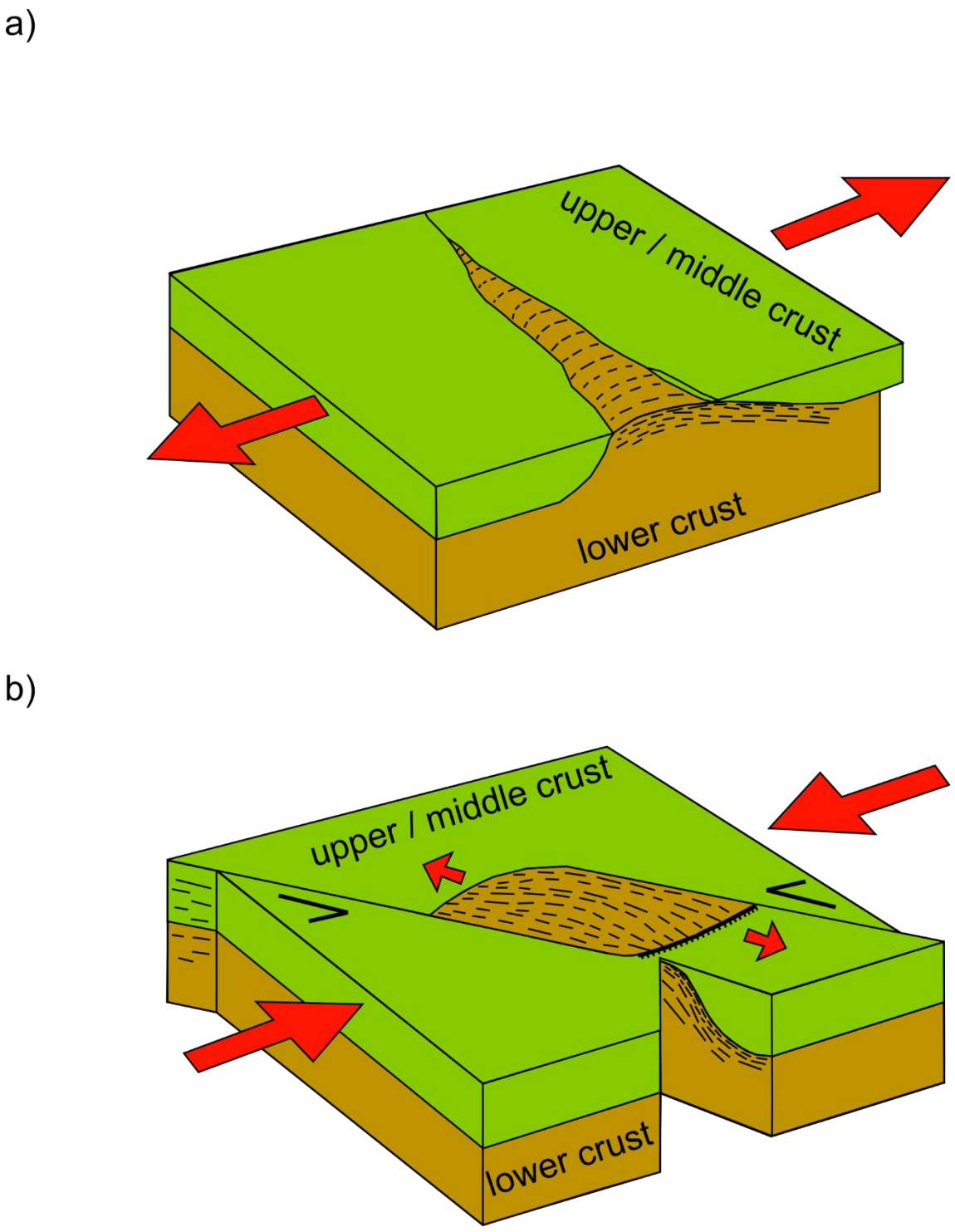

Figure 2.1 a) Typical metamorphic core complex formed in regional extension; b) Strike-slip core complex, formed in regional constriction by local extension associated with a jog in a strike-slip shear zone

2.2 The Najd shear zones system

The Arabian Nubian shield (ANS) in Egypt, Saudi Arabia and Sudan is composed of ~870 - 630 Ma Neoproterozoic juvenile arc terranes and remains of ophiolite belts which amalgamated during the closing of the Mozambique ocean and the associated assembly of Gondwanaland (Johnson et al., 2004; Stern, 1994; Stern and Johnson, 2010). Most of the ANS consists of low-grade metavolcanics, metasediments with scattered intrusive arc-type and few A-type granitoids. All units are affected by the Najd fault System (NFS), a network of crustal-scale sinistral strike-slip zones 2000 km long and 400 km wide, which cut and partly reactivate older tectonic elements in the shield (Stern, 1994; Fig. 2.2). Development of this shear zone network during and following the collision of West- and East Gondwana resulted in E-W shortening with a northwards trend of escape tectonic (Abdelsalam and Stern, 1996; Burke and Sengör, 1986; Stern, 1994). This was accompanied by the exhumation of metamorphic domes (e.g. Fritz et al., 2002; Blasband et al., 2000; Brooijmans et al., 2003; Abd El-Naby et al., 2008; Abu-Alam and Stüwe, 2009). We studied one of these domes in NW Saudi Arabia: the Qazaz Dome, which is associated with the sinistral Qazaz strike-slip shear zone, one of the largest Najd structures with a length of at least 140 km (Stern and Johnson, 2010; Genna et al., 2002; Figs. 2.2, 2.3).

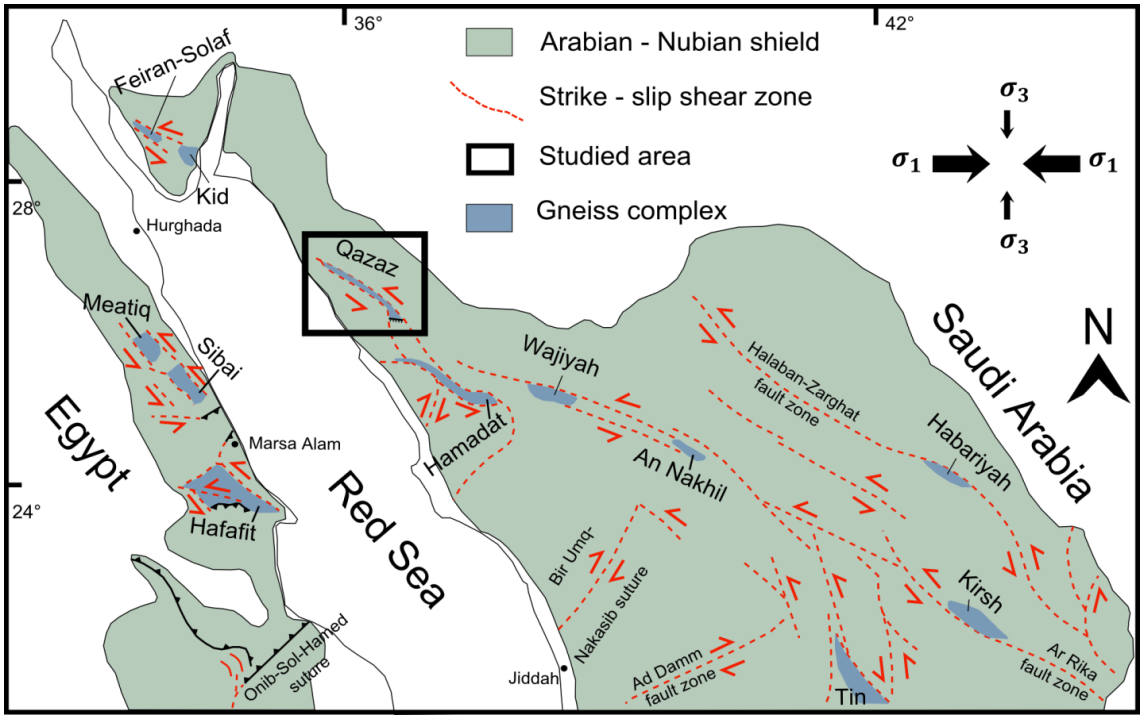

Figure 2.2 Overview map of the Najd shear zones and the gneiss complexes in the Arabian-Nubian Shield; modified after Abu-Alam and Stüwe (2009)

2.3 Qazaz metamorphic complex

The Qazaz Dome developed in a low-relief area with nearly continuous exposure in the desert of Saudi Arabia. It is a triangular dome of medium- to high-grade gneisses surrounded by low-grade mylonite zones and very low-grade metapelite, conglomerate and volcanic rocks of the Neoproterozoic Thalbah and Bayda Groups (Fig. 2.3a, b). The Thalbah group sediments have been deposited unconformable on the Imdan plutonic complex (660 ± 4 Ma) and were intruded by the Liban complex (621 ± 7 Ma), which appears to bracket deposition between 660 - 620 Ma (Johnson et al., 2011). However, the age of the group is debated, and new U-Pb dates of detrital zircons from two of the three formations that make up the Thalbah group (Bezenjani et al., 2014) suggest depositional ages of ≤ 596 ± 10 Ma (Hashim Formation) and ≤ 612 ± 7 Ma (Zhufar Formation). The Qazaz shear zone is locally 3 - 4 km wide with a dominance of vertical foliations and gently plunging stretching lineations. It is an anastomosing complex of high-strain branches with high-grade mylonitized rocks in the core (Fig. 2.3a). Adjacent to the Qazaz Dome, the shear zone splits into two strike-slip zones with similar sinistral shear sense, which flank the dome as described below. The activity of the Qazaz shear branches is bracketed between ~630 and 580 Ma (Calvez et al., 1984; Kennedy et al., 2009) based on displacement of dated granitoids.

The Qazaz Dome is characterized by a dominant gently SW-NE-dipping mylonitic foliation with NW-SE or NS trending gently plunging stretching lineations developed in granitic gneisses (Fig. 2.3c). The age of gneisses (protolith) in the dome itself is given by SHRIMP zircon dating as 725-696 Ma (Johnson and Woldehaimanot, 2003). Towards the southern detachment, the gentle southern dip of the mylonitic foliation increases to a maximum of 40° (Fig. 2.3c, 2.4). The detachment includes parts of the Qazaz gneisses and metasediments of the Thalbah group with a strong south-dipping mylonitic shape fabric (Fig. 2.3c). The footwall contains high-strain migmatites, high metamorphic grade mylonites with σ-type feldspar clasts and garnet clasts with strain shadows, giving a dominant top to the south shear sense (Fig. 2.5). These high-grade shear sense markers and shape fabrics are overprinted by lower grade S-C shear bands and chlorite veins representing the same movement direction and shear sense, suggesting synkinematic exhumation of the dome. The hanging wall of the Qazaz Dome to the south and west is composed of rocks of the Thalbah Group. These are weakly to moderately deformed with

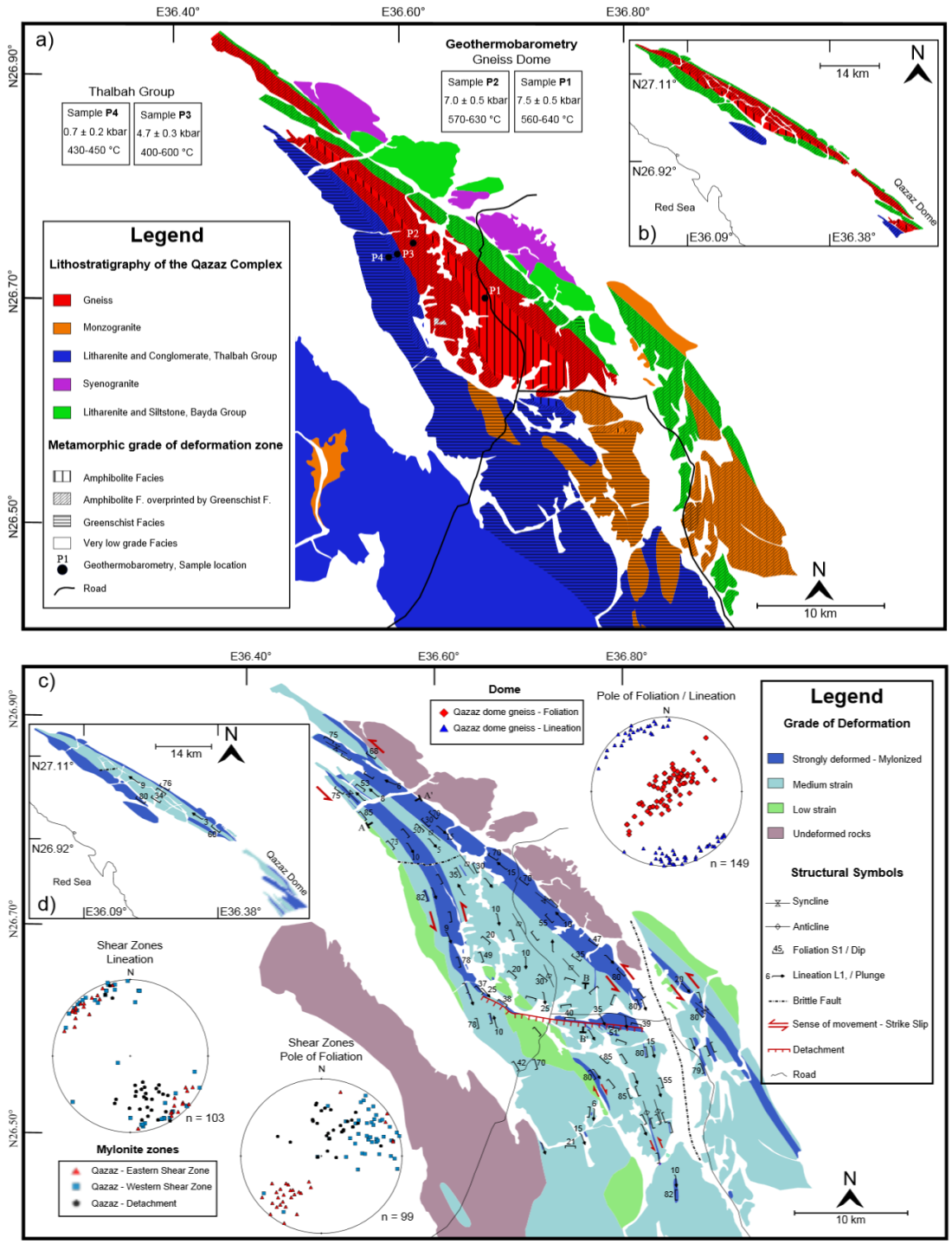

Figure 2.3 a) Lithological and metamorphic map of the Qazaz complex; b, d) Inset maps showing the shear zone northwest of the Qazaz Dome; c) Structural map of the Qazaz complex

open upright folds south of and alongside the dome and the Qazaz shear zone, but undeformed further away (Fig. 2.3c, d). To the SE, the Thalbah group is invaded by small, mostly undeformed monzogranite bodies that are not affected by the main strike-slip or detachment mylonitization, although some minor shear zones occur at the contact of the

granite and the metasediments. The gently dipping mylonitic foliation in the Qazaz Dome is affected by km-scale folds with NNW-SSE trending steep axial planes, which are open in the SE but become increasingly tight to the NW (Fig. 2.3c, 2.6c-e). In the NW apex of the Dome a single tight to isoclinal antiform dominates the mylonite zone and grades into the Qazaz shear zone. Up to 20 km north of the Qazaz Dome, this fold is still recognizable since the strike-slip Qazaz shear zone has gently plunging lineations throughout, but a foliation that changes from subvertical in the shear zone limbs, to horizontal in the centre (Fig. 2.3d, 2.6e, 2.7 inset). Further NW, only vertical foliations are present in the Qazaz shear zone. The west side of the Qazaz Dome is flanked by a sinistral strike-slip shear zone, which overprints the high-grade mylonitic fabrics in the western part of the gneiss dome with a lower grade shear band cleavage.

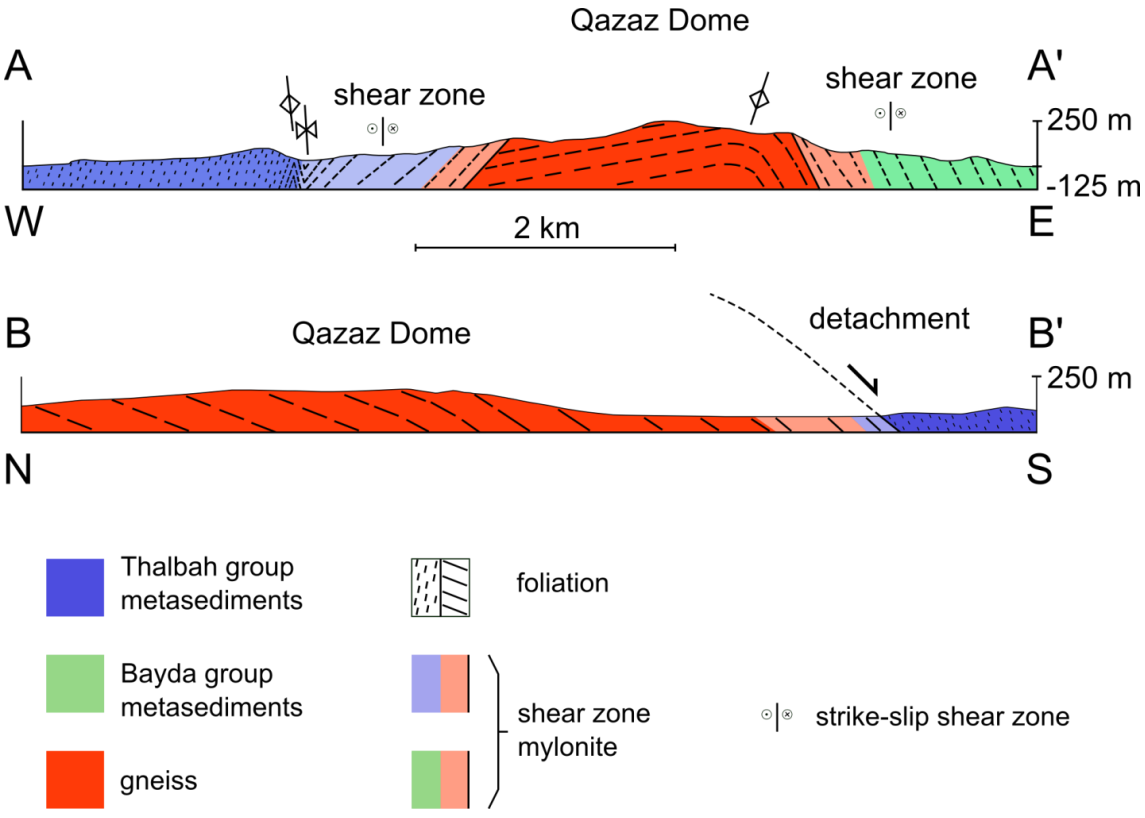

Figure 2.4 Profiles through the Qazaz Dome, marked in Fig. 3c

The western shear zone shows a steep mylonitic foliation with a westwards dip and stretching lineations are gently plunging with a NW-SE to N-S trend (Fig. 2.3c). In the SW corner of the Dome, the strike-slip shear zone changes direction and grades into the extensional detachment described above, while the stretching lineations in both segments

have the same orientation with a plunge of 10 to 35 degrees (Fig. 2.3c). There is no indication of any overprint, suggesting that the strike-slip and detachment segments operated simultaneously as one continuous shear zone. The gently dipping mylonitic fabric in the central parts of the dome gradually steepens and grades into the western shear zone and southern detachment without overprint and without a significant change in orientation of the main lineations (Fig. 2.3c, 2.7).

The eastern branch of the Qazaz shear zone is a sinistral shear zone with steep foliations and gently plunging stretching lineations similar to the western branch; it likewise has a greenschist facies mylonitic fabric with prominent shear band cleavage that overprints the gently south dipping amphibolite-grade mylonites of the central dome. Locally, the older mylonitic foliation is folded, and two parallel stretching lineations of different age can be found. The eastern branch is therefore younger than the detachment and formed later than the other structures. The eastern branch also transects the contact of the dome with the Bayda group in the south, interrupted by a sinistral brittle fault in the wadi (Fig. 2.3c).

2.4 Depth of Emplacement

Mineral exchange thermobarometers (i.e. garnet-biotite of Hodges and Crowley, 1985; muscovite-plagioclase of Green and Usdansky, 1986 and hornblende-plagioclase of Holland and Blundy, 1994) and the Al-in-hornblende barometer of Johnson and Rutherford (1989) were used to calculate peak metamorphic conditions for several samples across the shear zone to determine the maximum depth of burial. The hornblende-plagioclase thermometer and the Al-in-hornblende barometer are based on calibrations of igneous systems, but can be used for the metamorphic system (e.g. Mancini et al., 1996; Schärer and Labrousse, 2003). The calculated pressure and temperature conditions based on hornblende-bearing assemblages agree with the conditions that were calculated by the garnet-biotite and the muscovite-plagioclase thermobarometers. A sample from the core of the Dome (Fig. 3a, P1: 26.6956° N, 36.6996° E) attained peak metamorphic conditions of 560 - 640 °C and 7.5 ± 0.5 kbar (crustal depth of 24 - 28 km; for an overburden density 2850 kg/m3 and assuming lithostatic conditions). A high-grade gneiss sample near the periphery of the Dome (P2: 26.7455° N, 36.6193° E) gave a pressure-temperature range of 570 - 630 °C and 7.0 ± 0.5 kbar (crustal depth of 22 - 26 km). A schist sample from

the western Qazaz shear zone branch (P3: 26.7347° N, 36.6034° E) reached peak conditions of 400 - 460 °C and 4.4 - 5.0 kbar (crustal depth of 15.5 - 17.5 km). A sample from the base of the Thalbah group at a distance of ~120 m from P3, SW of the western Qazaz shear zone branch (P4: 26.7331° N, 36.6004° E), shows greenschist facies conditions of 430 - 450 °C and 0.7 ± 0.2 kbar (crustal depth of 1.5 - 3.5 km). Clearly, the local metamorphic gradient is telescoped with significant uplift of the dome with respect to the Thalbah group due to movement on the shear zones.

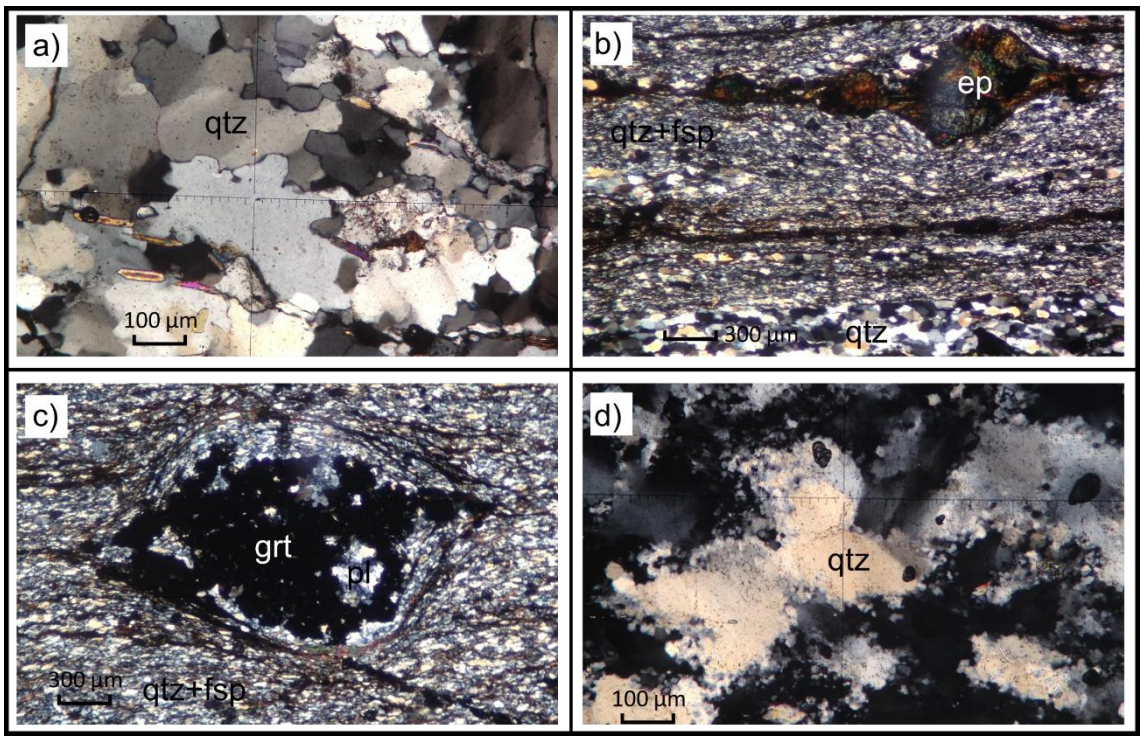

Figure 2.5 a) Quartz (qtz) with irregular grain boundaries with lobate structures, developed by grain boundary migration (GBM) recrystallization. Amphibolite facies, Centre of the Qazaz Dome; b) feldspar (fsp) porphyroclasts replaced by epidote (ep). Quartz shows a typical dynamical recrystallization fabric of subgrain rotation (SGR). Upper greenschist facies, Western shear zone; c) quartz with subgrain rotation (SGR) recrystallization and garnet crystals with irregular rims of plagioclase. Lower amphibolites facies, Western shear zone; d) relicts of GBM recrystallization, overprinted by lower temperature bulging recrystallization (BLG). Gneiss, detachment, S-side Qazaz Dome

The metamorphic grade of mylonitization in the Qazaz Dome and the shear zones was assessed from the microstructure using recrystallization characteristics of quartz and feldspar as an indicator (Stipp et al., 2002; Passchier and Trouw, 2005). The microstructure varies consistently with the barometry (Fig. 2.3a). The highest grade fabrics are found in the central and southern parts of the dome, with typical high temperature grain boundary migration (GBM) recrystallization of quartz with lobate grain boundaries, coarse grained

(>350µm) recrystallization of feldspars, and bulbous feldspar-quartz boundaries (Stipp et al., 2002; Fig. 2.5a). These fabrics grade to the south and to west into greenschist facies mylonitic fabrics, with subgrain boundary rotation or even bulging recrystallization of quartz; recrystallization to fine grain-size and brittle deformation of feldspar, and abundant development of shear band cleavage (Stipp et al., 2002; Fig. 2.5b-d).

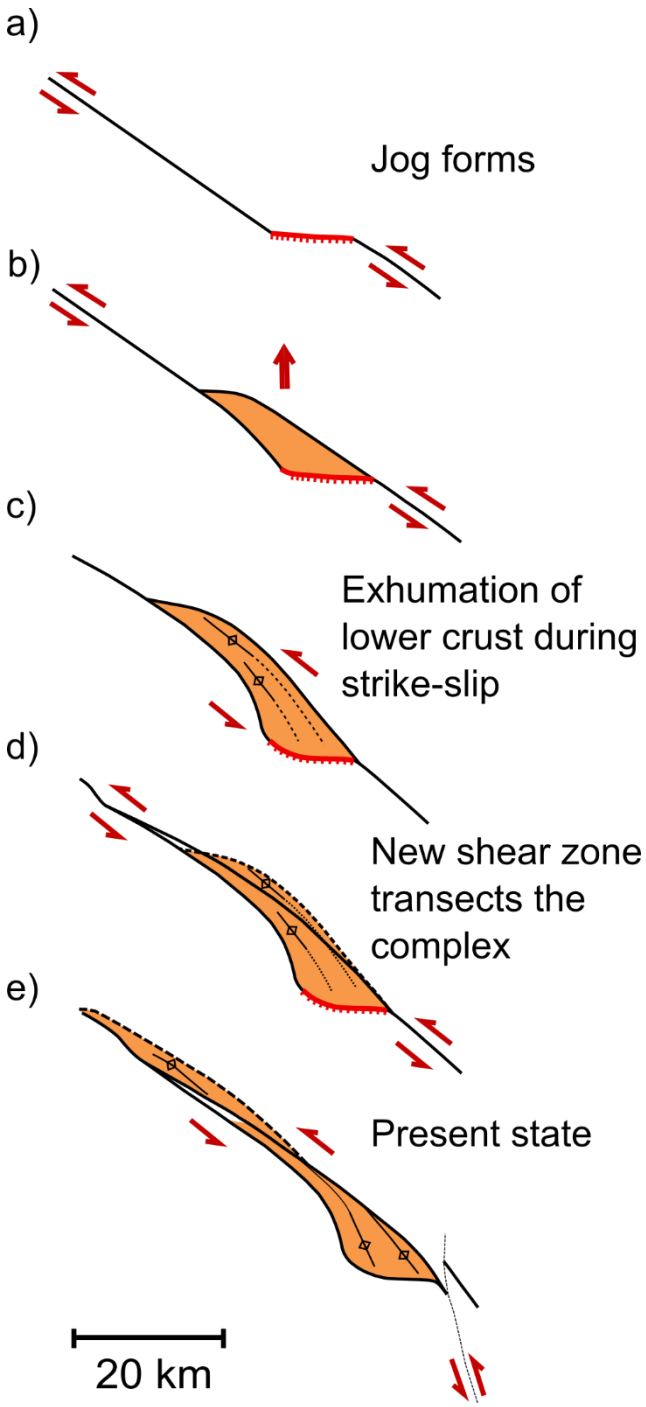

Figure 2.6 a-e) Proposed sequence in the development of the Qazaz complex along the Qazaz strike-slip shear zone

The greenschist facies mylonites along the western, eastern and southern side of the core complex show remains of an earlier high temperature fabric (Fig. 2.5d). The overprinting of coarse-grained quartz bands with lobate grain boundaries by shear band cleavage and bulging recrystallization indicate exhumation and cooling during ongoing mylonitization (Fig. 2.5d). Garnet crystals in samples from close to P3 in the western shear zone show irregular rims of plagioclase (Fig. 2.5c) in a primary volcanic rock, an indicator for decompression during the growth of the crystals. Calculated peak metamorphism of P3 classify this part as a middle crustal segment, which could be the deeper part of the Thalbah group. The kinematics of the shear zone and a steep metamorphic gradient of over 200 °C and 4.0 kbar in an E-W profile between the gneiss and the metasediments of the Thalbah group show that the southern Qazaz complex is a typical extensional detachment structure.

2.5 Discussion

Field and microstructural evidence shows that the Qazaz Dome is a high-grade metamorphic dome that has been brought into contact with adjacent low-grade metasediments by movement on ductile shear zones. The emplacement of the footwall high-grade dome by exhumation along a gently S-dipping detachment and emplacement against low-grade hanging wall metasediments is typical of a metamorphic core complex (Tirel et al., 2008; Huet et al., 2010). However, the relationship with strike-slip shear zones is different from other core complexes (Fig. 2.1). From field and microstructural data, we envisage the following scenario for development of the Qazaz Dome (Fig. 2.6). During development of the crustal scale vertical strike-slip Qazaz shear zone between ~630 - 580 Ma, a 10 km size jog formed as a gently south-dipping detachment, probably in response to a local pre-existing fabric (Fig. 2.6a). Progressive strike-slip after the jog formed led to exhumation of the middle and lower crust underlying the jog zone (Fig. 2.6b), which in turn considerably changed the local strength profile of the crust. The developing core complex is affected by regional shortening oblique to the strike-slip shear zone segments. The uplifted high-temperature dome underwent ductile E-W internal shortening leading to folding of previously gently-dipping planar fabric of foliation in the dome, at some distance from the detachment (Fig. 2.6c). Since the earlier exhumed part underwent lateral constriction for a longer time, folding is tightest furthest away from the detachment zone leading to a triangular shape of the dome (Fig. 2.6e; 2.7). This process created an unusual

strike-slip shear zone segment with an internal antiformal folded foliation in its core (Fig. 2.3c, 2.7 inset). If the detachment shear zone has a dip of 40º throughout, as observed at the surface, 25 km of vertical exhumation may have been accommodated by 30 km of horizontal slip on the Qazaz shear zone. The triangular core complex that formed in this way alongside the strike-slip zone was subsequently transected by a newly developing eastern branch of the Qazaz shear zone, which separated and displaced its NE side (Fig. 2.6d-e). This may have happened in reaction to cooling and strengthening of the distal side after slip on the western shear zone ceased. Sinistral displacement on the eastern branch is estimated to be at least 30 km, based on strain intensity in the shear zone, and displacement of marker horizons in satellite images (Fig. 2.6d). The accumulated displacement along the Qazaz shear zone can therefore be at least 60 km including the estimated 30 km of strike-slip displacement associated with exhumation of the central Qazaz Dome. Finally, a brittle sinistral strike-slip fault offset the eastern branch itself in a late stage of Najd shear zone activity (Fig. 2.3c, 2.6e).

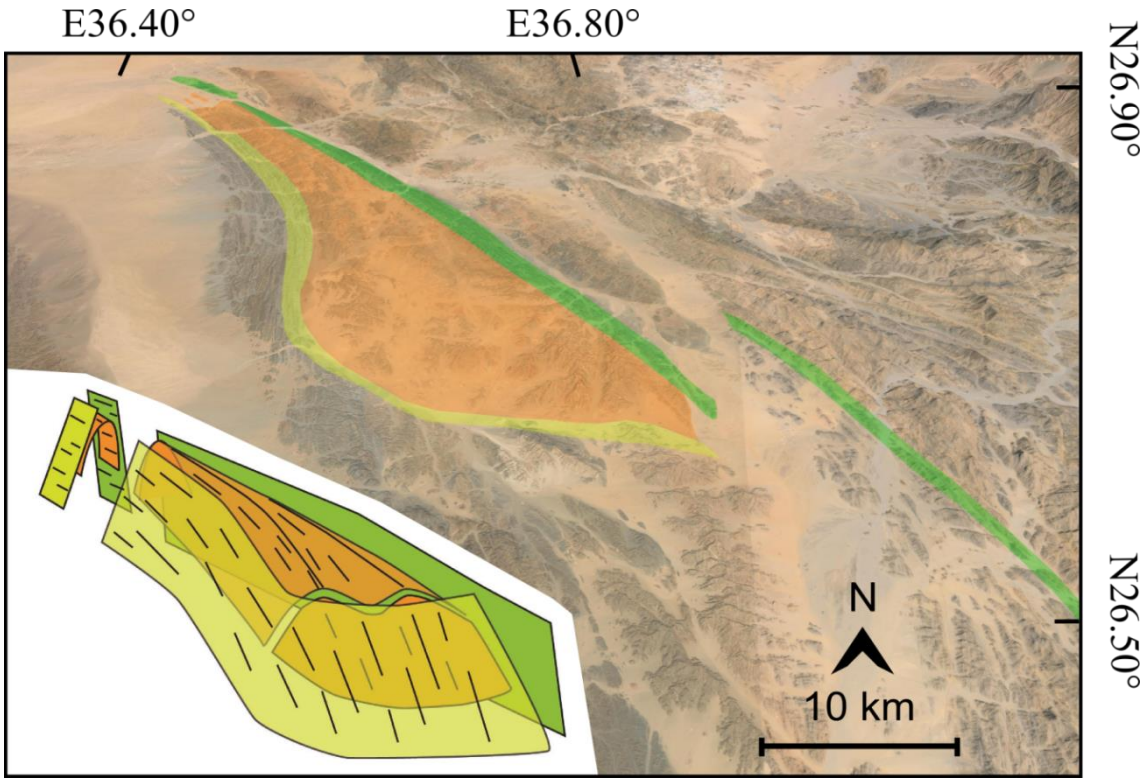

Figure 2.7 Annotated satellite image and 3-D cartoon of the present structure of the Qazaz complex. Black dashes indicate the orientation of the stretching lineation in the mylonites. Folding in the internal part of the dome is highlighted by an EW section

The deformation pattern in the low-grade Thalbah and Bayda Group metasediments surrounding the Qazaz Dome (Fig. 2.3c) also support a model where the Qazaz Dome formed in a regime of strike-slip linked detachment, accommodating regional E-W crustal shortening (Fig. 2.2, 2.3c). It is even conceivable that deposition of part of these metasediments is connected with development of the extensional jog. The most likely candidates that may show a similar development to the Qazaz Dome are other gneiss domes in the Najd Fault system such as and Hafafit complex (Fowler and Osman, 2009) and the Kirsh gneiss Dome (Al-Saleh, 2012, Fig. 2.2). The Sha'it-Nugrus shear zone of the Hafafit dome shows an identical transition from a strike-slip to a detachment fault as in the Qazaz Dome (Fowler and Osman, 2009).

Gneiss domes superficially similar to the Qazaz Dome also occur in a number of other tectonic settings. A-type domes in the Aegean (Jolivet et al., 2004b, 2010; Le Pourhiet et al., 2012) and the gneiss domes in the central Pyrenees (van den Eeckhout and Zwart, 1988; Denèle et al., 2007) superficially resemble the Qazaz Dome, but have a more complex history and no permanent link to crustal-scale strike-slip shear zones. Core complexes along the Lewis and Clark fault zone in the Rocky Mountains (Foster et al., 2007) differ from the Qazaz Dome in that the core complexes are the dominant structure, with strike-slip faults playing an accommodating role. The Niğde massif along the Central Anatolian fault zone in Turkey (Whitney et al., 2007) and domes along the Red River Shear Zones in Southern China and Indochina may have formed in a similar way as the Qazaz Dome, but are reported to have formed with a more complex history including a transtension phase (Jolivet et al., 2001). Further research on these structures, and along major strike slip fault systems will have to show if other isolated metamorphic domes formed in a similar way to the Qazaz Dome.

2.6 Conclusions

The development of metamorphic core complexes is generally thought to involve crustal scale extensional processes of crustal thinning with exhumation of the lower crust. The Qazaz Dome shows that core complexes can form along crustal-scale strike-slip shear zones which accommodated crustal shortening. The synchronous activity of strike-slip shear zones and a detachment-jog is an extremely effective way to exhume deeper crustal rocks under constrictional conditions. Strike-slip core complexes similar to the Qazaz

Dome may therefore be present unrecognized along many other crustal scale strike-slip shear zones where they have been transposed by ongoing strike-slip deformation. Development of a strike-slip core complex will locally change the thermal profile of the crust and can have far reaching effects on local crustal strength and the functioning of crustal-scale strike-slip shear zones.

2.7 References

Abd El-Naby, H., Frisch, W. and Siebel, W., 2008. Tectonometamorphic evolution of the Wadi Hafafit Culmination (central Eastern Desert, Egypt). Implication for Neoproterozoic core complex exhumation in NE Africa: Geologica Acta, 6, 293-312.

Abdelsalam, M.G., and Stern, R.J., 1996. Sutures and shear zones in the Arabian-Nubian Shield: J. African Earth Sciences, V. 23, No. 3, p. 289-310.

Abu-Alam, T. S. and Stüwe, K., 2009. Exhumation during oblique transpression: The Feiran–Solaf region, Egypt: Journal of Metamorphic Geology, 27, 439-459.

Al-Saleh, A. M., 2012. The Kirsh gneiss dome: an extensional metamorphic complex from the SE Arabian shield: Arabian Journal of Geosciences, 5, 335-344. DOI 10.1007/s12517-010-0179-1.

Bezenjani, R. N., Pease, V., Whitehouse, M. J., Shalaby, M. H., Kadi K. A. and Kozdroj, W., 2014. Detrital zircon geochronology and provenance of the Neoproterozoic Hammamat Group (Igla Basin), Egypt and the Thalbah Group, NW Saudi Arabia: Implications for regional collision tectonics. Precambrian Research, V. 245, p. 225-243.

Blasband, B., White, S., Brooijmans, P., De Boorder, H. and Visser, W., 2000. Late Proterozoic extensional collapse in Arabian-Nubian Shield: Journal of the Geological Society of London, 157, 615-628.

Brooijmans, P., Blasband, B., White, S. H., Visser, W. J. and Dirks, P., 2003. Geothermobarometric evidence for a metamorphic core complex in Sinai, Egypt: Precambrian Research, 123, 249-268.

Burke, K. and Sengör, C., 1986. Tectonic escape in the evolution of the continental crust, in Reflection Seismology: The Continental Crust, (ed. M. Barazangi, L. Brown), Geodyn. Ser. 14, pp. 41-53. Washington, DC: Am. Geophys. Union.

Calvez, J.-Y., Alsac, C., Delfour, J., Kemp, J., and Pellaton, C., 1984. Geologic evolution of western, central, and eastern parts of the northern Precambrian Shield, Kingdom of Saudi Arabia. Faculty of Earth Sciences Bulletin 6, 24-48.

Crittenden, M. D., Coney, P. J., and Davis, G. H. (Eds.), 1980. Cordilleran Metamorphic Core Complexes: Mem. Geol. Soc. Am., 153, 490 pp.

Davis, G. A., and Coney, P. J., 1979. Geological development of metamorphic core complexes: Geology, 7, 120-124.

Davis, G. A., Lister, G. S., and Reynolds, S. J., 1986. Structural evolution of the Whipple and South Mountains shear zones, southwestern United States. Geology 14, 7-10.

Denèle, Y., Olivier, P., Gleizes, G. and Barbey, P., 2007. The Hospitalet gneiss dome (Pyrenees) revisited: lateral flow during Variscan transpression in the middle crust, Terra Nova, 19, 6, 445-453.

van den Eeckhout, B., and Zwart, H. J., 1988. Hercynian crustal-scale extensional shear zone in the Pyrenees. Geology, 16, 135-138.

Foster, D. A., Doughty, P. T., Kalakay, T. J., Fanning, C. M., Coyner, S., Grice, W. C., and Vogle, J., 2007. Kinematics and timing of exhumation of metamorphic core complexes along the Lewis and Clark fault zone, northern Rocky Mountains, USA. Geological Society of America Special Papers, 434; 207-232 doi:10.1130/2007.2434 (10).

Fowler, A., and Osman, A. F., 2009. The Sha'it-Nugrus shear zone separating Central and South Eastern Deserts, Egypt: A post-arc collision low-angle normal ductile shear zone: Journal of African Earth Sciences, 53, 16-32.

Fritz, H., Dallmeyer, D. R., Wallbrecher, E., Loizenbauer, J., Hoinkes, G., Neumayr, P. and Khudeir, A. A., 2002. Neoproterozoic tectonothermal evolution of the Central Eastern Desert, Egypt: a slow velocity tectonic process of core complex exhumation: Journal of African Earth Sciences, 34, 137-155.

Genna, A., Nehlig, P., Le Goff, E., Guerrot, C., and Shanti, M., 2002. Proterozoic tectonism of the Arabian Shield: Precambrian Research, 117, 21-40.

Green, N., and Usdansky, S., 1986. Ternary-feldspar mixing relations and thermobarometry: American Mineralogist, 71, 1109-1117.

Hodges, K., and Crowley, P., 1985. Error estimation and empirical geothermobarometry for pelitic systems: American Mineralogist, 70, 702-709.

Holland, T., and Bundy, J., 1994. Non-ideal interactions in calcic amphiboles and their bearing on amphibole-plagioclase thermometry: Contributions to Mineralogy and Petrology, 116, 433-447.

Huet, B., Le Pourhiet, L., Labrousse, L., Burov, E., and Jolivet, L., 2010. Post-orogenic extension and metamorphic core complexes in a heterogeneous crust: the role of crustal layering inherited from collision, Application to the Cyclades (Aegean domain): Geophysical Journal International, V. 184, Issue 2, pages 611-625.

Johnson, P.R., Kattan, F.H., and Al-Saleh, A.M., 2004. Neoproterozoic ophiolites in the Arabian Shield: Field relations and structure: In Kusky, T. M. Precambrian Ophiolites and related rocks. Developments in Precambrian Geology, V. 13 (K. C. Condie, Series Editor), Elsevier.

Johnson, M. and Rutherford, M., 1989. Experimental calibration of the aluminum-in-hornblende geobarometer with application to Long Valley caldera (California) volcanic rocks: Geology, 17, 837-841.

Johnson, P. R., and Woldehaimanot, B., 2003. Development of the Arabian -Nubian Shield: Perspectives on accretion and deformation in the northern East African Orogen and the assembly of Gondwana: Geology Society London. Special Publication 206, 289-325.

Johnson, P. R., Andresen, A., Collins, A. S., Fowler, A. R., Fritz, H., Ghebreab, W., Kusky, T., and Stern, R. J., 2011. Late Cryogenian-Ediacaran history of the Arabian-Nubian Shield: A review of depositional, plutonic, structural, and tectonic events in the losing stages of the northern East African Orogen: Journal of African Earth Sciences, V. 61, p. 167–232.

Jolivet, L., Beyssac, O., Goffé, B., Avigad, D., Lepvrier, C., Maluski, H. and Thang, T. T., 2001. Oligo-Miocene midcrustal subhorizontal shear zone in Indochina. Tectonics, V. 20, NO.1, pages 46-57.

Jolivet L., Famin V., Mehl C., Parra T., Aubourg C., Hébert R. and Philippot P., 2004b. Progressive strain localisation, boudinage and extensional metamorphic complexes, the Aegean Sea case: in D.L. Whitney, C. Teyssier, 203 and C. S. Siddoway, Gneiss Domes in Orogeny, GSA Special Papers, 380, pp. 185–210.

Jolivet, L., Lecomte, L., Huet, B., Denèle, Y., Lacombe, O., Labrousse, L., Le Pourhiet, L. and Mehl, C., 2010. The North Cycladic Detachment System. Earth and Planetary Science Letters, 289, 87-104, doi: 10.1016/j.epsl.2009.10.032.

Kennedy, A., Johnson, P. R., and Kattan, F.H., 2009. SHRIMP geochronology in the northern Arabian Shield: part III data acquisition, 2006, Saudi Geological Survey Open File Report, Jeddah.

Le Pourhiet, L., Huet, B., May, D. A., Labrousse, L., and Jolivet, L., 2012. Kinematic interpretation of the 3D shapes of metamorphic core complexes. Geochemistry, Geophysics, Geosystems, 13, 9 1-17, Doi: 10.1029/2012GC004271.

Lister, G. S., Banga, G., and Feenstra, A., 1984. Metamorphic core complexes of Cordilleran type in the Cyclades, Aegean Sea, Greece: Geology, 12, 221–225.

Mancini, F., Sillanpää, R., Marshall, B., and Papunen, H., 1996. Magnesian hornblende from a metamorphosed ultramafic body in southwestern Finland: crystal chemistry and petrological implications: The Canadian Mineralogist, 34, 835–844.

Passchier, C. W., and Trouw R. A. J., 2005. Microtectonics: Springer Verlag. 366 pp.

Schärer, U., and Labrousse, L., 2003. Dating the exhumation of UHP rocks and associated crustal melting in the Norwegian Caledonides: Contributions to Mineralogy and Petrology, 144, 758–770.

Stern, R.J., 1994. Arc assembly and continental collision in the Neoproterozoic East African orogen: Implications for the consolidation of Gondwana: Annu Rev of Earth and Planet Sci, V. 22, p. 319–351.

Stern, R.J., and Johnson, P., 2010. Continental lithosphere of the Arabian Plate: A geologic, petrologic, and geophysical synthesis: Earth Science Reviews, 101, 29-67.

Stipp, M., Holger, S., Heilbronner, R., and Schmid, S. F., 2002. Dynamic recrystallization of quartz: correlation between natural and experimental conditions: Geological Society London Special Publications 200: 171-190.

Tirel, C., Brun, J.-P., and Burov, E., 2008. Dynamics and structural development of metamorphic core complexes: Journal of Geophysical Research, B04403, Doi: 10.1029/2005JB003694.

Wernicke, B., 1981. Low-angle normal faults in the Basin and Range Province: Nappe tectonics in an extending orogen: Nature, 291, 645-648.

Whitney, D. L., Teyssier, C., and Heizler, M. T., 2007. Gneiss domes, metamorphic core complexes, and wrench zones: Thermal and structural evolution of the Nigde Massif, central Anatolia. Tectonics, Vol. 26, TC5002, doi: 10.1029/2006TC002040.

3. Numerical models of branching brittle and ductile shear zones

Abstract

Continental collision zones are usually associated with large-scale strike-slip shear zones. In most cases these shear zones are complex and consists of multiple branches of varying width, length, and total displacement. Here, we present 2-D numerical models to simulate the formation of such branching brittle and ductile shear localization on geological timescales for different rheological rock properties. The numerical models reproduce branching shear zone patterns starting from a relatively homogeneous initial setup and demonstrate that different kinds of strain weakening results in different types of shear zones. We show that during its evolution towards a complex brittle shear zone system, local-scale changes occur in the kinematics of the host rocks, which affect the development of the shear zones through affecting the orientation of new brittle shear localization. Our simulations show, the development of antithetic faults in a brittle shear zone system is closely linked to the decreasing of the angle of friction during the deformation. Furthermore, the characteristic of ductile shear zones to localize in a wider or in a narrow zone is strongly dependent of the reduction of the effective viscosity during the deformation. In addition, the interaction of syn- and antithetic ductile shear zones within the main shear fault results in complex shear-related structures, consistent with observations.

This chapter will be submitted:

Meyer S., Kaus B.J.P., and Passchier C. (in review). Numerical models of branching brittle and ductile shear zones. Geochemistry Geophysics Geosystems.

3.1 Introduction

Crustal scale strike-slip shear zones play an essential role in accommodating the Earth's plate tectonic displacement pattern and are locations where earthquakes occur. Crustal-scale shear zones operated in either brittle or ductile regimes predominantly depending on the depth within the crust at which they formed. Well known examples are the San Andreas, North-Anatolian and Dead Sea Faults. The San Andreas Fault is such an example for a shear zone in a brittle regime with a complex geometry of synthetic and antithetic faults, in that the weakening of the shear fault by the frictional behavior is still under debate (Scholz, 2000; Zoback, 2000; Carpenter et al., 2011). However, previous numerical models showed that the weakening behavior has a highly effect on the localization of shear zones (Huismans and Beaumont, 2003). But still it is not clear how that process controls the development of brittle shear faults in a strike-slip motion to form a complex network of shear zones, which are observed on several places on earth.

There are also numerous fossil crustal scale shear zones, mostly in Precambrian terranes, where the deeper edifice of such structures can be studied (ductile shear zones). Although detailed and quantitative studies have usually been limited to simple, straight planar shear zone segments (Passchier, 1990a, b, 1998; Grujic and Mancktelow, 1998; Piazolo et al., 2001; Schrank et al., 2008), field work shows that in most cases the straight segments form part of a complex systems of kilometers-wide anastomosing and branching shear zones (Passchier et al. 1997; Faure et al. 2005; Archanjo, 2008; Culshaw et al., 2011). Ductile shear zones differ in their characteristics in length, width, shear sense and amount of displacements. Field studies on high-temperature shear zones indicated that shear localization is often associated with a weakening processes, which can be grain size reduction, dynamic recrystallization, chemical alterations of minerals and shear heating, among others (Etheridge and Wilkie, 1979; Brun and Cobbold, 1980; Regenauer-Lieb and Yuen, 1998; Braun et al., 1999; De Bresser et al., 2001; Kaus and Podladchikov, 2006; Bürgmann and Dresen, 2008; Platt and Behr, 2011a, b, Sullivan et al., 2013; Montési, 2013). Most previous theoretical studies focused on lithospheric extensional, transform faults or on the behavior of single ductile and brittle shear zones (Mancktelow, 2002; Huismans and Beaumont; 2003; Hieronymus, 2004; Mancktelow, 2007; Choi et al., 2008; Gerya, 2010a, 2012, 2013). The research on this topic showed that the rheological properties, especially the weakening mechanism, exert an influence on the shear localizations. No work has been carried out on how individual shear zone strands interact in a strike-

slip regime, how they form a larger branching shearing system and what the effect of strain weakening is on the geometry of branching shear zones.

Here we present a 2-D forward model to study in a systematic way the influence of different rock rheological regimes on the development of complex strike-slip shear zone systems at different crustal depths.

3.2 Modeling approach (Methology)

The numerical model is based on a visco-elastic-plastic (VEP) code named MILAMIN_VEP (Kaus, 2010; Thielmann and Kaus, 2012), which solves the incompressible Stokes equations for VEP rocks in combination with the energy conservation equation (see Thielmann and Kaus (2012) for a more extensive description). For the upper crust we employ a Drucker-Prager yield criterion which is the 2-D simulation equivalent with the Mohr-Coulomb plasticity for incompressible deformation with the general equation for shear stress (τ):

$$\tau = C + \mu\, \sigma_n$$

$$\mu = \tan(\phi) \qquad (1)$$

where C is the cohesion, μ the coefficient of internal friction, σ_n the normal stress and ϕ the angle of internal friction described by Vermeer and De Borst (1984). We computed the second invariant total stress tensor (σ_{II}):

$$\sigma_{II} = \sqrt{0.5\left(\sigma_{xx}^2 + \sigma_{yy}^2 + 2\sigma_{xy}^2\right)} \qquad (2)$$

where σ_{xx}, σ_{yy} are the normal stress in x and y-direction and σ_{xy} the shear stress. Shear zones are interpreted as a weaker zone in comparison to the surrounding undeformed rock (Chéry et al. 2001; Provost and Houston, 2003; Carpenter et al., 2011). The strain-weakening in a brittle-plastic regime is controlled by frictional processes in the Mohr-Coulomb plasticity (Huismans and Beaumont, 2007). We use the friction angle and the cohesion to control the weakening of the material by ongoing deformation in our numerical models (Poliakov and Buck, 1998; Lavier et al., 2000). The relation of the friction angle and the cohesion is described by the yield stress:

$$\sigma_y = -0.5\left(\sigma_{xx} + \sigma_{yy}\right)\sin(\phi) + C\cos(\phi) \qquad (3)$$

Brittle strain localizations occur where the plastic yield stress (σ_y) is reached by the second invariant of the total stress tensor (σ_{II}):

$$\sigma_{II} > \sigma_y \tag{4}$$

$$F = \sigma_{II} - \sigma_y \tag{5}$$

where F is the yield function with the term $F \leq 0$ for brittle deformation. The initial rheological properties of the matrix are 30° for the friction angle and 35 MPa for the cohesion, which linearly weakens with increasing critical strain at stated intervals (Fig. 3.1b). This leads to weakening represented by a lower yield stress value (σ_y) (3).

The mechanical code for simulating ductile shear zones is based on a power-law rheology, which is strongly viscosity-dependent. The rheology is a Maxwell VEP system:

$$\dot{\varepsilon}_{ij} = \dot{\varepsilon}_{ij}^{\text{viscous}} + \dot{\varepsilon}_{ij}^{\text{elastic}} + \dot{\varepsilon}_{ij}^{\text{plastic}} = \frac{1}{2\eta_{\text{eff}}}\tau_{ij} + \frac{1}{2G}\frac{D\tau_{ij}}{Dt} + \dot{\lambda}\frac{\delta Q}{\delta \sigma_{ij}} \tag{6}$$

where $\dot{\varepsilon}_{ij}$ is the deviatoric strain-rate, G the elastic shear modulus, τ_{ij} the deviatoric stress, $\dot{\lambda}$ the plastic multiplier and Q the associated plastic flow potential. Natural ductile shear zones are characterized by a fine-grained matrix, where the high-strain zone regards to the P-T field lead to crystal-plastic processes and dynamic recrystallization. The reduction of the grain-size results in a weakening of the material within the shear zone in comparison to the neighbor host rock. In our numerical models we used the physical law that a decrease in effective viscosity leads to an increase of the strain-rate. η_{eff} is the effective viscosity and can be described by power-law creep:

$$\eta_{eff} = \eta_0 (e_{II}/e_0)^{1/n-1} \exp\left(k\left(\frac{1}{T_1} - \frac{1}{T_0}\right)\right) \tag{7}$$

where η_0, n are the specified material viscosity at the initial stage for T_0 (Tab. A1) and the stress exponent. e_{II} is the second invariant of shear strain rate, e_0 a reference strain-rate, k is the Arrhenius type temperature dependency of viscosity, T the temperature, and T_0 a reference temperature.

We implement a factor (A) to reduce the effective viscosity from an initial value of 1 to a linked end-value related to the critical strain (Fig. 3.1c), shown by the equation:

$$\eta_{def} = A\,\eta_{eff} \tag{8}$$

3.3 Model setup

The models constructed in this study represent a horizontal large-scale piece of the crust that is 300 km in length and 150 km wide at different crustal levels, simulating brittle shear localization in the upper crust (5-12 km), and ductile shear zones in the lower crust (20-25 km) with Mohr Coulomb plasticity and viscous power-law rheology, respectively (Fig. 3.1). We implement two different rock properties in the models: a dry upper crust to simulate brittle localization, and a lower crust to simulate the ductile shear zones (Burg and Schmalholz, 2008; Tab. A1). To initiate the shear zones, we use heterogeneities that have a granitic composition (Tirel et al., 2008) and a round shape in the center of the model. The effect of the shape, the size and the number of initial heterogeneities on the results will be discussed in section 4.1.1.

The boundary conditions for the velocities are as follows (Fig. 3.1a): The right and left boundaries are periodic, the bottom is fixed in the reference frame and the top boundary has a prescribed horizontal velocity such that the overall strain-rate ($\dot{\varepsilon}_{BG}$) is constant throughout the simulation. This generates a dextral shear flow (simple shear), where the maximum compressive stress is oriented with an angle of 40 - 45° to the imposed shear direction (Fig. 3.1a) and lies parallel to the plane of the model. The model represents a horizontal segment of the crust with a uniform temperature, and a total lithostatic pressure that is added to the dynamic pressure of the model. The boundary condition for the temperature consists of heat flow through the sides (periodic boundary), while the top and bottom are isothermal. The heat source is given by the initial temperature and during the simulation by shear heating (T_s), which transforms the elastic and plastic deformation into thermal energy,

$$T_s = \chi\, \tau_{ij}(\dot{\varepsilon}_{ij}^{viscous} + \dot{\varepsilon}_{ij}^{plastic}) \qquad (9)$$

where τ_{ij} is the deviatoric stress, χ the efficiency of shear heating and $\dot{\varepsilon}_{ij}$ the deviatoric strain-rate. In all model runs we used $\chi = 1$ as a standard. Shear heating is present in all brittle and ductile shear zone simulations as an additional weakening parameter. We employed a lower and upper viscosity cutoff of 10^{18} and 10^{26} Pa s to avoid numerical instabilities. The numerical Lagrangian mesh consists of about 1.4 million quadrilateral finite elements with linear shape functions for velocity, temperature and discontinuous linear function for pressure (checkerboard pressure field, Q1-P0). During the simulation periodic remeshing is applied if elements are too distorted and we use particles to track material properties and stresses.

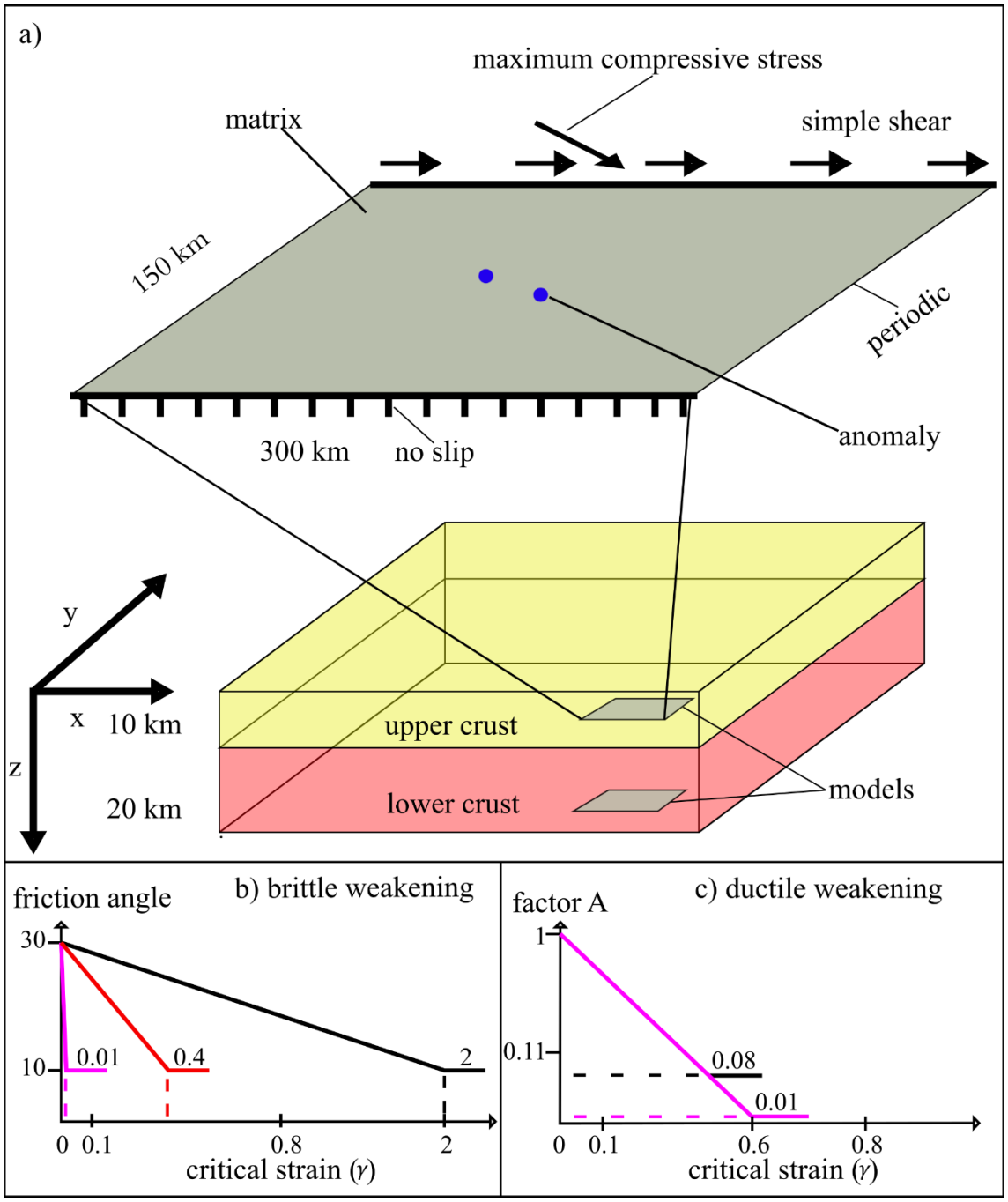

Figure 3.1 a) Setup of the large-scale models for different crustal levels, simulated by a bulk simple shear; b) brittle weakening; friction angle and cohesion decrease with progressive critical strain (γ), start value of friction angle is 30 °. The cohesion decreases by 35 MPa to 1 MPa; c) ductile weakening, the viscosity decreases with progressive strain by a factor A with a start value of 1.

In the following model runs we will change the rheological parameters in equations (4-8) to understand how these values affect the localization of brittle / ductile shear zones, and if the parameters have an influence on the geometry of complex branching strike-slip shear zones.

3.4 Results

3.4.1 Brittle strain localization

For sufficiently large stresses, the upper crust is brittle which can be described by Mohr-Coulomb plasticity. In the first simulation (reference model) we use standard rock properties (Tab. A1) for the upper crust, to show in different time-span the development of brittle shear zones. We employ an overall strain-rate of $10^{-14}\mathrm{s}^{-1}$ with a lithostatic pressure of 264.9 MPa and 300 °C, which represent the pressure-temperature conditions for a horizontal model in the upper crust (10 km depth). Furthermore we implemented two anomalies in the center of the matrix and we used a specified material viscosity of 1.2768×10^{21} Pa s for the upper crust (Burg and Schmalholz, 2008) and 7.4893×10^{20} Pa s for granite in the intrusion used to nucleate the shear zones (Tirel et al., 2008).

The top of the model moves to the right, where the maximum compressive stress is oriented to an angle of 40-45° to the imposed shear direction (dextral shear sense, Fig. 3.1a). In all simulations (we performed more than ~100 in total) the first brittle shear zones grow at an angle of 5-8° to the imposed shear direction with a dextral shear sense (Fig. 3.2a). The main faults (R - faults) spread to the sides of the model and join at the center at 0.11 Ma (Fig. 3.2b), which leads to a complex geometry of the branches in the form of a “bridge structure”. The term “branch” is used for an active shear zone, which is connected by joining or splitting with a further shear localization. In a later stage, two new shear zones develop that have a different shear sense (Fig. 3.2c), namely one set of synthetic faults with an orientation of 166-168° (P - faults) and a second set of antithetic faults at 20-75° to the imposed shear direction (R’ - faults). The shear zones in our simulation have orientations that are typical for Riedel structures, described by Cloos (1928) and Riedel (1929), with the exception of the R’-faults which have a larger variation in orientation. In the early model stages, the R’-faults grew at an angle between 40-50°. After 13% strain, new R’-faults developed at a higher angle (between 70-75°) to the applied shear direction (Fig. 3.2c).

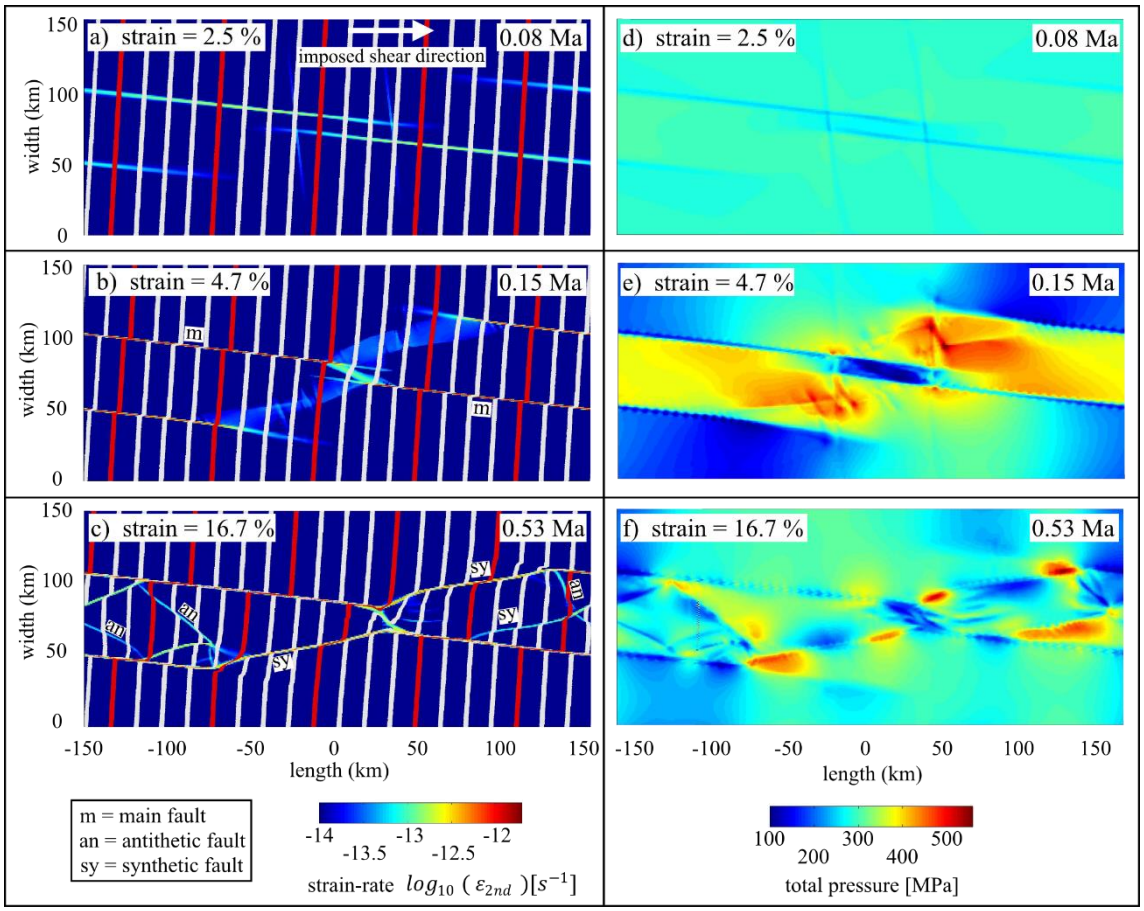

Figure 3.2 Model development for a case with reference parameters in the brittle regime (Tab. A1) and two anomalies in the center with an overall strain-rate of $\dot{\varepsilon}_0 = 10^{-14}\ s^{-1}$, showing; a) The development of the main faults in the strain rate field; b) The interaction of the main faults and weak growth of synthetic faults; c) The development of a complex shear zone system with anti- /synthetic faults; d-f) Shows the evolution of the total pressure [in MPa] at the same time steps. In a-c, vertical white and red lines are originally vertical passive strain markers that show deformation in the model

The simulation of shear zones in the model is based on a pressure dependent brittle-plastic regime, therefore we plotted the pressure distribution including the lithostatic pressure during the run. During early stages, the shear zones exhibit a decrease of pressure relative to the surrounded matrix, which is a feature of shear bands in a pressure-dependent rheology (Mohr-Coulomb plasticity, Fig. 3.2d-e, Mancktelow, 2006). The center of the model is dominated by a low-pressure zone attributable to the anomaly at the starting-point of the model. The higher position of the left anomaly, and therefore the higher position of the initiated shear zone on the left side of the model, related to the dextral shear movement initiate a new shear band in an extensional setting. The increasing number of variously-oriented shear branches (relative to the imposed shear direction) results in a more complex geometry and simultaneously to a further change in the pressure distribution in a later stage. The gentle bending trend of the newly developed syn- and antithetic

faults shows high-pressure zones with a difference of 400 MPa to the low-pressure zones along the straight part of the shear branches (Fig. 3.2f). A further observation is that the shear zone branches, which connect to the opposite side of the imposed shearing, show a high pressure zone of the material between the shear branches (junction zone). In summary, the results show that the more complex geometry of shear branches subsequently affects the nucleation of the newly-initiated shear zones (e.g. R'-faults) and the pressure distribution of the rocks.

3.4.1.1 Influence of heterogeneities and material properties on shear localization

In a homogeneous model with identical rock parameters and rheology, no brittle localization occurs. For the previous simulation, we used values of $\eta_0 = 1.28 \times 10^{21}$ Pa s for the matrix (upper crust, Burg and Schmalholz, 2008) and $\eta_0 = 7.49 \times 10^{20}$ Pa s for the anomaly, which is a typical value for granite (Tirel et al., 2008). How heterogeneous does the material of the anomaly have to be in comparison to the matrix in order to localize brittle shear zones? It is therefore interesting to test the effect of various model parameters on shear zone development. We ran several numerical models that employ different viscosities, friction angles and cohesion of the anomaly to simulate brittle shear zones under different rock properties or rock types. Simulations in which we reduced the specified material viscosity difference between matrix and anomaly suggest that even a small difference of > 0.1 % leads to shear localization. Furthermore, we performed 10 model runs with the identical rock parameters for the anomaly and the matrix but with a variation in the strain weakening. The results show, that a tiny difference in the friction angle (> 1°) between the matrix and the anomaly leads to heterogeneous behavior and initiate a shear zone nucleation. In comparison to the previous runs, the localized main faults show no connection by R'-faults and P-faults, whereas the shear zones stayed at the final stage parallel and isolated (similar to Fig. 3.2a). In the previous simulations, we used anomalies as an appropriate method to simulate heterogeneous conditions, within an otherwise homogeneous matrix. Supplying the models with a different anomaly shape showed that this does not play a significant role in the development of brittle shear zones. The variation of the size of the anomaly indicate a similar result to the previous observation except that the anomaly exhibits enough particles to form a rheological contrast to the surrounded matrix. Therefore we decided to use a standard round shape with a size of 100 meter radius, which represents a rheological variation of the material in the case of a granite

intrusion. The position of the anomaly determined the nucleation site of shear localization. In models with only one anomaly a single shear zone occurs, whereas the periodic boundary conditions lead to further heterogeneous influences which eventually a more complex network of R, R' and P-faults (Fig. 3.3a). The models with two anomalies can have two different configurations. In the case of an upper position of the left anomaly in comparison to the right anomaly by a dextral shear sense, the new shear branch grows with an extensional component in the center of the model (Fig. 3.2a-c).

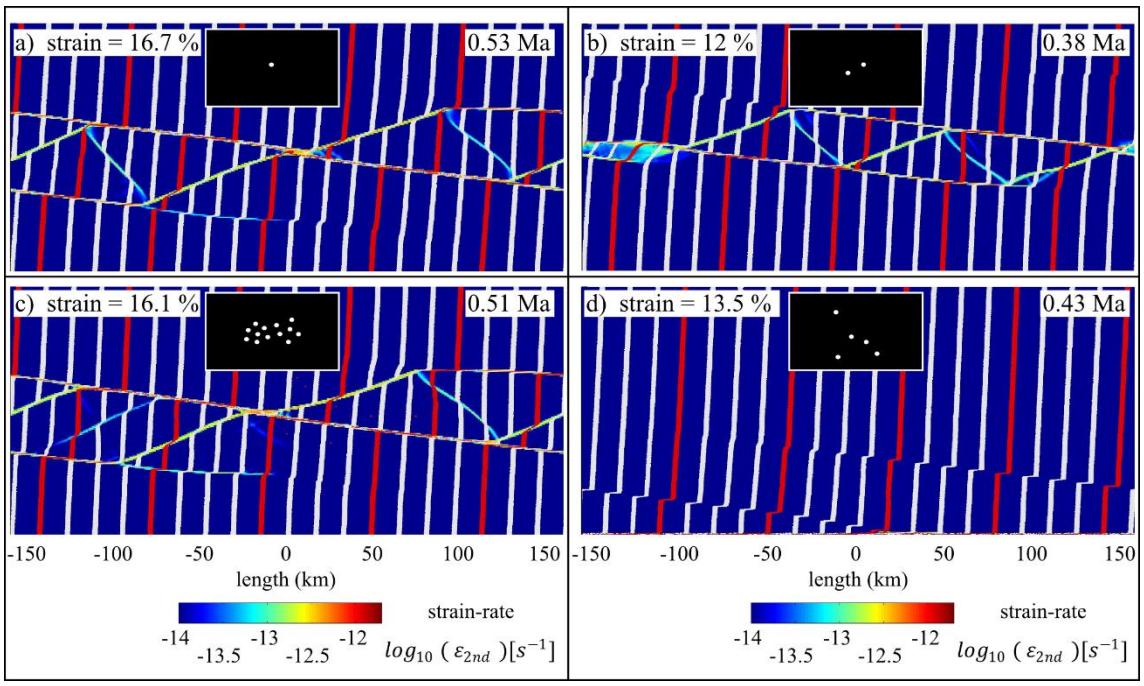

Figure 3.3 Setup with different numbers of anomalies under a constant overall strain-rate of $\dot{\varepsilon}_0 = 10^{-14}\ s^{-1}$ and with reference rock properties (Tab. A1); a) One anomaly; b) Two anomalies; c) More than 12 anomalies; d) Boundary effect –starting-point of the anomaly is very close to the lower boundary

The opposite starting position simulates a fault in a compressional setting, which indicates similar orientations of R, R' and P-faults (Fig. 3.3b).The runs with more than two anomalies show that only one dominant shear zone was formed (Fig. 3.3c). Shear localization affects the surrounding matrix as well, and if the anomalies are close together, one shear zone develops and the neighboring point remains inactive. In further tests, we initiated shear zones close to the boundaries. Based on the boundary effect at the top and bottom of the model, the shear zones close to both of these boundaries were strongly active and disturbed the shear localization within the model (Fig. 3.3d). Therefore it is important to have anomalies that are sufficiently far from the top / bottom boundary in order to avoid

the boundary effect. We conclude that the number of anomalies does not play an important role in the geometry of the shear branches network. We therefore use two anomalies to control the initial localization and to form a complex network of brittle shear zones to understand the rheological effects on these geometries.

3.4.1.2 Effect of crustal depth on shear zone patterns

Shear zones can be formed in different crustal depths, and with increasing depth, the rheology of the material changes due to increasing temperature and pressure. Such fault zones can form crustal-scale structures which pass through the ductile as well as the brittle regime of the crust. Our following numerical models show the influence of different pressure-temperature conditions on the development of brittle shear zones. The three dimensional effect of a continuous shear zone through the crust cannot be simulated in our 2-D models. We ran a total of 25 numerical models with reference properties (Tab. A1) to regulate the overall strain-rate ($\dot{\varepsilon_0}$), pressure (P) and temperature (T). We varied the depth of the models from 2 to 14 km in 2 km steps under a constant overall strain-rate of $\dot{\varepsilon_o} = 10^{-14}\ s^{-1}$ (Tab. A1). The temperature change with depth is based on a geotherm of T≈273 K+ (25z), where z is the depth in km. The results show that variations in pressure do not have a significant effect on the geometry of shear localization. Increasing the temperature over 330° C, which simulates a depth of 12-14 km, led to a viscous behavior of the material and no shear localization occurs. Increasing the lithostatic pressure to a value comparable to the depth of a lower crust (>14 km depth) with a temperature of 330 °C, showed no localizations of brittle shear zones. In a system of constant overall strain-rate, the shear stress is proportional to the effective viscosity (7, 10).

$$\sigma_{xy} = 2\,\mu_{\text{eff}} * \dot{\varepsilon}_{BG} \qquad (10)$$

An increase of temperature reduces the effective viscosity and the shear stress (σ_{xy}) until it is less than the yield stress (σ_y), which occurs when the temperature exceeds 330° C in our model. An increase in overall strain-rate results in shear localization even at temperatures over 330°C, consistent with the fact that according to eq. 10, this results in larger shear stresses. The reference models have no shear localization if $\dot{\varepsilon}_o = \leq 10^{-15} s^{-1}$. At a higher value of overall strain-rate $\dot{\varepsilon}_o = \geq 10^{-15} s^{-1}$, the shear geometry is similar to those in the previous models but with a significant increase in the numbers of shear branches. To summarize, the models show that the variation of the lithostatic pressure have no influence on the development of brittle shear zones, whereas the temperature has an indirect effect of the shear localization. Furthermore we confirm with our models that

the brittle-ductile transition zone depends on many factors including rheology, temperature and strain-rate (Sibson, 1980; Hobbs et al., 1986; Handy et al., 2007).

3.4.1.3 Effect of initial viscosity on rheology

In the previous simulations, we used the rock properties of the upper crust (Burg and Schmalholz, 2008) for the matrix with a stress exponent (n) of 3.3, a viscosity (η) of $1.28 * 10^{21}$ and a reference strain-rate of $e_0 = 10^{-15} s^{-1}$ (eq. 7). To simulate a brittle fracture, we used the Mohr Coulomb yield plasticity (eq. 3) in relation to the elasto-visco behavior. This implies that the localization of a brittle shear zone in the code is determined by a reduction of the effective viscosity (eq. 7). The results of section 3.4.1.2 describe the effect of effective viscosity on shear localization.

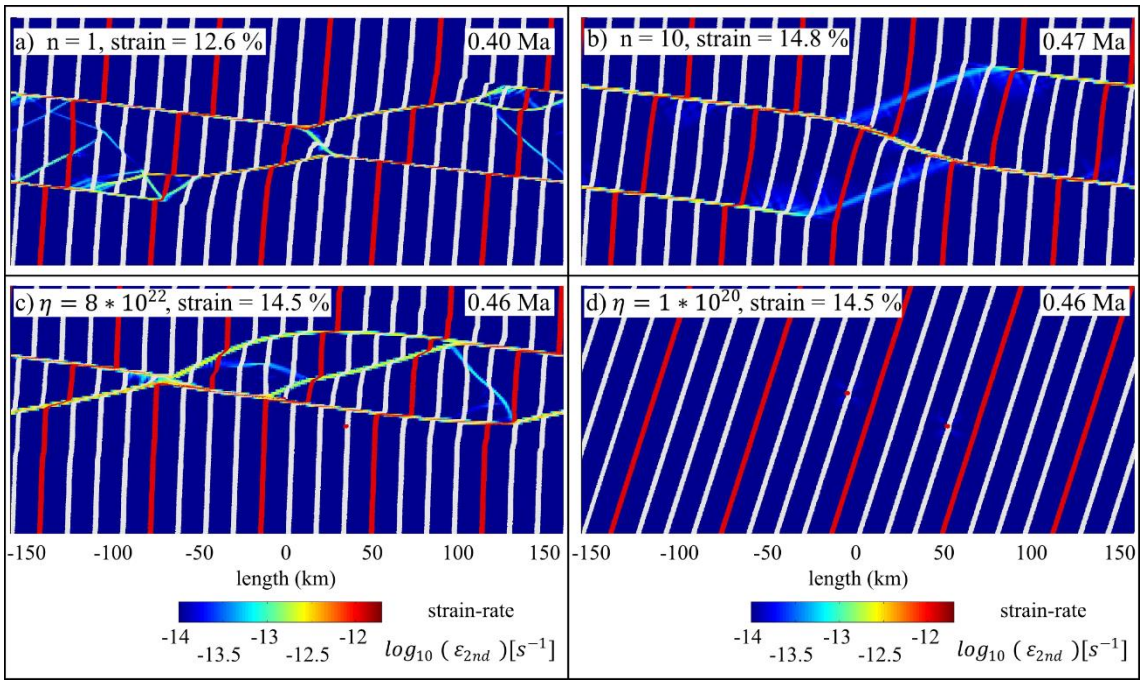

Figure 3.4 Effect of rheological parameters with a constant overall strain-rate on the geometry of shear zones in the models; a-b) Effect of increasing the stress exponent (n); c) Increasing the viscosity, similar shear localization; d) decreasing the viscosity, no shear localization – viscous behavior

We performed 6 additional simulations in which we varied the initial matrix viscosity from $10^{19} - 10^{23}$ Pa s. The resulting deformation geometries indicate that an initial viscosity lower than 10^{20} Pa s leads to a viscous model behavior with no shear localization, whereas viscosities between $10^{21} - 10^{22}$ Pa s show a similar geometry with main, synthetic and antithetic faults. The main faults have a stronger activity with an increase in

viscosity, and simultaneously, the synthetic and antithetic faults have lower strain rates, resulting in a simpler geometry (Fig. 3.4c-d).

3.4.1.4 Effect of strain softening

With ongoing deformation, grain-size reduction through damage results in a weaker behavior of the cataclastic zones. Previous studies have indicated the importance of strain softening on plate tectonics (Gueydan et al., 2014), which includes cohesion loss (Buck, 1993), frictional strength reduction (Bos and Spiers, 2002) and fluid pressure variations (Sibson, 1990; Chester, 1993; Rice 1992; Faulkner and Rutter, 2001; Carpenter et al., 2011). Strain softening can be simulated in a strain-rate (Behn et al., 2002) or strain dependent weakening (Huismans and Beaumont, 2003), while the former represents the fault weakness on a seismic timescale, the latter does so on a geological timescale. Previous studies on lithospheric extensional and on transform fault models showed that strain softening has a strong effect on the development of shear zones (Lavier et al., 2000; Huismans and Beaumont, 2003; Hieronymus, 2004; Choi et al., 2008; Gerya, 2010a, 2012, 2013; Alken et al., 2011, 2012). In contrast to the previous studies, our numerical models represent a horizontal profile within the crust with a constant lithostatic pressure. We simulated shear zones in a strike-slip motion with a focus to understanding the influence of the strain-softening on the development of complex network of shear zones. A further point is the interaction of the branched shear zones in relation to the weakening behavior of the material. Therefore we tested the effects of a decrease of the friction angle and cohesion in relation to variation of the critical strain (γ) on the geometry of branching shear zones. We focused the first models on the friction angle and the cohesion with a constant critical strain of 0.6 under reference properties (Tab. A1). The results of the decrease in cohesion from an initial value of 35 MPa can be subdivided into three groups: (1) localization of parallel main faults for a reduction of the cohesion to $\geq$ 20 MPa, (2) joining of the main faults for a value of $4 < C < 20$ MPa and (3) localization of weak synthetic faults together with the main faults for a cohesion $\leq$ 3 MPa (Fig. 3.5a, b). The next set of models focused on the friction angle, while cohesion was kept constant, with a critical strain of 0.6. An initial value of $\phi = 30°$ is a close approximation for a dry upper crust and the Beyerlee's law. We ran 15 models, in which we decreased the initial value friction angle of 30° down to a value of 10°. The results indicate shear localization of main faults accompanied by synthetic faults for a friction angle of $12° < \phi < 30°$. Antithetic faults developed only if the friction angle is reduced to $\leq$ 12° (Fig. 3.5c, d).

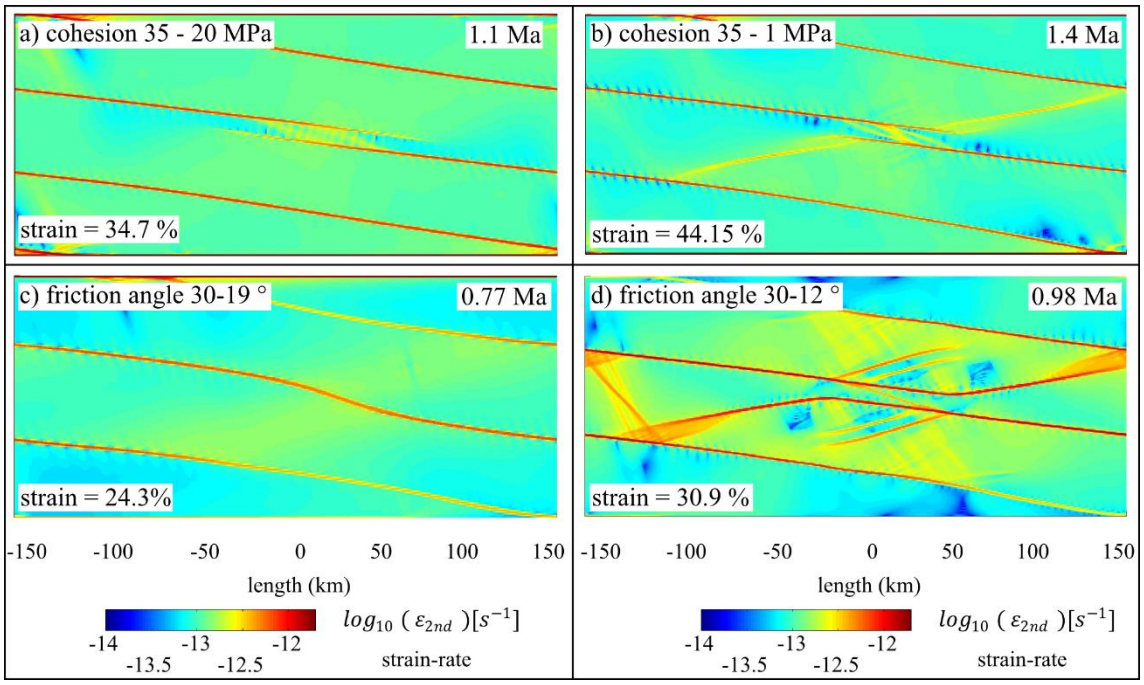

Figure 3.5 Effect of strain weakening on shear zone geometry; a-b) Effect of decreasing the friction angle by various amounts with ongoing critical strain; c-d) Effect of a decrease in the cohesion

Next, we varied the critical strain to simulate different softening behavior of the material. We employed models with a simultaneous reduction of the friction angle (ϕ) by 30° to 10° and cohesion (C) by 35 MPa to 1 MPa, the reduction of the yield stress σ_y led to a weaker behavior of the material. In the first models, we used a critical strain of 0.01, which results in a very rapid weakening of the matrix. The weak rheological behavior of the material leads to a high number of brittle shear localizations in a short amount of time, which formed a complex system of main, syn- and antithetic faults. Furthermore the synthetic faults show a stronger variation in the displacement along the branches and a more bending trend (Fig. 3.6a). By increasing the critical strain to 0.6, the geometry of shear zones is more compact and has a stronger concentration of strain on a smaller number of shear zones. The main faults are characterized by a thinner zone of localization in comparison to the soft models (Fig. 3.6b). The connection of shear branches formed by simultaneously active antithetic and synthetic faults over a longer period of time. In the following models, we employed a critical strain ≥ 2, which resulted in main faults that were active for a longer period of time and in synthetic faults with weak antithetic shear zones. To clarify the difference in shear zone geometry, we computed the proportion of synthetic and antithetic faults in the models. In order to do this in a controlled manner, we defined

a “shear zone”, as any zone where the strain-rate is at least twice the overall strain-rate, while the vorticity characterized the shear sense of the shear zone.

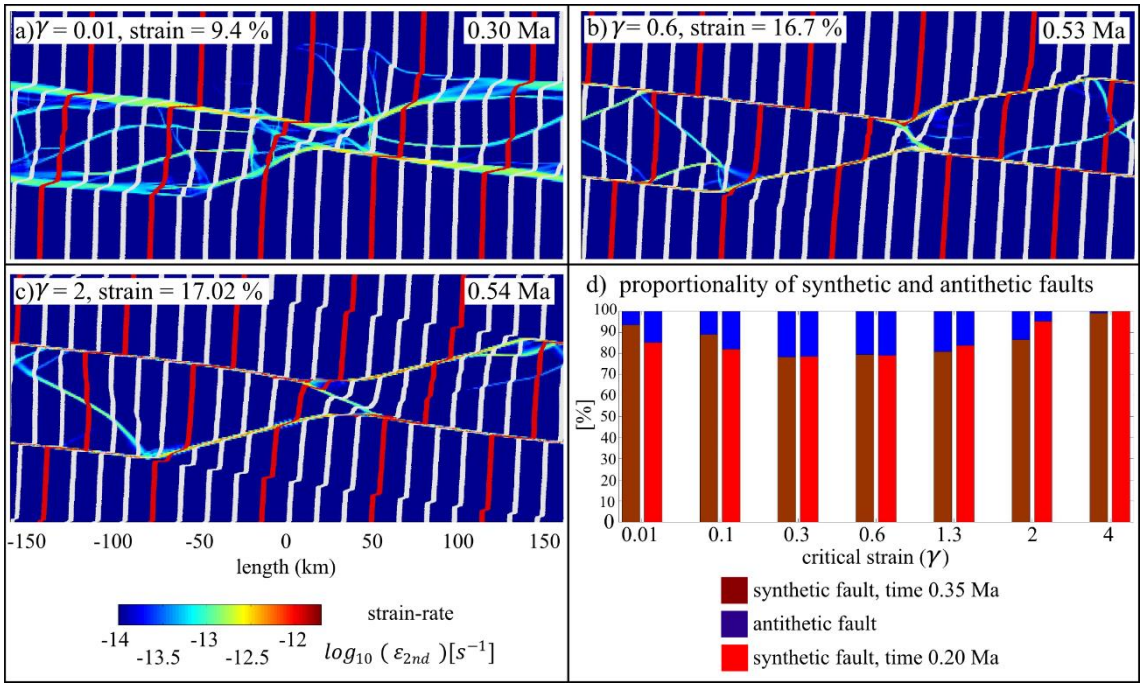

Figure 3.6 Weakening controlled by the reduction of friction angle and cohesion with ongoing strain. In all models the friction angle and the cohesion is decreased from 30 to 10° and 35 to 1 MPa under different critical strain; a) Rapid strain weakening with γ = 0.01; b) Intermediate conditions with γ = 0.6; c) Slow weakening with γ = 2, d) Activity of syn- and antithetic faults under different critical strain

The results after 0.35 Ma show a maximum proportion of antithetic faults with a critical strain between 0.3 - 0.6, where 22% of the shear zones have a sinistral shear sense (antithetic faults). A higher or lower value of the critical strain shows a reduction of the proportion of antithetic faults (Fig. 3.6d). During the analysis we observed a variation in the activity (strain-rate) of the shear zones; the interaction of the shear branches affects the surrounding shear localization and leads to a change in activity. The proportionality of the faults at an early stage (0.20 Ma) of development indicates a change of the percentage-amount of antithetic faults in comparison to a later stage. The activity of the antithetic faults is relatively high at a low critical strain, and increases for a higher critical strain. The maximum proportionality of antithetic faults occurs at a critical strain of 0.3 - 0.6. The models with a critical strain of 0.01 - 0.1 exhibit a trend of a higher activity of antithetic faults during early stages of the simulation, and a reduction with increasing strain (Fig. 3.6d).

Summarizing, the implementation of strain-weakening in the models showed that the complexity of brittle branching shear zones patterns is more dependent on the friction angle than on the cohesion and that antithetic faults occur with a friction angle lower than 12°. Furthermore computing the proportionality of the faults indicated that the rate of decrease of the frictional strength strongly influences the activity of antithetic faults.

3.4.2 Ductile shear zone localization

Our simulations of ductile shear zones differ from previous simulations in crustal profile depth, deformation mechanics and rock properties. We employed as a matrix the properties for a lower crust (Burg and Schmalholz, 2008) with a viscosity of $\eta_0 = 3.0484 * 10^{21}$Pa s, a stress exponent of n = 3 and for the anomaly a granite rock type with the viscosity of $\eta_0 = 7.4893 * 10^{20}$ Pa s (Tirel et al., 2008) with a stress exponent of n = 3.2. The models were performed at a depth of 20 km in the lower crust with a lithostatic pressure of 530 MPa, a temperature of 500° C and an overall strain-rate ($\dot{\varepsilon}_0$) of $10^{-14}\ s^{-1}$. Strain weakening is initiated by reducing the initial viscosity by a factor of 1 to 0.01, over a strain (γ) of 0.6 (Fig. 3.1c) in a power-law rheology. The positions of the anomalies are similar to the setup of the previous brittle runs (Fig. 3.1a, 2).

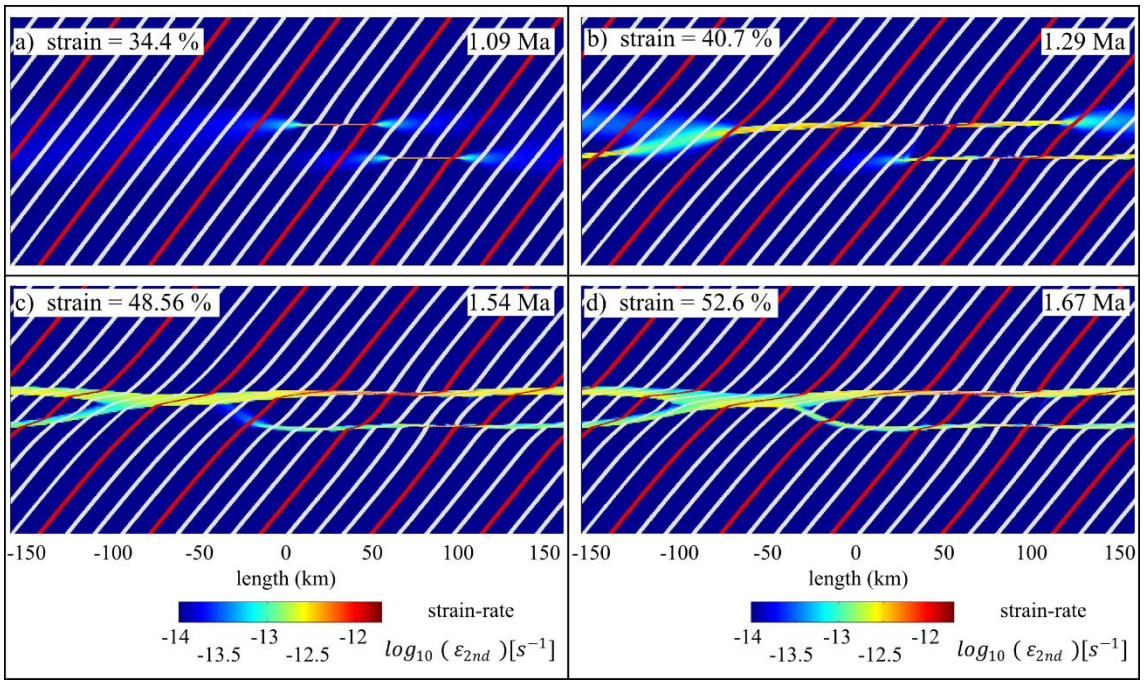

Figure 3.7 a-d) Evolution in different time-steps of ductile shear localizations, constant strain-rate

The first ductile shear zone develops at a strain of 34.4 % after 1.09 Ma along the two anomalies in the center of the model. The shear zones are first oriented parallel to the imposed shear direction in a narrow zone and fan out towards at their termination (Fig. 7a). After 1.29 and 1.54 Ma, the tip of the main shear zone changes its orientation by 25° to join the upper shear branch (Fig. 3.7b-d). In the zone of interaction, the shear zones widen considerably. In general, the shear branches vary in shear zone thickness. The main faults feature a dextral shear sense with some minor sinistral shear zones at 115° to the imposed shear direction. The shear branches differ in their displacement, and the interaction of the lower branch with the upper shear localization led to a decrease in the activity of the lower shear branch. Every branch remained active over the duration of the simulation.

3.4.2.1 Effect of heterogeneous material (number of anomalies)

The presence of heterogeneities is important in the development of localized ductile shear zones, and as in the brittle simulations, a small variation in viscosity or in the weakening parameters is sufficient to produce localized shear zones along the boundary of the anomaly and matrix. Simulations with only one anomaly led to a single shear zone parallel to the imposed shear directions with a uniform shear sense (Fig. 3.8a).

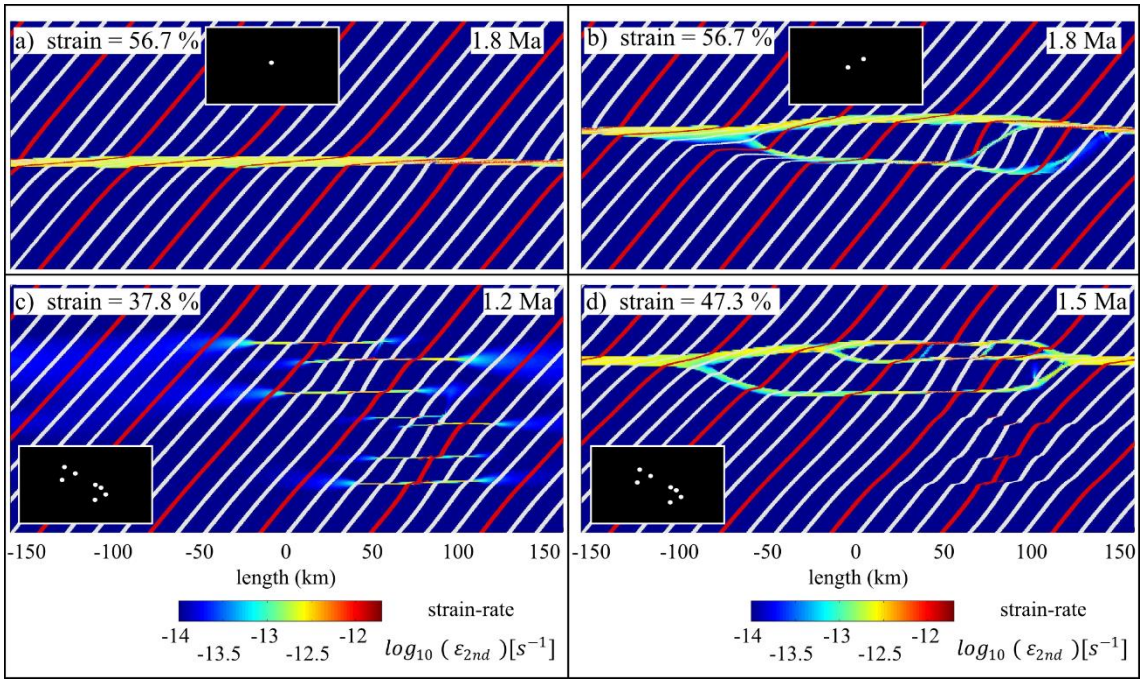

Figure 3.8 Shear localization under a constant overall strain-rate for different number of initial anomalies; a) One anomaly; b) Two anomalies with a different starting position and in which the left anomaly has a lower position; c-d) More than 6 anomalies after a time-step of 1.2 and 1.5 Ma

In subsequent simulations, we implemented two anomalies in the center and varied the vertical positions of the left anomaly to simulate extensional and compression conditions for the interaction of the shear branches. The results show that the model with a lower position of the left anomaly (compression setting) leads to new branches of synthetic shear zones with an angle between 125° to 140° and 35° to the bulk shear direction (Fig. 3.8b). The combination of a dextral shear sense together with the orientation of 125° of the side shear branches increases the local differential stress by compression and leads to new shear zone localizations. In comparison to the previous cases (Fig. 3.7d) with a lower position of the anomaly, the shear zone is more stable. In a subsequent simulation, we employed more than 7 anomalies in the model and the results initially showed a simultaneous activity of all shear zones (Fig. 3.8c). After 1.26 Ma the activity of the shear zones changed, and the upper shear branches became the dominant structures and formed a system of branching shear zones (Fig. 3.8d). In comparison to previous simulations, the shear zones are parallel to the imposed shear direction and are connected at angles of 25-30° and 135°. The geometry of the ductile shear zone branches are similar to the results of simulations with two anomalies, it differs only in the number of branches. We decided to use two anomalies during the following simulations, consistent with the earlier brittle simulations.

3.4.2.2 Internal and External influence of material behavior

The numerical modeling of ductile shear zones based on power-law rheology, as a consequences the shear localization are zones of a reduced effective viscosity. In terms of the eq. 10, the stress exponent and the initial viscosity are variables of the effective viscosity. We were interested in the influences of these parameters on the development of ductile shear zones. In general rock types differ in their initial viscosity (μ_0) and stress exponent (n), for the models we used the reference setup (Tab. A1) with an overall strain-rate of $10^{-14}\mathrm{s}^{-1}$ and a constant value for the anomaly (granite; Tirel et al., 2008) with a viscosity of $\eta_0 = 3.0484 \times 10^{21}$ Pa s and a stress exponent of n = 3.2. In the following simulations, we changed the stress exponent, and in subsequent model the initial viscosity of the matrix. The stress exponent describes the creep law of the deformation. A linear viscous material (Newtonian) has a stress exponent of n = 1, for a fine-grained material the grain boundary sliding can be controlled by diffusion (n = 1) or by dislocations (n = 2) (Bürgmann and Dresen, 2008; Hansen et al., 2011). These deformation mechanisms are grain-size dependent. The climb-controlled dislocation creep has a stress exponent

between n = 3-6, which is a grain-size intensitive creep. Numerical studies with an exponential flow law showed that the regulation of the stress exponent to a larger value can simulate pinch-and-swell structures similar to experiments which based on power-law regimes for diffusion creep or dislocation creep (Schmalholz and Fletcher, 2011). In addition to the results of Schmalholz and Fletcher (2011) we decided to use a constant value for the grain-size and by varying the stress exponent to simulate different power-law rheological regimes. Deformation experiments on fine-grained quartz showed that a flow regime of dislocation creep leads to the development of a crystallographic preferred orientation with a grain flattening fabric of quartz, together with typical microstructures of recovery creep (Rutter and Brodie, 2004). In general the study of quartz in a plastic flow are reported with a stress exponent lower than 3 (Paterson, 1989; Paterson and Luan, 1990; Rutter and Brodie, 2004). High-strain tests on olivine showed that the main flow mechanism during the deformation is the dislocation accommodated grain-boundary sliding with a stress exponent between n = 4.1 (Hansen et al., 2012). In our numerical models we used in the previous runs a stress exponent of n = 3 for the matrix, to predict a dislocation creep as a main flow mechanism for the material of the lower crust (Burg and Schmalholz, 2008).

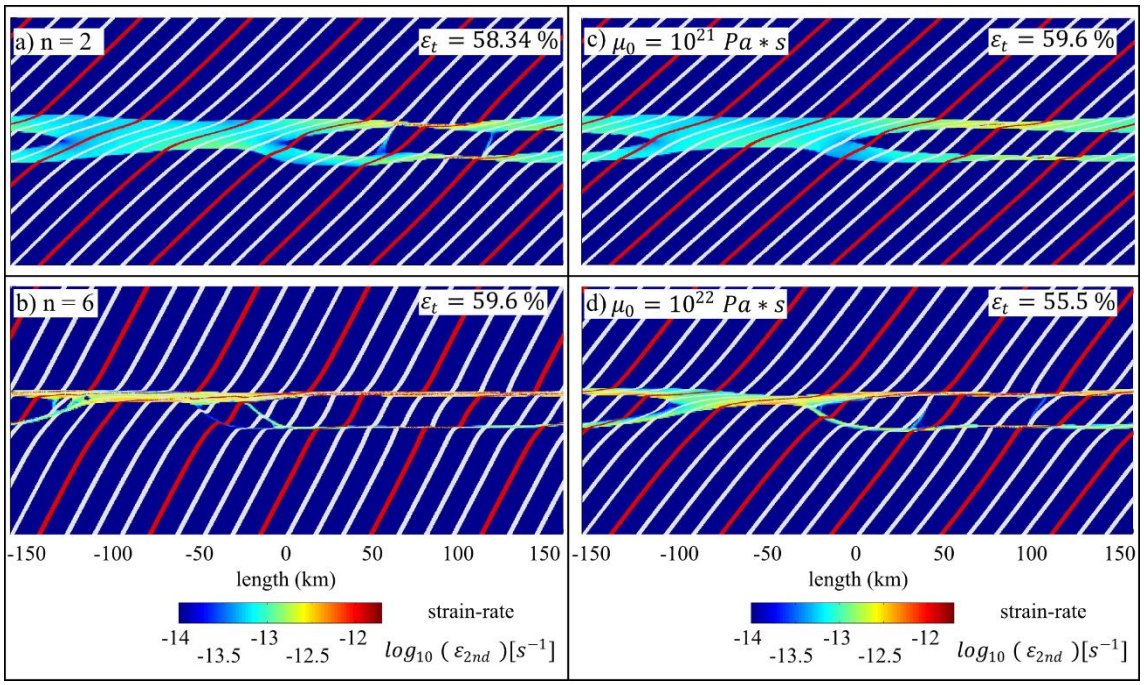

Figure 3.9 Influence of stress exponent and viscosity on the development of ductile shear zones; a-b) Variation of the stress exponent n = 2, 6 under constant overall strain-rate, time-step of ~1.8 Ma; c-d) Influence of the initial viscosity, time-step ~1.8 Ma

To understand the effect of the stress exponent on the development and on the interaction of the shear zones, we employed values of n between 1 and 10. The results showed that models with n = 1 result in weak shear localization that fans out in a narrow zone around the anomaly after 1.8 Ma. The simulation with n = 2 formed a system of two shear branches and a wide zone of the model was affected by deformation. The width of single shear branches varies between 2 and 6 km and the connected zone is more than 35 km wide (Fig. 3.9a). Models with a stress exponent between 4 and 10 differ in the width of the ductile shear localization relative to the previous runs. The upper shear localization develops into a strong active shear branch with a width of 2-6 km, whereas the lower shear localization concentrates in a narrow zone with less slip motion. After 1.2 Ma, the shear branches joined at an angle of 40-45° and 160° to the bulk shear direction (Fig. 3.9b). As a summary, for n < 3 the shear zones are wider and more regular in shape. For stress exponents n > 3, the strain is concentrated in a narrower zone, while the main shear branch has an larger amount of displacement in comparison to the models with a lower n.

As matrix viscosity has an influence on the power-law rheology (eq. 9), we varied this parameter to simulate different crustal strengths. The results show that a decrease of viscosity (η_0) results in more splays fanning outwards from the main shear zone while a wider zone is affected by deformation (Fig. 3.9c). An initial viscosity smaller than 10^{21}Pa s results in viscous flow of the model and no shear localization occurs. For initial viscosities with a value larger than 8 x 10^{22} Pa s normal shear localization occurs with a typical geometry and stronger localization along the shear branches (Fig. 3.9c, d).

Summarizing the results, our simulations show that the initial viscosity has an effect on the shear zone geometry whereby a lower viscosity leads to a weaker behavior of the material. The width of the ductile shear branches and the zone of connection is wider in comparison to the models with a higher initial viscosity.

3.4.2.3 Effect of strain weakening

Field observation showed that the rock behavior of the sheared zones is weaker in comparison to the surrounded host rock. The study of ductile shear zones indicate that high strain zones are associated with strain-softening due to grain size reduction, crystallographic preferred orientation, or metamorphic reactions (Poirier, 1980; Gueydan et al, 2003; Park et al., 2006; Platt and Behr, 2011a, b; Rennie et al., 2013). Gueydan et al., (2003, 2014) implement the two level mixing theory (Montési, 2007) in their numerical models to study the effect of a strain-weakening by a feldspar to mica reaction. Thielmann

and Kaus (2012) used shear heating to simulate a strain-softening in the lower crust to occur shear zones, whereas Jammes et al. (2015) implement a low-temperature linear strain-weakening by decreasing the cohesion. In contrast to the previous investigations, we focused our study on understanding the relation of the rate and amount of effective viscosity (strain-weakening) reduction on the characteristics of branched ductile shear zones. In order to-systematically analyze different values for the change of the effective viscosity, we used a factor described in eq. 8 (Fig. 3.1c). We perform this weakening in a linear fashion with ongoing critical strain (γ). In order to test the effect of this weakening on model outcome, we ran a total of 6 models with a constant background strain-rate of $10^{-14}s^{-1}$ and with a constant weakening for the anomaly with a critical strain of 0.1 to 1.5 and a factor that varied between 1-0.1. The initial viscosity of the matrix with 3.0484 x 10^{21}Pa s (lower crust; Burg and Schmalholz, 2008) was decreased by a factor which has the initial value of 1 to an end value between 1-0.01 with a constant critical strain of 0.6 over a time-span of 1.8 - 2 Ma (55 - 63% strain, Fig. 3.10a, b). The results showed that the weakening process during the deformation is crucial for the development of shear localizations. In the numerical models with a factor higher than 0.55 appeared no ductile shear zones appeared (Fig. 3.11).

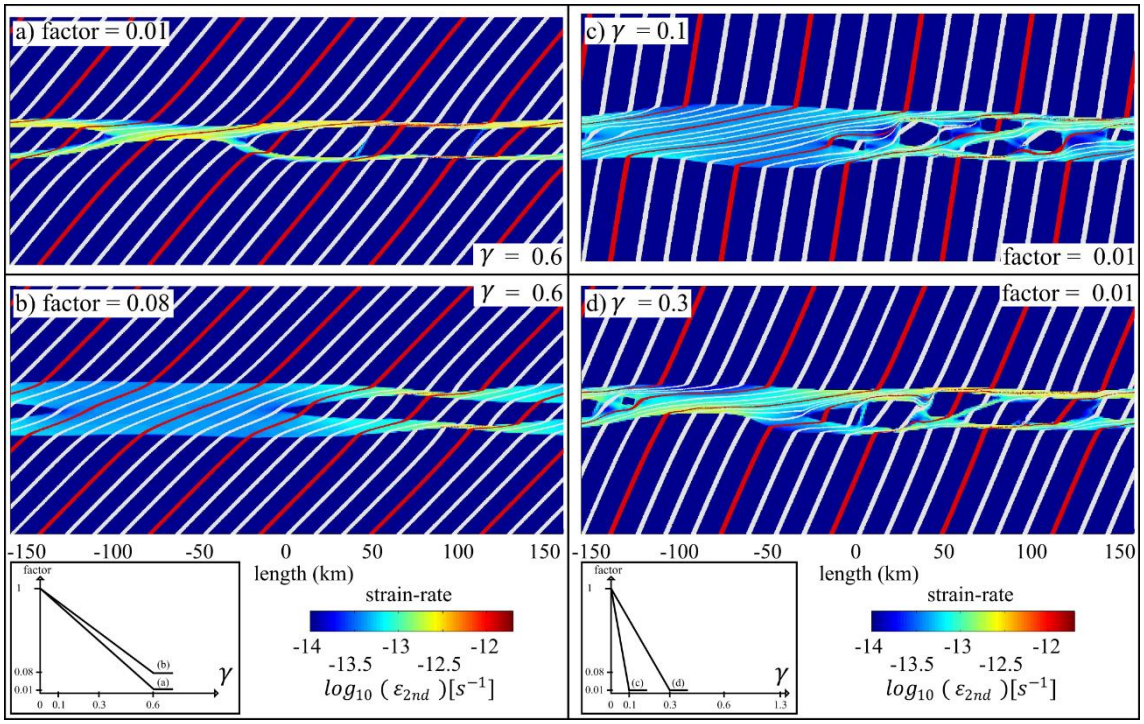

Figure 3.10 Comparison of the models with a different factor and critical strain under constant overall strain-rate of $10^{-14}s^{-1}$ for a time-step 1.8 – 2 Ma; a-b) Changing of the factor by constant critical strain 0.6; c) Critical strain γ = 0.1 with a factor 1 - 0.01; d) Increasing of the critical strain to γ = 0.3

Weak single shear zones develop when a factor between 0.55 - 0.25 was applied in addition the shear zones were active only for a small time period. The shear localization is limited to a small zone with a length of 10 - 20 km, the reason is the rapid inactivity of the shear zones. A decrease of the factor to a value between 0.25 - 0.12 leads to a more stable activity of the shear branches with the result that the shear zones form a weak connection of the shear strands. The shear zones are more intensely localized close to the anomaly and have a more disperse strain to the junction zone. With a critical value of ≤ 0.12 as a factor, the shear zone strands showed a continuous activity during the entirety of the simulations (Fig. 3.11), unlike the previous runs. The characteristics of these shear zones are that at a distance from the anomaly the strain fans out and affects a wider zone, whereas the width of the shear zone strands and the junction zone varies between 3 - 30 km (Fig. 3.10a).

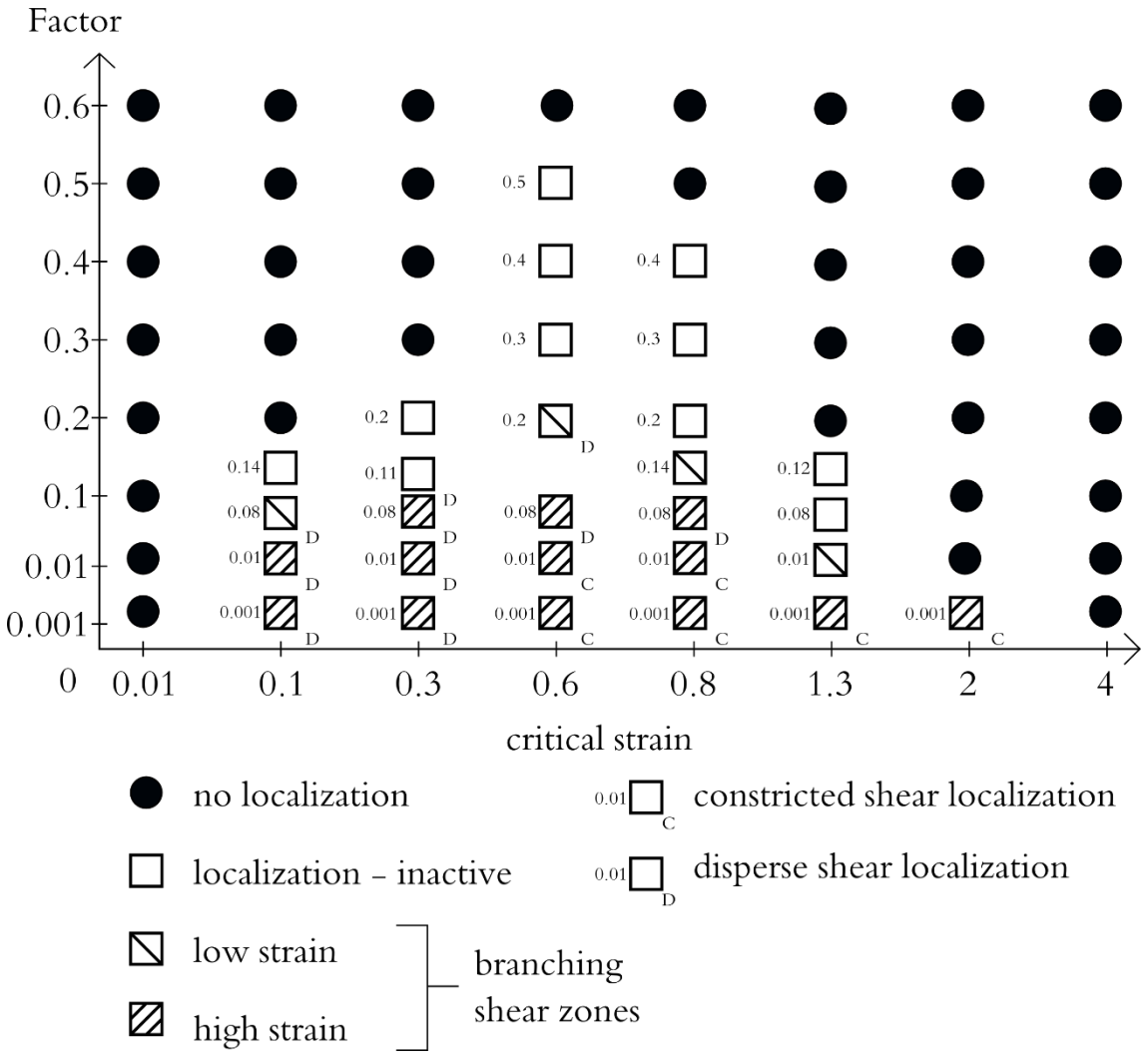

Figure 3.11 Influence of strain-weakening on ductile shear localization by decrease in viscosity by a factor linked to a critical strain (γ) under constant overall strain-rate $10^{-14}s^{-1}$, after a time-step of 1.8 to 2 Ma

A further decrease of the factor to a value between 0.03 and 0.01 leads to constricted shear branches with high strain, whereas the width of the shear zone branches and the junction zone varies between 3-10 km (Fig. 3.10b). Strain-softening of the material has a significant influence on the characteristics of the development of shear zones and the width of the shear strands. A weak behavior of the material with a reduction of more than 1/100 of the initial viscosity by ongoing strain leads to narrow high strain zones (Fig. 3.11, constricted shear localization).

Next, we employed different critical strain values (γ) under a constant reduction of the factor to 0.01 for a time-span of 1.8-2 Ma (55-63% strain, Fig. 3.10c, d). The results show that shear zones develop in a limited field for a critical strain of 0.1 and 2 (Fig. 3.11), whereas the maximum limit can be extended for values of $\gamma \geq 2$ in an advanced stage with a strain of 94%. The results show that the localized shear zones for a factor of 0.01 in a critical strain field of 0.1-2 differ in thickness of the strands, in the geometry and in intensity of localization. The shear localization for γ = 0.1-0.3 is characterized by a wide junction zone with a width of more than 30 km and by development of internal synthetic faults between the main faults.

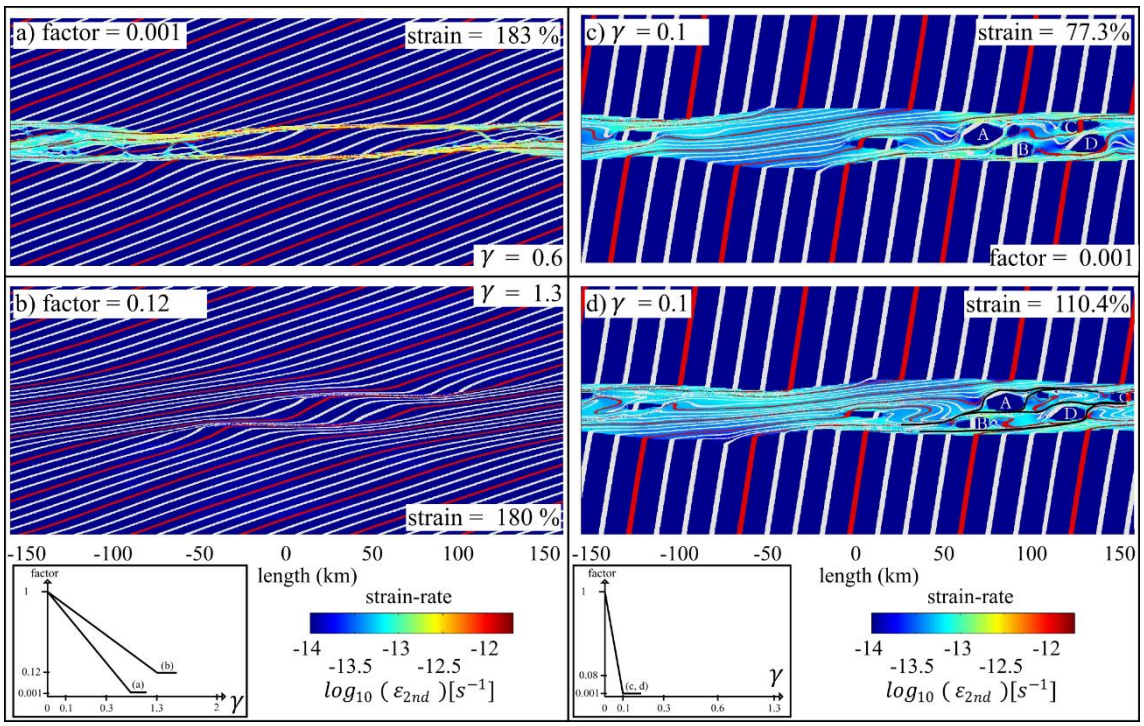

Figure 3.12 a) Constricted shear zones with internal shear-related folds, initiation of synthetic faults; b) Inactive shear zones, unsheared zones are surrounded by high-strain zones; c-d) Evolution of undeformed blocs and shear-related folds. Example of a dispersed shear zone with a different movement of the undeformed blocs (A, B, C, D), development of shear-related folds. Black lines represent the high strain zones to illustrate the anastomosing trend

The new synthetic faults with an angle of 160° to the imposed shear direction form an anastomosing network of shear zones (Fig. 3.10c, d), whereas the material between the high strain zones stay undeformed (unsheared zones). An increase of the critical strain to ≥ 0.6 led to a stronger localization in a thinner zone, and a thinner junction zone with a width of 5-10 km (Fig. 3.10a). These constricted shear zones show a strong localization with a simplified geometry in comparison to the previous results. The overview of the distribution of the shear localization indicates a maximum of development of shear zones even with a higher value for a factor > 2 for the model runs with a critical strain of 0.6 to 0.8. Summarizing we found only the constricted shear zones in a limited range for a critical strain value ≥ 0.6 and a factor of ≤ 0.01.

Extension of the numerical models over a time-span of 3.18 Ma with a strain of more than ~100 % gives similar geometries compared to previous runs, but these differ in the width and the number of shear zones. During advanced stages of the constricted models, new antithetic and synthetic shear zones develop with an angle of 140°-115° and 45° to the imposed shear direction between the shear branches (Fig. 3.12a), whereas the dispersed models show a similar trend in an earlier stage of the runs. In an advanced stage of the modeling of dispersed shear zones (critical strain 0.1-0.3), the new developed synthetic and antithetic high strain branches form an anastomosing structure (Fig. 3.12c, d). The junction zone display transition of unsheared zones to highly strained domains, indicated by asymmetric shear-folds of the strain-markers with a complex geometry. The variations of geometry are associated by an initiated shape of open shear-related late folds to tightening shear -induced flattening folds. These shear related folds differ by their wavelength and amplitudes whereby the disperse shear zones (critical strain 0.1-0.3) indicate a higher number of large-scale folds.

3.5 Discussion and applications to field examples

Most of the crustal-scale strike slip shear zones exhibit a complex network of shear zone branches in a brittle (e.g. San Andreas Fault; Wallace, 1990) or ductile (e.g. Nadj shear zone; Stern,1994) regime. The rheological behavior of the material is the key to better understanding the variations in the geometry of such shear zones. Examples of large-scale shear zones show a straight as well as a curvy trace of the fault at the earth's surface, furthermore the slip motion can be right-lateral or left-lateral according to the

orientation of the shear localizations to the imposed shear direction. One of the well exposed classical examples of a complex network of brittle shear zone is the San Andreas Fault (SAF). Studies on the SAF have illustrated that the material within the shear zone is weaker than the surrounding rocks (Brune et al., 1969; Lachenbruch and Sass, 1980; Zoback et al., 1987; Zoback, 2000; Carpenter et al., 2011), but the weakness is still under debate (Scholz, 2000). Research on foliated cataclasis has given us an overview regarding values for a decrease in frictional coefficient from 0.6 to 0.1 (Collettini et al., 2009, Faulkner et al., 2010) by ongoing strain. Previous work on the San Andreas Fault confirmed the weaker theory of the shear zone with a measurement of the frictional coefficient of 0.21 at 2.7 km depth (Carpenter et al., 2011). In general the explanation of the small value of the frictional strength can be related to different variables, pore pressure for example may be one of the important factor (Chester, 1993; Rice 1992; Faulkner and Rutter, 2001; Carpenter et al., 2011). Numerical 3-D simulation of the strike-slip deformation in the upper crust and modeling with thin plates indicate a much lower value of the friction coefficient of the sheared zone in relation to the surrounding rocks if a best fit to the

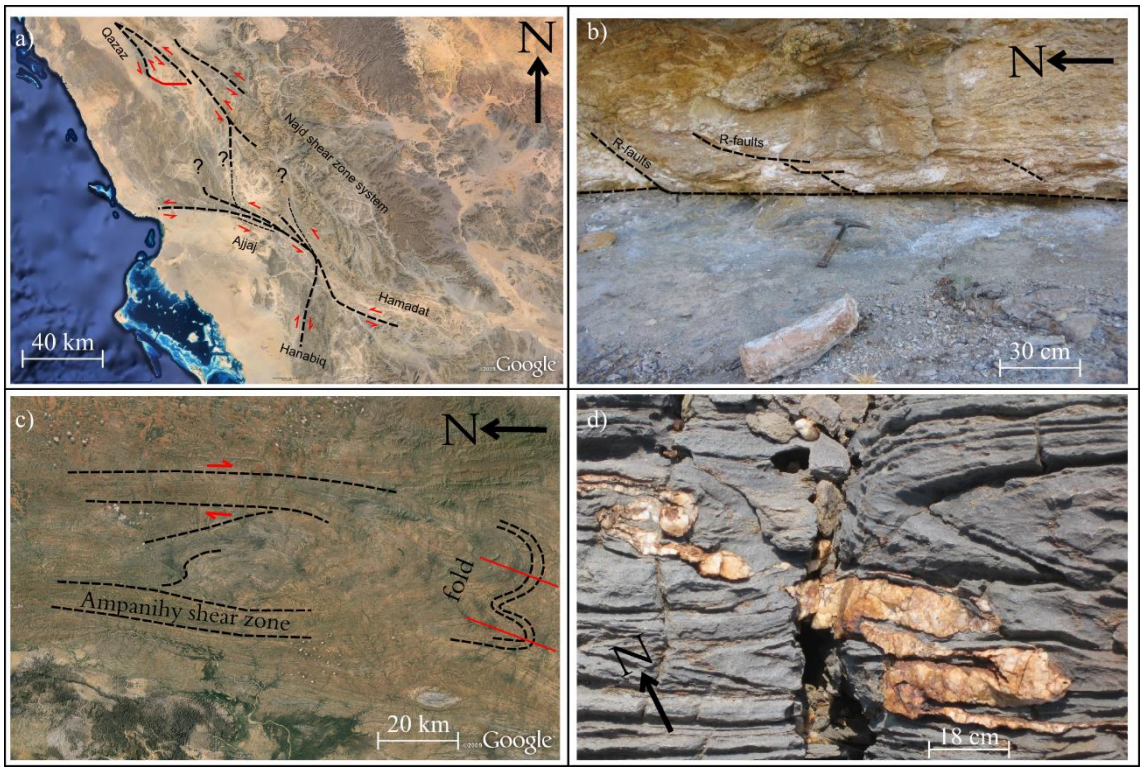

Figure 3.13 a) Network of anastomosing ductile shear zones - Qazaz, Ajjaj, Hanabiq and Hamadat shear zones, Najd shear zone system in Saudi Arabia; b) Riedel shear zones in foliated cataclasite, Güney Detachment, Aydin, Turkey; c) 10-20 km wide shear zones with F3 folds in quartzo-feldspathic granulites, southern Madagascar (Martelat et al., 1999; De Witt et al., 2001); d) Shear related folds of quartz veins in a graphitic marble, Brandberg-West-Fm, Goantagab, Namibia

natural example of the SAF is to be obtained by the model (Bird and Kong, 1994; Chéry et al., 2001; Popov et al., 2012). In our numerical 2-D models we focused the study primarily on the geometry of brittle shear zones and the interaction of the shear branches dependent on the strain-softening. The first step to understand the development of complex shear zone system dependent on the frictional behavior is to work with a simplified strain-softening. The results show that the development of antithetic faults (R') depends on a decrease of the friction angle and is not related to cohesion. Antithetic faults occur in our simulations by a decrease of the friction angle from an initial of 30° to a value lower than 12° (frictional coefficient <0.21). Furthermore the R'-faults appeared at a later geological time-span in the models (Fig. 3.2, 3.15a, b). The final mature fault system with synthetic and antithetic faults shows similarities to natural examples, e.g. the SAF described by Wallace (1990) or the Anatolian Fault (Barka and Kadinsky-Cade, 1988). We observed that the rate of decrease of the frictional strength plays an important role in the activity (strain-rate) of antithetic faults (Fig. 3.6d). The models exhibit the highest proportionality (slip motion) of antithetic faults for a critical strain of 0.3-0.6. During the development of the brittle shear zone network, the numerical models showed a variation in the activity of the synthetic and antithetic faults related to the time-span. One reasonable explanation is the constant overall strain-rate (boundary conditions): The dominant dextral shear sense in the model accommodates the highest displacement of the preferred oriented synthetic and main faults. Accordingly, the synthetic and main faults are more influenced by strain-weakening than antithetic faults with ongoing deformation, which changes the activity of the shear branches with ongoing strain (Fig. 3.6d). The simplified relationship of the linear weakening gives us an idea about the relation of the frictional behavior to the activity (strain-rate) of different types of shear strands, but may be more complex in natural examples.

In general field studies (Davis et al., 1999; Katz et al., 2004), shear experiments (Schreurs et al., 1994), numerical models (McKinnon and Garrido de la Barra, 1998) and analogue models (Naylor et al., 1986; Marques et al., 2001; Coelho et al., 2006) are consistent with Coulomb theory where R and R' are oriented at $45° \pm \phi/2$ to the maximum compressive stress (Fig. 3.13d). A number of field studies on small-scale Riedel structures indicate a variation in the orientation of R and R'-faults, for example in the Jurassic Navajo Sandstone (Capitol Reef National Park, Utah; Katz et al., 2004) or in the foliated cataclasite, Güney Detachment (NW of Aydin, Turkey - Gessner et al., 2001; Fig. 3.12b). One explanation could be the internal rotation by granular flow between the shear

branches or a multiple deformation phase (Bell, 1986; Ham and Bell, 2004; Katz et al., 2004). In our numerical model, the antithetic faults imply a similar trend of a variation at an angle between 20°-75° to the imposed shear direction (Fig. 3.14c). Our simulations suggest that the development of R-faults during early stages leads to a change of the maximum compressive stress direction between the shear faults (junction zone) of an initial value of 45° to an angle of 10°.

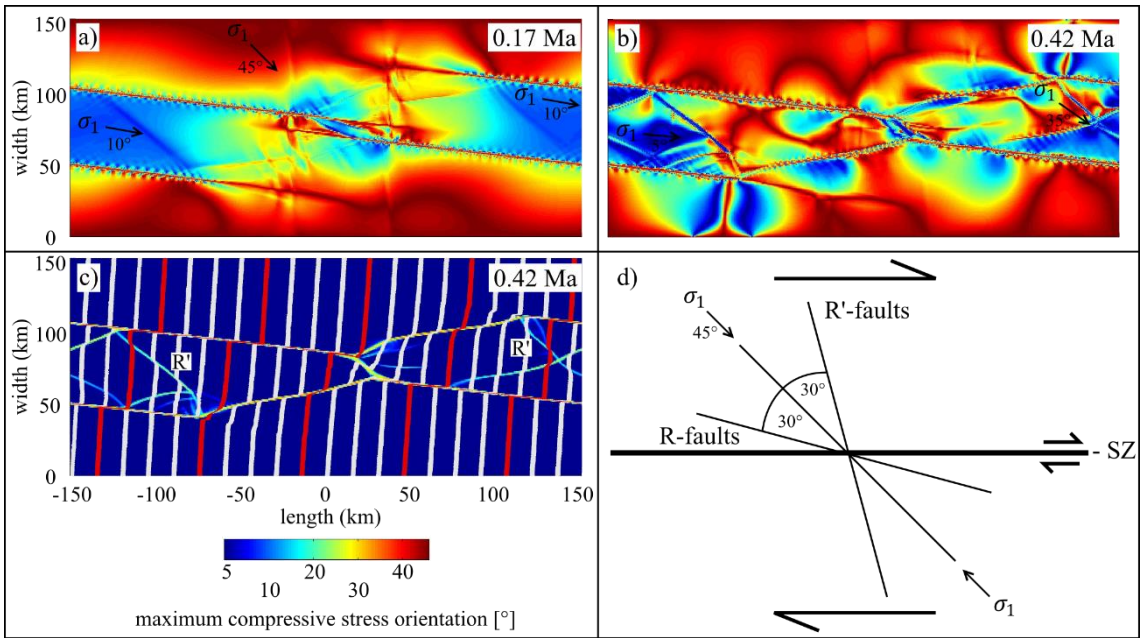

Figure 3.14 Distribution of the maximum compressive stress orientation on a brittle shear localization, γ=0.6; a-c) The interaction of the shear zone branches leads to local variations in the compressive stress direction between 10 - 45°, time-step 0.17 to 0.42 Ma; c) Overview of shear localization, R'-faults indicate a bending trend and different angles to the imposed shear direction; d) Geometry of syn- and antithetic faults in dextral simple shear, SZ is the imposed shear direction

The low - angle of the maximum compressive stress forms antithetic faults (R') at a range of ~40°. The angle of the compressive stress component is therefore not a stable value. For complex branched shear zones, the angle varied locally in a range between 5° and 45°, which explains the bending trend of the wide-range oriented antithetic faults between 20°-75° (Fig. 3.2c, Fig. 3.14a-c). A change of the maximum compressive stress in the evolution of the Riedel - shears may be a suitable explanation for the variation of the antithetic faults on small-scale as well as large-scale field examples.

The simulations suggest that the bending trend of the syn- and antithetic faults affects also the distribution of the total pressure. The numerical models shows that during early stages, total pressure is typically reduced along the shear zones compared to the host rock,

as described by Mancktelow (2006). With ongoing strain, the distribution of pressure changes in relationship with newly formed synthetic and antithetic faults. The cross-linking shear faults are separated by a high-pressure zone, which is related to the bending trend of the localization whereas the straighter trend of the faults indicates a low-pressure zone (Fig. 3.2f). Fluid flow to from the high to the low-pressure zone will locally change the shear strength of the shear zone in relation to a weakening effect by mineral reactions or the effect of pore pressure (Sibson, 1990; Rice, 1992; Ridley, 1993; Connolly and Podladchikov, 2000; Jeffries et al., 2006).

Field studies on exposed large -and small-scale ductile shear zones has shown that their fault incline in a straight line, whereas a higher number of shear localization have distinguishable bending (anastomosing) to form a complex network (e.g. Carreras et al., 2010). Detailed analysis of the single shear branch exhibit different characteristics with regards to the width, length, shear sense and displacement (Carreras et al., 2001; Fusseis et al., 2006; Bürgmann and Dresen, 2008). The Najd shear zone is an example of a huge system up to 400 km wide and 2000 km long; an anastomosing constricted structure with an individual variation of shear, from scale of meters to a few kilometers wide (Fig. 3.13a, (Stern, 1994)). Our numerical models show that the change of the effective viscosity during deformation (strain-softening) has the greatest effect on the geometry of shear zones and therefore on the evolution of the complex shear zone network. The transition from a dispersed to a constricted shear zone (Fig. 3.10a-b, 3.15c-d) is located in a limited range to the factor ~100 and a critical strain ~0.5. These bounds show that the development of different types of shear localization is sensitive to the mechanical conditions. Estimates from field examples indicate similar values for the reduction of viscosity along ductile shear zones (Burgmann and Dresen, 2008; Mehl and Hirth, 2008). Numerical studies also show well-developed ductile shear zones illustrated by a strain-weakening with a critical strain of 0.5, as reported by Gueydan et al. (2014). The weakening process in natural shear zones is much more complex than our modeled linear behavior with a critical strain and a factor. Simulations with bimineralic material, reported by Jammes et al., (2015), showed that the heterogeneous property of the material has an influence on the development on ductile shear zones and their geometry. Even so our simplified models demonstrate how the change of the effective viscosity affects the shear geometries: in the numerical models a ductile shear zone occurs at a smaller change in viscosity at a critical strain between 0.6 and 0.8. These simulations give us an interesting view of these interactions and may be a

suitable explanation for the variation of the shear zone width on well-exposed field examples like that-of Madagascar or the Najd shear zone in Saudi Arabia (Fig. 3.13a, c). Another typical characteristic feature of anastomosing shear zones are lozenges of less deformed material surrounded by sheared localizations, which indicate internal fold structures, exposed for example in southern Madagascar, southern Switzerland and in northeastern Spain (Fig. 3.13c, (Simpson, 1982; Martelat et al., 1999; Carreras, 2001; Ponce et al., 2013)). In our numerical models over an advanced time-span (> 90 % strain), new synthetic and antithetic faults developed and formed by interconnecting delineate undeformed blocs (lozenge) within the main shear zones (Fig. 3.15d). The development of lozenge in the numerical models show similarities to the described theories (Pollard and Aydin, 1984; Pennacchioni, 2005; Mann, 2007; Ponce et al., 2013). These new high strain zones tend to be anastomosing structure, which increase the complexity of the internal shear zone geometry. The distribution strain-rate along the shear zones is highly inhomogeneous, as demonstrated by the different activity of high-angle shear zone strands oriented between 140° and 115°, or at 45° to the imposed shear direction (Fig. 3.12a). The movement of the undeformed blocs within the shear zone indicated a horizontal variation in flow along the shear direction (Fig. 3.12c, d). The combination of the different oriented shear components linked to the heterogeneous main flow produce shear related folds (Fig. 3.12c-d, 3.15d), which can be described as a flow perturbation.

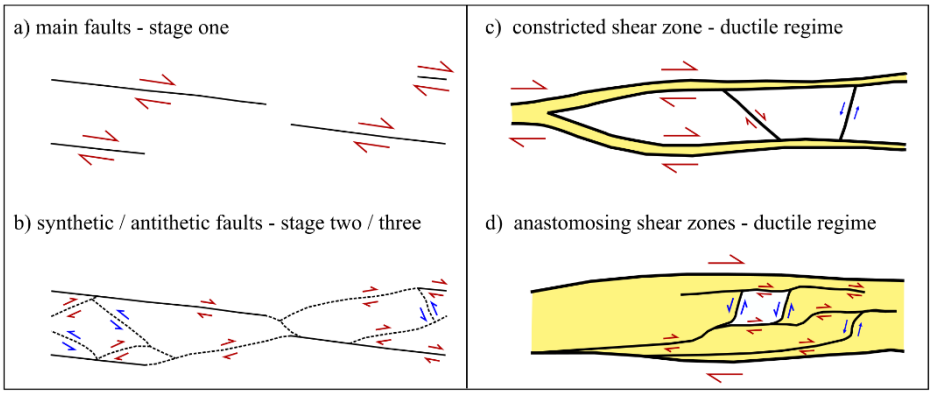

Figure 3.15 Numerical results of brittle and ductile shear localization; a-b) Development of Riedel shear zones to a complex network of brittle faults, anti- and synthetic faults indicating different orientations in the propagation; c-d) Showing the interconnection of shear strands and the development of anastomosing pattern of syn- and antithetic faults within the dispersed shear zones, which bounds lozenges

The evolution of the folds showed an increase of complexity of the geometry as deformation proceeds, whereby the initial structures formed during early stages are characterized as open folds with an axial surface of 90° to the shear direction. At later stages, the open folds start to be tighter and their axial surfaces rotate parallel to the imposed shear direction. Local zones of high strain, mostly between the undeformed blocs, display the complex geometry of verging overturned folds (Fig. 3.12a, d) and several types of shear-related folds. Differences in wavelength, thickness and amplitude of the folds are influenced by changes of the internal flow perturbation, whereas the viscosity contrast plays no role in the model. Similar structures of shear-related late folds (Howard, 1968; Platt, 1983; Mandal et al., 2004) were described by Carreras et al. (2005) on a classical example in north-eastern Spain. The development of the fold structures has been suggested in literature to be caused by local or general perturbations of flow, related to rigid objects or rheological effects of different material properties between the layers (Cobbold and Quinquis, 1980; Lister and Williams, 1983; Platt, 1983; Bons and Jessell, 1998). Studies on the shear related late folds in Cadaqués described the folds in relation to a change of the kinematics, reported by Carerras et al. (2005). Our numerical models demonstrate that the evolution of internal time-dependence synthetic and antithetic high strain zones in combination with the main shear flow within the shear zone generate shear-related folds.

3.6 Conclusion

The development of shear branches is strongly affected by weakening mechanics under brittle and ductile conditions - a minor change in the rheology results in a new geometry of the shear zones. The time-dependent evolution of the brittle shear branches changes the internal stress field of the surrounding rocks, which promotes new shear zones to form with orientations differing from their predecessors. In addition to these effects, variations in the trend of the new faults lead to an irregular distribution of pressure along the shear zones. Furthermore, the numerical model runs show that the strike-slip shear branches are dominated by synthetic shear, whereas the maximum activity of antithetic faults is associated with a strain-weakening with a critical strain between 0.3 and 0.6. A lower value of the critical strain (0.01) leads to a more pronounced bending trend of the shear zones and to a higher number of shear faults. The change of the frictional strength during deformation is essential in the develop antithetic faults: we observed for

a linear behavior of the weakening that the friction angle has to be reduced to a value lower than 12 ° for such fault zones to occur.

The evolution of particular types of ductile shear zones is also limited by critical values in the reduction of the effective viscosity and to a specific range of critical strain. A decrease of the initial effective viscosity by a factor of 1/10 during the deformation is required to develop ductile shear zones in the simulations, with the largest shear zone diversity occurring where the total strain is between 0.3-0.8. The numerical models show that the interaction of variously-oriented syn- /antithetic shear branches together with the continuous activity of the main shear component leads to shear-related folds and undeformed blocs within the shear zone. The time-dependent evolution of undeformed blocs together with their movement within the shear zone, initiate new shear zones at a higher-angle to the imposed shear direction. At large deformation the dominant horizontal shear overprints the high-angle shear zones, whereby the shear-related folds are the relics of the past which show the complexity of the interaction of anastomosed shear zones. However, the weakening and therefore the mechanism behind the change in effective viscosity during deformation affects the geometries of the shear zone system, and leads to different characteristics of the ductile shear branches.

3.7 References

Allken, V., Huismans R. S., and Thieulot, C., 2011. Three dimensional numerical modeling of upper crustal extensional systems, J. Geophys. Res., vol. 116, B10409.

Allken, V., Huismans, R. S., and Thieulot, C., 2012. Factors controlling the mode of rift interaction in brittle-ductile coupled systems: a 3D numerical study, Geochem. Geophys. Geosyst., vol. 13, Q05010.

Archanjo C. J., Hollanda, M. H. B. M., Rodrigues, S. W. O., Neves, B. B. B., and Armstrong, R., 2008. Fabrics of pre- and syntectonic granite plutons and chronology of shear zones in the Eastern Borborema Province, NE Brazil. Journal of Structural Geology 30, 310-326.

Barka A. A., and Kadinsky-Cade, K., 1988. Strike-slip fault geometry in Turkey and its influence on earthquake activity. Tectonics 7, 663-84.

Behn, M. D., Lin, J., and Zuber, M. T., 2002. A continuum mechanics model for normal faulting using a strain-rate softening rheology: Implications for thermal and rheological controls on continental and oceanic rifting, Earth Planet. Sci. Lett., 202, 725-740.

Bell, T.H., 1986. Foliation development and refraction in metamorphic rocks: reactivation of earlier foliations and decrenulation due to shifting patterns of deformation partitioning. Journal of Metamorphic Geology 4, 421-444.

Bird, P., and Kong, X., 1994. Computer simulations of California tectonics confirm very low strength of major faults, Geol. Soc. Am. Bull., 106, 159-174.

Bos, B., and Spiers, C. J., 2002. Frictional-viscous flow of phyllosilicate-bearing fault rock: Microphysical model and implications for crustal strength profiles, J. Geophys. Res., 107(B2), 2028, doi:10.1029/2001JB000301.

Bons, P.D., and Jessell, M.W., 1998. Folding in experimental mylonites, in: Snoke, A.W. (Ed.), Fault-Related Rocks-A Photographic Atlas, pp. 366-367.

Braun, J., Chéry, J., Poliakov, A. N. B., Mainprice, D., Vauchez, A., Tommasi, A., and Daignières, M., 1999. A simple parameterization of strain localization in the ductile regime due to grain size reduction: a case study for olivine. Journal of Geophysical Research 104, 25167-25181.

de Bresser, J. H. P., ter Heege, J. H., and Spiers, C. J., 2001. Grain size reduction by dynamic recrystallization: can it result in major rheological weakening? International Journal of Earth Sciences 90, 28-45.

Brun, J.-P., and Cobbold, P. R., 1980. Strain heating and thermal softening in continental shear zones: a review. Journal of Structural Geology 2, 149-158.

Brune, J. N., Henyey, T. L., and Roy, R. F., 1969. Heat flow, stress, and rate of slip along the San Andreas Fault, California. J. Geophys. Res. 74, 3821-3827.

Buck, W. R., 1993. Effect of lithospheric thickness on the formation of high- and low-angle normal faults, Geology, 21, 933-936.

Burg, J. and Schmalholz, S., 2008. Viscous heating allows thrusting to overcome crus tal-scale buckling: Numerical investigation with application to the himalayan syntaxes. Earth and Planetary Science Letters.

Bürgmann, R., and Dresen, G., 2008. Rheology of the lower crust and upper mantle: Evidence from rock mechanics, geodesy, and field observations: Annual Review of Earth and Planetary Sciences, v. 36, doi: 10.1146/annurev.earth.36.031207.124326.

Carpenter, B. M., Marone, C., and Saffer, D. M., 2011. Weakness of the San Andreas Fault revealed by samples from the active fault zone. Nature Geoscience 4, 251-254, doi:10.1038/ngeo1089.

Carreras, J., 2001. Zooming on Northern Cap de Creus shear zones. Journal of Structural Geology 23, 1457-1486.

Carreras, J., Druguet, E., and Griera, A., 2005. Shear zone-related folds. Journal of Structural Geology 27, 1229-1251.

Carreras, J., Czeck, D. M., Druguet, E., and Hudleston, P. J., 2010. Structure and development of an anastomosing network of ductile shear zones. Journal of Structural Geology, 32 (5), 656-666.

Chéry, J., Zoback, M. D., and Hassani, R., 2001. An integrated mechanical model of the San Andreas fault in central and northern California. Journal of Geophysical Research, 106, 22,051-22,066.

Chester, F.M., Evans, J. P., and Biegel, R. L., 1993. Internal structure and weakening mechanism sof the San Andreas Fault. J. Geophys. Res. 98, 771-786.

Choi, E., Lavier, L., and Gurnis, M., 2008. Thermomechanics of mid-ocean ridge segmentation, Phys. Earth Planet. Int., vol. 171, pp. 374-386.

Cloos, H., 1928. Experimenten zur inneren Tektonic. Centralblatt für Mineralogie und Paleontologie B, 609.

Cobbold, P.R., and Quinquis, H., 1980. Development of sheath folds in shear regimes. Journal of Structural Geology 2, 119-126.

Coelho, S., Passchier, C., and Marques, F., 2006. Riedel shear control on the development of pennant veins: field example and analogue modelling. J. Struct. Geol. 28:1658-1669.

Collettini, C., Niemeijer, A., Viti, C., and Marone, C., 2009. Fault zone fabric and fault weakness. Nature 462, 907-910. http://dx.doi.org/10.1038/nature08585.

Connolly, J. A. D. and Podladchikov, Y. Y., 2000. Temperature-dependent viscoelastic compaction and compartmentalization in sedimentary basins. Tectonophysics, 324, 137-168.

Culshaw, N.G., Gerbi, C., Marsh, J. H., and Plug, L., 2011. Heterogeneous amphibolite facies deformation of a granulite facies layered protolith: Matches Island Shear System, Parry Sound Domain, Grenville Province, Ontario, Canada. Journal of Structural Geology, 33, 875-890.

Davis, G.H., Bump, A. P., Garcia, P. E., and Ahlgren, S. G., 1999. Conjugate Riedel deformation band shear zones. Journal of Structural Geology 22, 169-190.

Etheridge, M.A., and Wilkie, J. C., 1979. Grainsize reduction, grain boundary sliding and the flow strength of mylonites. Tectonophysics 58, 159-178.

Faulkner, D. R., and Rutter, J. H., 2001. Can the maintenance of overpressured fluids in large strike-slip fault zones explain their apparent weakness? Geology 29, 503-506.

Faulkner, D. R., Jackson, C. A. L., Lunn, R. J., Schlische, R. W., Shipton, Z. K., C. A. J. Wibberley, C. A. J., and Withjack, M. O., 2010. A review of recent developments concerning the structure, mechanics and fluid flow properties of fault zones, J. Struct. Geol., 32, 1557–1575, doi:10.1016/j.jsg.2010.06.009.

Faure M., Be Mezeme, E., Duguet, M., and Talbot, J-Y., 2005. Paleozoic tectonic evolution of medio-Europa from the example of the French Massif Central and Massif Armoricain. - In: Carosi R., Dias R., Iacopini D., and Rosenbaum G., Eds., The southern Variscan belt, J. of the Virtual Explorer, 19, Paper 5.

Fusseis, F., Handy, M.R., and Schrank, C., 2006. Networking of shear zones at the brittle-to-viscous transition (Cap de Creus, NE Spain). Journal of Structural Geology 28, 1228-1243.

Gerya, T., 2010a. Dynamical instability produces transform faults at mid-ocean ridges, Science, vol. 329, pp. 1047–1050.

Gerya, T., 2012. Origin and models of oceanic transform faults, Tectonophys., vol. 522-523, pp. 34-56.

Gerya, T. V., 2013. Three dimensional thermomechanical modeling of oceanic spreading initiation and evolution, Phys. Earth Planet. Int., 2013, vol. 214, pp. 35-52.

Gessner K, Piazolo, S., Güngör, T., Ring U., and Passchier, C.W., 2001. Tectonic significance of deformation patterns in granitoid rocks of the Menderes Massif, southwest Turkey. International Journal of Earth Sciences 89: 766-780.

Gueydan, F., Leroy, Y. M., Jolivet, L., and Agard, P., 2003. Analysis of continental midcrustal strain localization induced by reaction-softening and microfracturing. J. Geophys. Res. 108 (B2), 2064. http://dx.doi.org/10.1029/2001JB000611.

Gueydan, F., Précigout, J., and Montési, L. G. J., 2014. Strain weakening enables continental plate tectonics, Tectonophysics, Volume 631, p. 189-196.

Grujic, D., and Mancktelow, N. S., 1998. Melt-bearing shear zones: analogue experiments and comparison with examples from southern Madagascar. Journal of Structural Geology 20, 673-680.

Handy, M. R., Hirth, G., and Bürgmann, R., 2007. Fault Structure and Rheology from the Frictional-Viscous Transition Downward. pp. 139-181 in: Tectonic Faults - Agents of Change on a Dynamic Earth, edited by M.R. Handy, G. Hirth, N. Hovius, Dahlem Workshop Report 95, 504 pp., The MIT Press, Cambridge, Mass., USA.

Hansen, L. N., Zimmerman, M. E., and Kohlstedt, D. L., 2011. Grain-boundary sliding in San Carlos olivine: Flow-law parameters and crystallographic-preferred orientation, J. Geophys. Res., 116, B08201, doi:10.1029/2011JB008220.

Hansen, L. N., Zimmerman, M. E., and Kohlstedt, D. L., 2012. The influence of microstructure on deformation of olivine in the grain-boundary sliding regime, J. Geophys. Res., 117, B09201, doi:10.1029/2012JB009305.

Ham, A.P., and Bell, T. H., 2004. Recycling of foliations during folding. Journal of Structural Geology 26, 1989-2009.

Hieronymus, C. F., 2004. Control on seafloor spreading geometries by stress-and strain-induced lithospheric weakening. Earth and Planetary Science Letters, 222 (1), 177-189.

Hobbs, B. E., Ord, A., and Teyssier, C., 1986. Earthquakes in the ductile regime. Pure and Applied Geophysics 124 (1–2), 309–336.

Howard, K. A., 1968. Flow direction in triclinic foliated rocks. American Journal of Science 266, 758-765.

Huismans, R. S., and Beaumont, C., 2003. Symmetric and asymmetric lithospheric extension: Relative effects of frictional-plastic and viscous strain softening, J. Geophys. Res., 108(B10), 2496, doi:10.1029/2002JB002026.

Huismans, R. S., and Beaumont, C., 2007. Roles of lithospheric strain softening and heterogeneity in determining the geometry of rifts and continental margins. Geological Society, London, Special Publications, 282 (1), 111-138.

Jammes, S., Lavier, L. L., and Reber, J. E., 2015. Localization and delocalization of deformation in a bimineralic material, J. Geophys. Res. Solid Earth, 120, doi: 10.1002/2015JB011890.

Jefferies, S. P., Holdsworth, R. E., Wibberley, C. A. J., Shimamoto, T., Spiers, C. J., Niemeijer, A. R., and Lloyd, G. E., 2006. The nature and importance of phyllonite development in crustal-scale fault cores: an example from the Median Tectonic Line, Japan. Journal of Structural Geology 28, 220-235.

Katz, Y., Weinberger, R., and Aydin, A., 2004. Geometry and kinematic evolution of Riedel shear structures, Capitol Reef National Park, Utah. Journal of Structural Geology 26, 491-501.

Kaus, B., and Podladchikov, Y., 2006. Initiation of localized shear zones in viscoelastoplastic rocks. J. Geophys. Res. 111. DOI: 10.1029/2005JB003652.

Kaus, B., 2010. Factors that control the angle of shear bands in geodynamic numerical models of brittle deformation Tectonophysics 484, 36-4.

Lachenbruch, A. H., and Sass, J. H., 1980. Heat flow and energetic of the San Andreas Fault Zone. J. Geophys. Res. 85, 6185-6223.

Lavier, L. L., Buck, W. R., and Poliakov, A. N. B., 2000. Factors controlling normal fault offset in an ideal brittle layer. Journal of Geophysical Research 105: doi: 10.1029/2000JB900108. issn: 0148-0227.

Lister, G.S., and Williams, P. F., 1983. The partitioning of deformation in flowing rock masses. Tectonophysics 92, 1–33.

Marques, F. O., and Coelho, S., 2001. Rotation of rigid elliptical cylinders in viscous simple shear flow: analogue experiments. Journal of Structural Geology 23, 609-617.

Martelat, J.E., Schulmann, K., Lardeaux, J. M., Nicollet, C., and Cardon, H., 1999. Granulite microfabrics and deformation mechanisms in southern Madagascar. J. Struct. Geol. 21:671-87.

Mancktelow, N. S., 2002. Finite-element modelling of shear zone development in visco-elastic materials and its implications for localisation of partial melting. Journal of Structural Geology 24, 1045-1053.

Mancktelow, N. S., 2006. How ductile are ductile shear zones? Geology, 34 (5), 345-348.

Mancktelow, N. S., 2007. Tectonic pressure: Theoretical concepts and modelled examples. Lithos. Volume 103 (2008), Issus 1-2, p. 149-177.

Mandal, N., Samanta, S. K., and Chakraborty, C., 2004. Problem of folding in ductile shear zones: a theoretical and experimental investigation. Journal of Structural Geology 26, 475-489.

Mann, P., 2007. Global catalogue, classification and tectonic origins of restraining- and releasing bends on active and ancient strike-slip fault systems. In: Cunningham,W. D., Mann, P. (Eds.) Tectonics of Strike-slip Restraining and Releasing Bends. Geological Society, London, Special Publications, 290, 367-385.

Mehl, L., and Hirth, G., 2008. Plagioclase preferred orientation in layered mylonites: Evaluation of flow laws for the lower crust, J. Geophys. Res., 113, B05202, Doi: 10.1029/2007JB005075.

McKinnon, S. D. and Garrido de la Barra, I., 1998. Fracture initiation, growth and effect on stress field: a numerical investigation. Journal of Structural Geology 20, 1673-1689.

Montési, L. G. J., 2007. A constitutive model for layer development in shear zones near Thebrittle-ductile transition. Geophys. Res. Lett. 34.

Montési, L. G. J., 2013. Fabric development as the key for forming ductile shear zones and enabling plate tectonics. Journal of Structural Geology 50, 254-266, doi: 10.1016/j.jsg. 2012.12.011.

Naylor, M. A., Mandl, G., and Sijpesteijn, C. H. K., 1986. Fault geometries in basement-induced wrench faulting under different initial stress states. Journal of Structural Geology 8, 737-752.

Park, Y., Yoo, S. -H., and Ree, J. -H., 2006. Weakening of deforming granitic rocks with layer development at middle crust. J. Struct. Geol. 28, 919-928. http://dx.doi.org/10.1016/ j.jsg.2006.02.005.

Passchier, C. W., 1990a. Reconstruction of deformation and flow parameters from deformed vein sets. Tectonophysics 180: 185-199.

Passchier, C. W., 1990b. A Mohr circle construction to plot the stretch history of material lines. Journal of Structural Geology 12: 513-515.

Passchier, C. W., den Brok, S. W. J., van Gool, J. A. M., Marker, M., and Manatschal, G., 1997. A laterally constricted shear zone system - the Nordre Strømfjord steep belt, Nagssugtoqidian Orogen, W. Greenland. Terra Nova 9, 199-202.

Passchier, C. W., 1998. Monoclinic model shear zones. Journal of Structural Geology 20, 1121-1137.

Paterson, M., S., 1989. The interaction of water with quartz and its influence in dislocation flow-an overview. In: Karato, S.I., Toriumi, M. (Eds.), Rheology of Solids and of the Earth, Oxford University Press, Oxford, pp. 107-142.

Paterson, M., S., Luan, F. C., 1990. Quartzite rheology under geological conditions. In: Knipe, R.J., Rutter, E.H. (Eds.), Deformation Mechanisms, Rheology and Tectonics. Geological Society Special Publication 54, pp. 299-307.

Pennacchioni, G., 2005. Control of the geometry of precursor brittle structures on the type of ductile shear zone in the Adamello tonalites, Southern Alps (Italy). Journal of Structural Geology 27, 627-644.

Piazolo, S., ten Grotenhuis, S. M., and Passchier, C. W., 2001. New apparatus for controlled general flow modelling of analog materials. Geological Society of America Memoir 193, 235-244.

Platt, J., P., 1983. Progressive folding in ductile shear zones. Journal of Structural Geology 5, 619-622.

Platt, J. P., and Behr, W. M., 2011a. Lithospheric shear zones as constant stress experiments. Geology 39, 127-130. http://dx.doi.org/10.1130/G31561.1.

Platt, J., P., and Behr, W. M., 2011b. Grainsize evolution in ductile shear zones: Implications for strain localization and the strength of the lithosphere. Journal of Structural Geology 33, 537-550. http://dx.doi.org/10.1016/j.jsg.2011.01.018.

Pollard, D. D., and Aydin, A. A., 1988. Progress in understanding jointing over the past century. Geological Society of America Bulletin 100, 1181-1204.

Poliakov, A. N. B. and Buck, W. R., 1998. In: Mechanics of stretching elastic-plastic-viscous layers: Applications to slow-spreading mid-ocean ridges. American Geophysical Union, Washington D.C.. 106: 3. Doi: 10.1029/GM106p0305.

Poirier, J. -P., 1980. Shear localization and shear instability in materials in the ductile field. J. Struct. Geol. 2, 135-142.

Popov, A., A., Sobolev, S. V., and Zoback, M. D., 2012. Modeling evolution of the San Andreas Fault system in northern and central California, Geochem. Geophys. Geosyst., 13, Q08016, doi:10.1029/2012GC004086.

Ponce, C., Druguet, E., and Carreras, J., 2013. Development of shear zone-related lozenges in foliated rocks. Journal of Structural Geology 50: 176-186.

Provost, A. -S., and Houston, H., 2003. Stress orientations in Northern and Central California; evidence for the evolution of frictional strength along the San Andreas plate boundary system. Journal of Geophysical Research, 108, 18.

Regenauer-Lieb, K., and Yuen, D., 1998. Rapid conversion of elastic energy into shear heating during incipient necking of the lithosphere. Geophysical Research Letters 25, 2737-2740.

Rennie, S., F., Fagereng, A., and Diener, J. F. A., 2013. Strain distribution within a km-scale, mid-crustal shear zone: The Kuckaus Mylonite Zone, Namibia. J. Struct. Geol. 56, 57-69.

Rice, J., R., 1992. in Fault Mechanics and Transport Properties of Rocks (eds. Evans, B. & Wong, T-F.) 475-503 (Academic).

Ridley, J., 1993. The relations between mean rock stress and fluid flow in the crust: with reference to vein-and lode-style gold deposits. Ore Geology Reviews 8, 23-37.

Riedel, W., 1929. Zur Mechanik Geologischer Brucherscheinungen. Zentralblatt für Mineralogie, Geologie und Paleontologie B, 354-368.

Rutter, E. H., and Brodie, K. H., 2004. Experimental intracrystalline plastic flow in hot-pressed synthetic quartzite prepared from Brazilian quartz crystals. Journal of Structural Geology, 26 (2), 259-270.

Schmalholz, S. M., and Fletcher, R. C., 2011. The exponential flow law applied to necking and folding of a ductile layer. Geophysical Journal International, 184 (1), 83-89.

Scholz, C., H., 2000. Evidence for a strong San Andreas Fault. Geology 28, 163-166.

Schrank, C., E., Handy, M. R., and Fusseis, F., 2008. Multiscaling of shear zones and the evolution of the brittle-to-viscous transition in continental crust. Journal of Geophysical Research 113, B01407, doi: 10.1029/2006JB004833.

Schreurs, G., 1994. Experiments on strike-slip faulting and block rotation. Geology 22, 567-570.

Sibson, R., H., 1980. Transient discontinuities in ductile shear zones. Journal of Structural Geology 2 (1-2), 165-171.

Sibson, R., H., 1990. Conditions for fault-valve behaviour, in Deformation Mechanisms, Rheology and Tectonics, edited by R. J. Knipe and E. H. Rutter, Geol. Soc. Spec. Publ., 54, 15-28.

Simpson, C., 1982. Strain and shape-fabric variations associated with ductile shear-zones. Journal of Structural Geology Volume 8, Issue 2, 1986, Pages 111-115, 117-122.

Stern, R., J., 1994. Arc assembly and continental collision in the Neoproterozoic East African orogen: Implications for the consolidation of Gondwana: Annu Rev of Earth and Planet Sci, V. 22, p. 319-351.

Sullivan, W., A., Boyd, A. S., and Monz, M. E., 2013. Strain localization in homogenous granite near the brittle–ductile transition: a case study of the Kellyland fault zone, Maine, USA. J. Struct. Geol. 56, 70-88. http://dx.doi.org/10.1016/j.jsg. 2013.09.00.

Thielmann, M., and Kaus, B. J. P., 2012. Shear heating induced lithospheric localization: does it result in subduction? Earth and Planetary Science Letters. Vol. 359-360. p. 1-13. doi:10.1016/j.epsl.2012.10.002.

Tirel, C., Brun, J. P., and Burov, E., 2008. Dynamics and structural development of metamorphic core complexes, J. Geophys. Res.113, p. B04403 10.1029/2005JB003694 25 pp.

Vermeer, P., and De Borst, R., 1984. Non-associated plasticity for soils, concrete and rock. Heron 29 (3), 1-64.

Wallace, R., 1990. The San Andreas fault system, California. U.S. Geological Survey Professional Paper 1515, 283.

de Wit, M. J., Bowring, S. A., Ashwal, L. D., Randianasolo, L. G., Morel, V. P. I., and Rambeloson, R. A., 2001. Age and tectonic evolution of Neoproterozoic ductile shear zones in southwestern Madagascar, with implications for Gondwana studies. Tectonics 20, 1-45.

Zoback, M., D., 1987. New evidence on the state of stress on the San Andreas Fault system. Science 238, 1105-1111.

Zoback, M., D., 2000. Strength of the San Andreas, Nature, 405, 31–32.

4. Lithology-driven shear zone nucleation: an example from the Wadi Filk (Jordan) and Hafafit (Egypt)

Abstract

In the Arabian-Nubian Shield, a wide range of small- to large-scale ductile shear zones have arisen with characteristics of isolated or anastomosed features. The Wadi Filk shear zone in Jordan represents a lithology-driven nucleation of paired shear zones associated with a pre-existing structure. Microstructural observations expose the development of a network of brittle Riedel shear zones in the granite of the Yutum Suite, related to an E-W shortening regime. At a later stage the brittle faults were emplaced by a rhyolithic melt, which indicated a chilled margin adjacent to the wall rock granite. The well-orientation of the dike to the maximum stress of the E-W shortening regime led to the reactivation of the pre-existing structure, with ductile overprinting. The ductile shear zone localized and propagated along the margins of the dike, which represented a weakness of the material resulted by a finer grain-size. Furthermore, detailed observation of the structure shows a sharp strain-gradient at the mm-scale from the margin of the dike to the wall rock granite, which shows no evidence of deformation. Such paired structures can be easily misinterpreted as the development of two shear zones in a homogeneous plutonic body, where the finer grain-size is a product of the dynamic recrystallization, which played a role during the deformation.

4.1 Introduction

Ductile shear zones are classified as high-strain zones surrounded by undeformed rocks. In general, the strain distribution within shear zones shows a gradient with a maximum displacement in the center, decreasing towards the margin (Coward 1976; Ramsay 1980; Simpson, 1983a, Passchier, 1986). At temperatures exceeding 300° C in granitic rocks, crystal plastic deformation and dynamic recrystallization leads to mylonization of

the rock (Bell and Etheridge, 1976; Sibson, 1977; Passchier and Trouw, 2005). Such mylonites are usually well-foliated and lineated (Hobbs et al., 1976; White et al., 1980; Tullis et al., 1982) with a high angle of foliation (~45°) in areas of lower shear strain, and a more sub-parallel foliation trend (relative to the imposed shear direction) in the high-strain domains. Natural ductile shear zones are disperse in their characteristics; they can be a straight isolated structures, or pairs or groups of sub-parallel to anastomosing zones (Ramsay and Graham 1970; Burg and Laurent 1978; Ramsay and Allison, 1979; Arbaret and Burg, 2003; Mancktelow and Pennacchioni, 2005). Since shear zones are distinct planar zones of high strain, numerous studies have been carried out to determine how and why they nucleate (Cobbold, 1977a, b; Poirier, 1980; Ramsay, 1980; White et al., 1980; Ingles et al., 1999). From these studies it is clear that shear zones are relatively weak domains that can theoretically nucleate in a homogeneous material. Numerical modeling shows that the implementation of power-law viscous flow and strain-softening (e.g. shear heating or mineral reactions) strongly affects the development of shear zones (Mancktelow, 2002, 2006; Thielmann and Kaus, 2012; Gueydan et al., 2003, 2014; Meyer et al., in review).

Despite the possibility of spontaneous nucleation in a homogeneous medium, most shear zones probably nucleate on pre-existing structures. The reason is that truly homogenous materials are rare in geology, and nucleation on some pre-existing structure is likely. The presence of brittle or heterogeneous discontinuities (e.g. a foliation in schists, Fusseis et al., 2006) in rocks causes a weak zone to develop into a ductile shear zone (Rudnicki, 1977; Segall and Pollard, 1983; Segall and Simpson, 1986; Kronenberg et al., 1990; Tullis et al., 1990; Guermani and Pennacchioni 1998; Takagi et al., 2000; Pennacchioni, 2005). Studies on mylonite in semi-brittle regimes have shown that earlier brittle fault rocks (pseudotachylite or cataclasite) are commonly reactivated and overprinted by ductile deformation (Segall and Simpson, 1986; Passchier et al., 1990; Tullis et al., 1990; Pennacchioni, 2005; Mancktelow and Pennacchioni, 2005; Fusseis et al., 2006)). Christiansen and Pollard (1997) have presented an example of nucleation of ductile shear zones along an aplite dike, wherein the fine-grained matrix and a different rock composition of the dike to the granitic wall rock initiated shear localizations by a weaker behavior. Another example of reactivation of pre-existing structures is that of ductile shear zones that have localized on the boundaries of bleached alteration halos of veins to form paired shear structures (Mancktelow and Pennacchioni, 2005).

This Chapter presents two new examples of shear zone geometries that are governed by lithology-related nucleation mechanism, and which are hard to recognize at first sight. In Wadi Filk, Jordan, paired ultra-mylonized shear zone developed in the margins of a rhyolithic dyke. In this case, a weak strain gradient penetrates the wall rock. An example from Wadi Hafafit in Egypt shows an extreme contrast where a strong mylonized dike cuts a pre-existing foliation of the wall rock at a high angle without overprint in the wall rock at all. The studied area belongs to an offset of the Arabian Nubian Shield in the East-West Gondwana collision zone. The observed structures illustrate the strong influence of pre-existing lithology on the development of ductile shear zones.

4.2 Geological overview

The studied areas in southwestern Jordan and the Eastern Desert in Egypt are characterized by Precambrian rocks and belong to the Arabian Nubian Shield (Fig. 4.1). The evolution of the East-West Gondwana orogeny described by Stern (2010) begins with the opening of the Mozambique Ocean (870-690 Ma) and its closing as a consequence of the collision of East and West Gondwana (630-550 Ma). The collision led to an east-west shortening, which formed a large system of large-scale sinistral strike-slip shear zones with a NW-SE trend, the Najd Shear zone system (Stern, 1994). The igneous rocks in the study area in southwest Jordan are typical post-collisional granitoids (Jarrar et al., 2003) dated at 640-540 Ma (Jarrar et al., 1993; Jarrar 1985; Brook et al., 1990). The Precambrian magmatic, metamorphic and sedimentary rocks can be subdivided into two complexes: The Araba (600-545 Ma) and the Aqaba (800-600 Ma) units. The calc-alkaline granites of the Aqaba complex were subject to a phase of deformation causing transformation to a gneissic rock with elongated feldspar trending E-NE (Jarrar, 1985). The younger Araba Unit is not affected by shear zones. The Wadi Filk mylonites are a part of the Yutum suite (Aqaba complex), which is a coarse-grained calc-alkaline granitic rock, cross-cut by younger bimodal syn-plutonic dikes (Jarrar et al., 2001, Fig. 4.1, 4.2). Mylonites developed in a rhyolithic dike that is chemically identical to the host rock granite. Jarrar (1985) reported a zircon-derived age of 608 Ma for these dikes. The studied area in the Central Eastern Desert in Egypt is part of the Nubian Shield and a western offset of the Najd shear zone system (Fig. 4.1). The rocks can be subdivided into two units: the upper Nugrus Unit

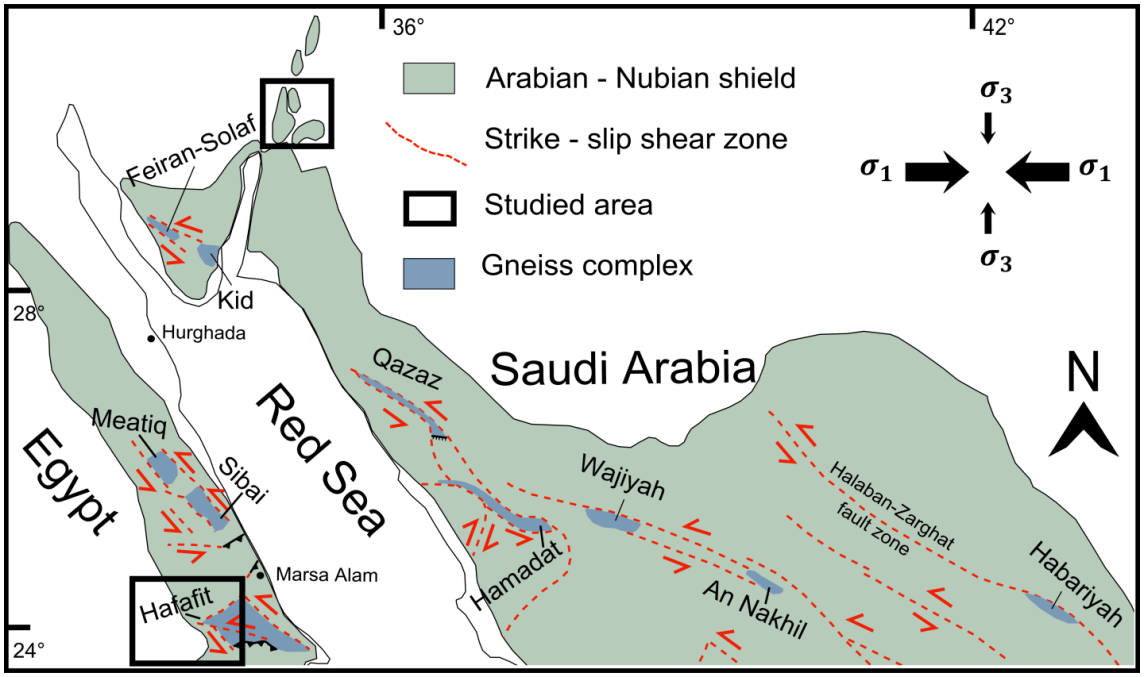

Figure 4.1 Overview map of the Arabian-Nubian Shield-modified after Meyer et al. (2014)

with mostly low-grade mica schists and ophiolitic rocks, and the Hafafit Unit consisting mainly of para- and ortho-gneisses together with amphibolite and ultramafic rocks (Abd El-Naby et al., 2008). Abd El-Naby (2008) reports two different metamorphic phases: a lower-grade greenschist facies event M1 (400 - 550 °C, 3.7 - 4.9 kbar), which is dominant in the Nugrus Unit, and an amphibolite facies event M2 (600 - 750 °C, 6-8 kbar) in the Hafafit Unit. The described metamorphic conditions are associated with collision processes around 620 - 640 Ma.

4.3 Wadi Filk mylonite - Jordan

The calk-alkaline granite in Wadi Filk is a homogenous medium- to coarse-grained rock with a matrix of quartz, plagioclase and alkali-feldspar. The undeformed granitoid shows several generations of syn-plutonic dikes (rhyolithic) with NW-SE or NE-SW trends which vary in width from 2 to15 m (Fig. 4.3a). The Wadi Filk mylonite is a NW-SE trending banded mylonitic structure (Fig. 4.3a), which consists of two vertical fine-grained ultra-mylonitic zones with a strong planar and linear fabric. Both mylonite zones show a sharp transition to the outside, and a gradual transition to the rhyolithic band between the shear zones (Fig. 4.2a, b).

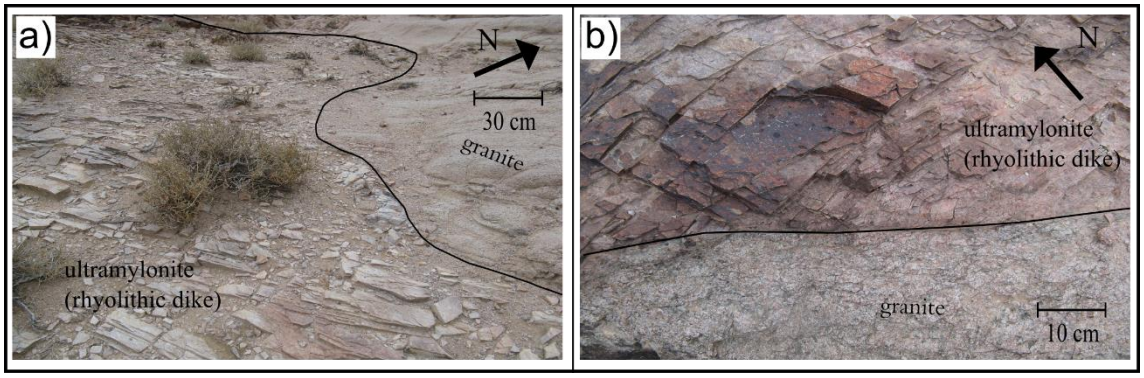

Figure 4.2 Wadi Filk mylonite; a) Curved shape of the transition zone from the granite to the rhyolithic, mylonized dike; b) Sharp boundary of the high strain zone to the undeformed granitic wall rock

The stretching lineation is subhorizontal with a NW-SE trend. The shear zones can be followed for at least several hundred metres in the existing exposure. The surrounding granite and dikes in the study area exhibit no mylonitic structures. The strain gradient is sharp towards the external granite, but gradual to the center of the dike between the two fine-grained bands.

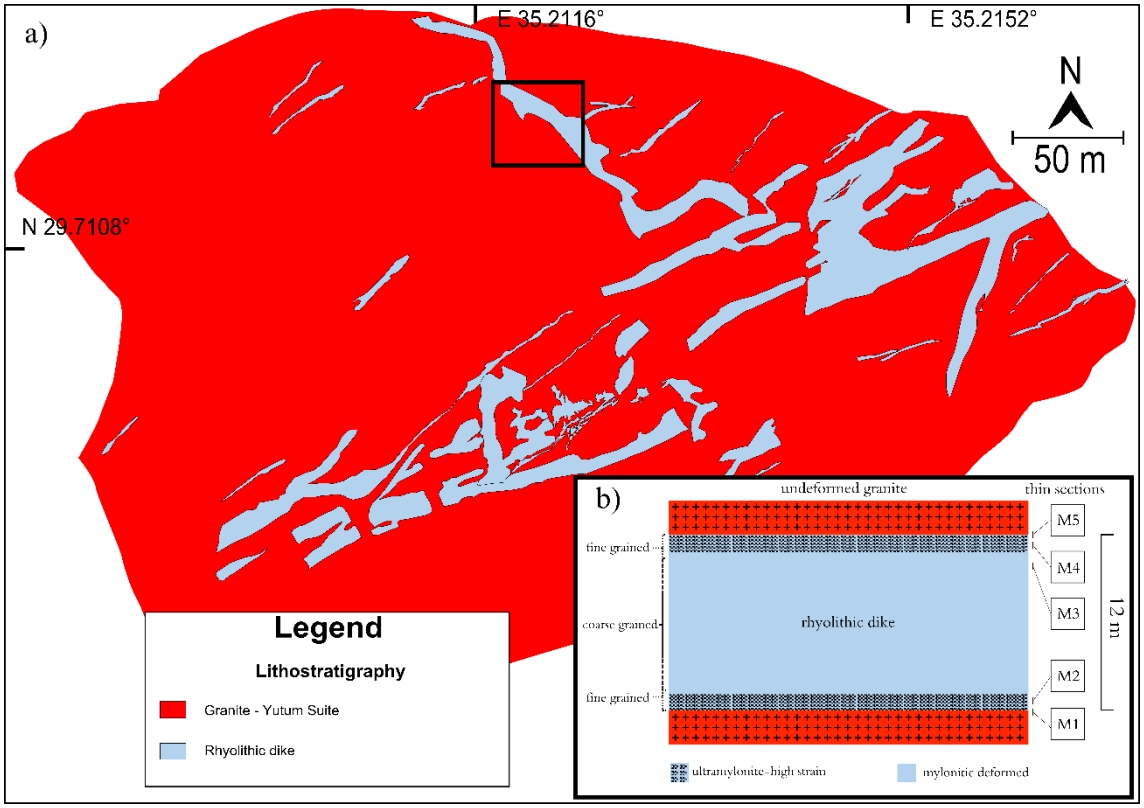

Figure 4.3 a) Overview of the granitic rock with rhyolithic dikes; b) Detailed sketch of the grain-size and the grade of deformation of the studied zone, with location of the samples M1-M5

The boundary between the fine-grained, ultra-mylonized dike material and the wall rock is usually straight line but shows local embayments which contain undeformed vein material. These were probably protected from mylonitization by the more coarse grained granitic rock (Fig. 4.2a, 4.4f). These embayments are most common on a cm scale, but some larger deviations from flat intrusion do occur (Fig. 4.2a).

4.3.1 Wadi Filk microstructure

The metamorphic grade of mylonization in the dike can be classified using recrystallization characteristics of quartz and feldspar to verify the temperature conditions (Stipp et al., 2002; Passchier and Trouw, 2005). The description of the microstructures starts with the wall rock granite (sample M1, M5, Fig. 4.2b), then deals with the inner part of the rhyolithic dike (sample M2, M3, M4, Fig. 4.2b).

The composition of the deformed coarse-grained granite (wall rock, sample M1, M5) is mostly plagioclase, K-feldspar and quartz minerals with a grain-size >400µm. Lobate grain boundaries between quartz and feldspar (Fig. 4.5a) crystals indicate the presence of a deformation phase within a higher temperature - between 550 and 600 °C (Stipp et al., 2002; Passchier and Trouw, 2005). Grain boundary migration (GBM) recrystallization fabrics are overprinted by undulose extinction and bulging recrystallization of quartz, as well as fabrics of brittle faulting, kinking and twinning structures of plagioclase. These fabrics belong to a younger second deformation phase at low- to medium-grade conditions of ~450 - 500 °C (Fig. 4.5b-d). The transition from the granite to the rhyolithic dike is a sharp curved contact, where the rhyolite has a grain-size of 30 - 200µm, much smaller than the 0.4 - 3mm grain size of the granite wall rock (Fig. 4.5d-f). The reduced grain size of the quartz-feldspar aggregate in the transition zone of the granite indicates a cohesive cataclasite behavior, where single branches of shear bands trend into the granite (Fig. 4.4, 4.5d). The large quartz grains exhibit loboid grain boundaries, indicating high-temperature grain boundary migration as the mechanism for grain growth (Fig. 4.5d). These pre-existing fabrics of the cataclastic zone are overprinted by undulose extinction and zones of small new grains of bulging to sub-grain rotation recrystallization of quartz. The second deformation features indicate a low- to medium-grade condition, and feldspar aggregates mainly behave brittle, as indicated by fracturing (Fig. 4.5e). The first 0.5 to 1 mm of the thin section of the dike is dominated by a strongly reduced, fine-grained matrix smaller than 10µm.

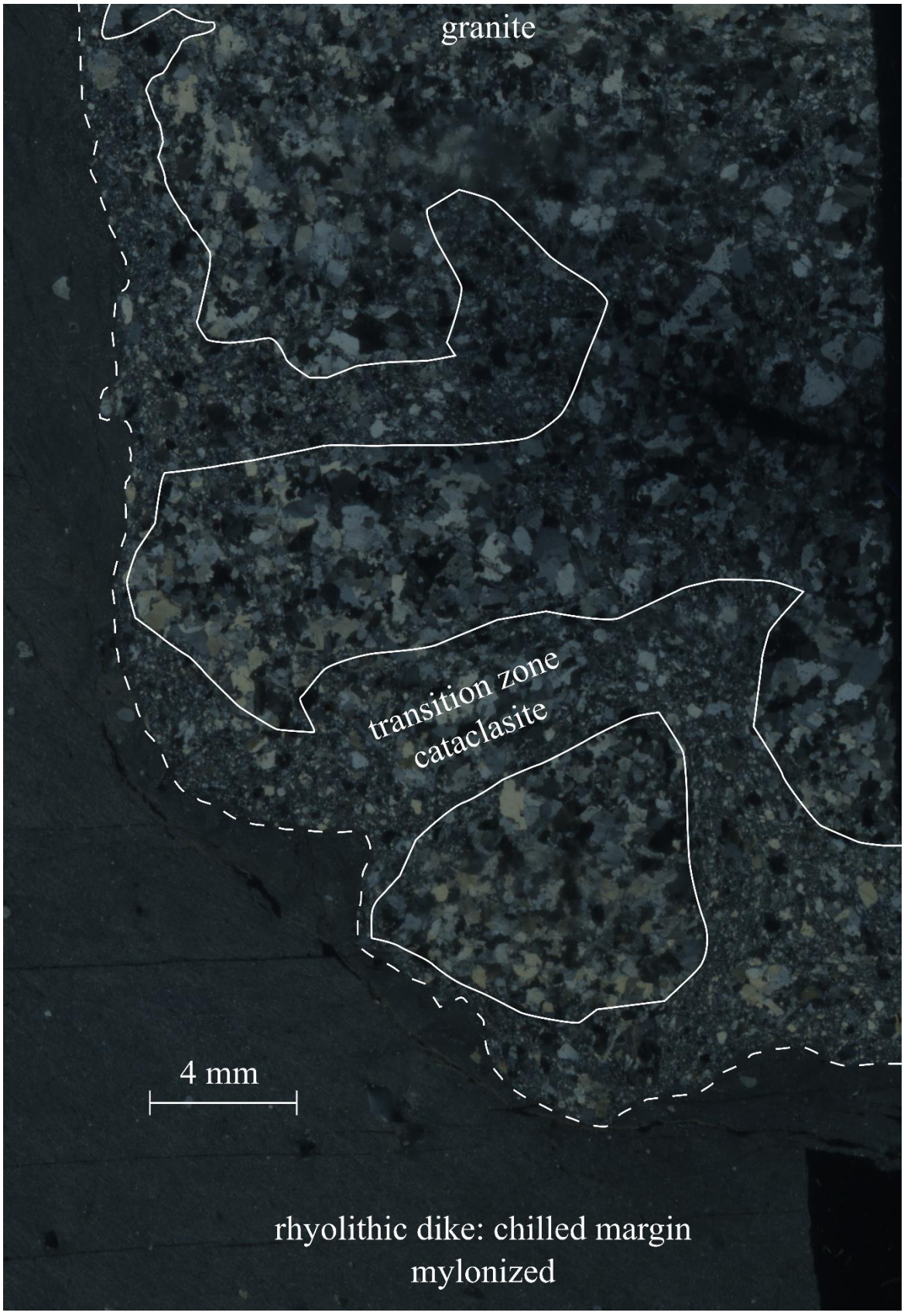

Figure 4.4 Photographic scan of M5, indicating the cataclastic fabric of the transition zone within the granite and the oriented recrystallized ground-mass of the rhyolithic chilled margin

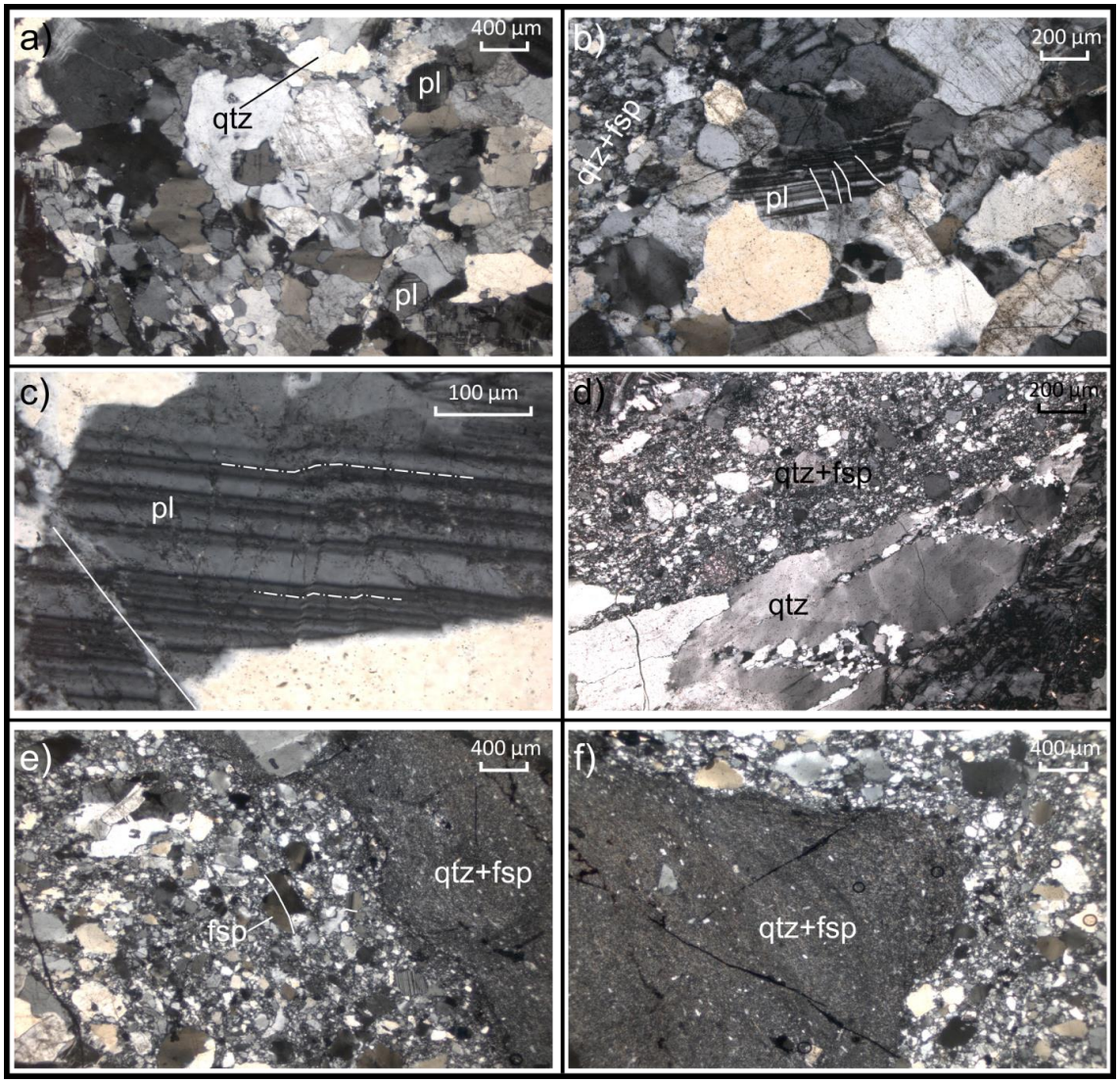

Figure 4.5 Thin section of the transition zone M1 and M5 a) Granitic wall rock, GBM of quartz and feldspar (pl) at relatively high temperature; b) brittle fracturing of plagioclase at lower temperature conditions; c) Brittle faults and kink fabrics in plagioclase; d) Upper half of the photograph shows a cataclastic shear band with a reduced grain-size of quartz and feldspar. The lower half shows a quartz grain with undulose extinction and bulging or subgrain rotation recrystallization (greenschist facies); e) Reduced grain size due to cataclastis with brittle fracturing of feldspar in the center (marked by a white line); f) Curvy trend of the transition zone, from the more coarse grained granite to the fine-grained matrix of quartz and feldspar with single feldspar porphyroclasts

The ultramylonitic matrix with a grain-size of ~30µm is mainly a mixture of dynamically recrystallized quartz and small feldspar grains. The ultramylonitic matrix contains a number of idiomorphic to hypidiomorphic porphyroclasts of feldspar and quartz. The feldspar porphyroclasts in the very fine-grained matrix show no evidence of deformation, whereas the feldspar component within the slightly more coarse-grained matrix (< 30µm) indicates brittle fracturing (Fig. 4.6a, b). The quartz aggregates are strongly deformed to sigmoids

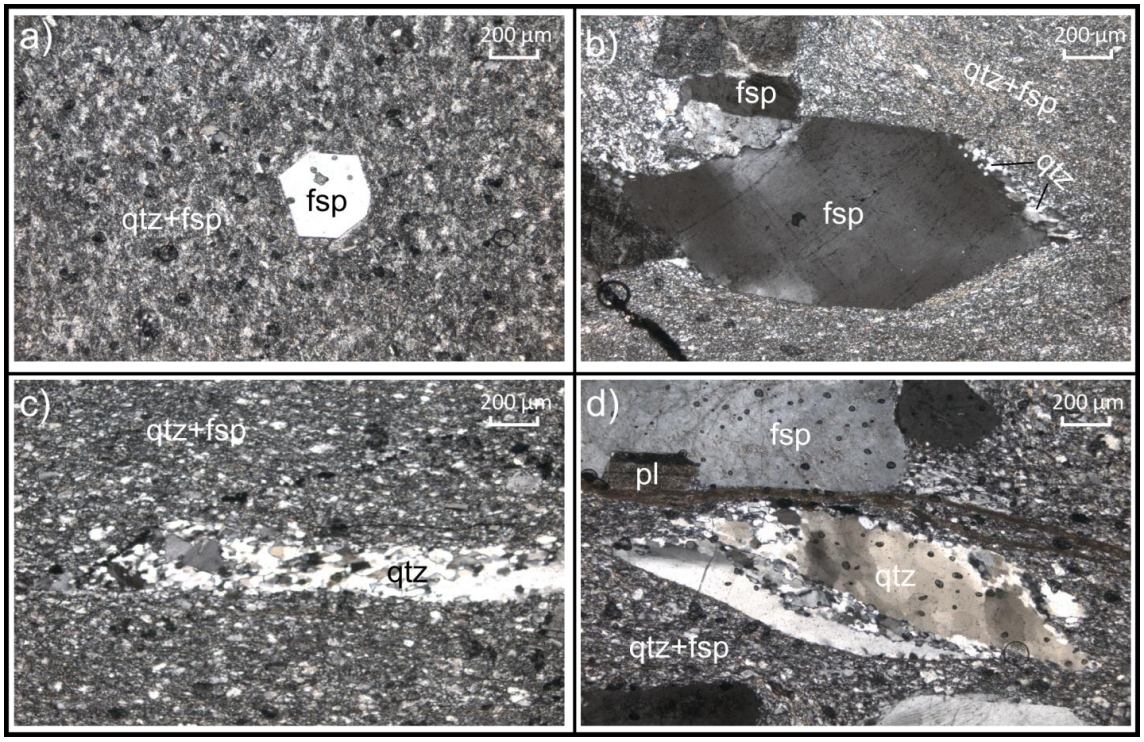

Figure 4.6 Thin section from the mylonites within the dike M2-M4, a) Undeformed K-feldspar porphyroclast in a fine grained quartzo - feldspathic ground mass; b) Feldspar porphyroclast forms sigma object with stair-stepping wing structure of recrystallized quartz grains; c) Quartz ribbon shaped fabrics in a quartzo-feldspathic ground-mas; d) Sigma shaped quartz porphyroclast indicating sinistral shear sense, new grains formed by bulging or subgrain rotation recrystallization

with an elongate shape (Fig. 4.6d, sinistral shear sense) partly affected by bulging or sub-grain rotation recrystallization (Fig. 4.6d). The volume of the recrystallized new grains varies from aggregate to aggregate, which indicates a variation in strain-rate within the shear zone under low- to medium-grade deformation conditions (450-500 °C). The thin section of the central part of the ultramylonite zone (M2, M4) is dominated by dynamic recrystallization of quartz. The fine-grained matrix exhibits a higher number of feldspar and quartz clasts, where plagioclase clasts are commonly developed into sigma structures with stair stepping to the left, indicating a sinistral shear sense. The wings are equidimensional grains of quartz, recrystallized by the bulging or sub-grain rotation mechanism (Fig. 4.6b). The quartz aggregates form elongated to ribbon-shaped fabrics, suggesting a higher strain-rate. The elongated quartz aggregates are composed of 20-30 % new grains and formed sigma objects with a sinistral shear sense (Fig. 4.6d). Furthermore, the thin section includes diagonal veins at an angle of 45 ° to the flow direction, filled by well-

developed spessartine minerals (garnet family), which represents medium grade conditions and suggests a similar trend for the temperature field as indicated by the described microstructures.

Thin section M3 is closer to the centre of the dike and shows a high number of porphyroclasts with a grain size >500µm. The phenocrysts of quartz have an elongated shape and provide evidence of subgrain rotation recrystallization, similar to the previous thin sections. The quartz aggregate forms mostly elongated fabrics and no ribbon shaped structures, whereas feldspar shows no evidence of ductile deformation. The deformation occured at low- to medium-grade with a temperature of 450-500 °C.

4.3.2 Quartz crystallographic preferred orientation (CPO) of Wadi Filk

The deformation of crystals by dislocation glide is characterized by movement of the dislocations along a specific crystallographic plane (Passchier and Trouw, 2005). The combination of a specific slip plane and a slip direction is called as a slip system. During deformation, single or multiple slip systems at different orientations in the crystal can operate simultaneously. The activity of the slip systems depends strongly on the metamorphic (temperature) and stress (strain-rate, differential stress) conditions during the deformation phase. An analysis of the c-axis orientation of quartz in the deformed granitoid rocks of Wadi Filk was carried out in order to determine the temperatures and kinematic conditions of deformation in the mylonites. Measurements were performed using a Fabric Analyser microscope (Prototype G60, Wilson et al., 2007; Wilson and Peternell, 2012), and the software INVESTIGATOR (Peternell et al., 2009) to select the orientation of the c-axis of each quartz mineral, with a resolution of 10µm. The quartz crystallographic preferred orientation was determined in three samples: One from the granite wall rock together with the transition zone and two from the mylonized rhyolithic dike. The distribution of the quartz c-axes of the coarse-grained granitic wall rock (sample M1) shows a distinct maximum close to the stretching lineation (L), which implies mainly prism <c> slip activity (Fig. 4.7a). Such a slip system operates under very high temperature conditions between 500 and 700 °C (Lister and Dornsiepen, 1982; Blumenfeld et al., 1986; Mainprice et al., 1986; Stipp et al., 2002; Peternell et al., 2010), which confirms

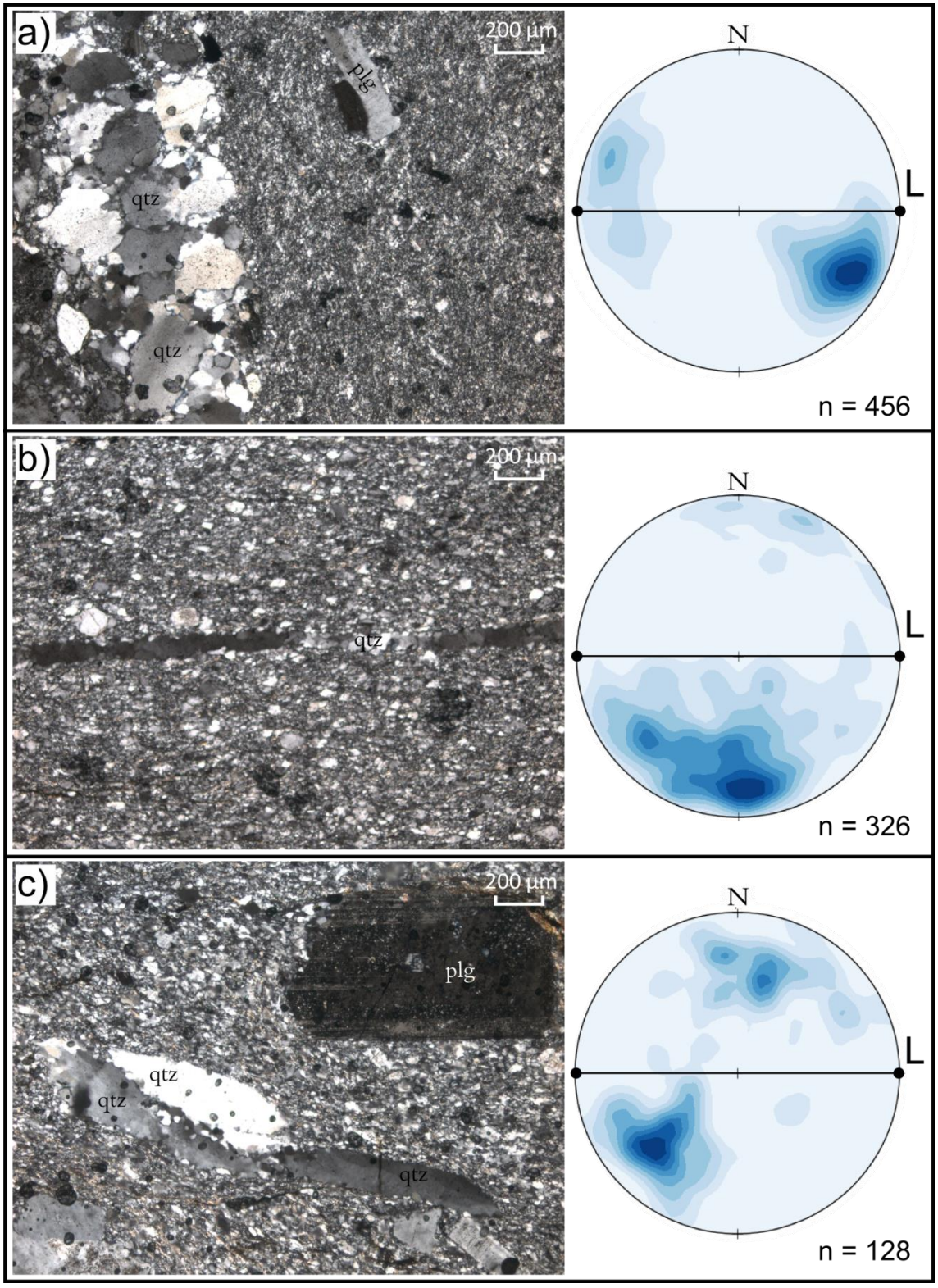

Figure 4.7 Photomicrographs from the mylonite in Wadi Filk and quartz c-axis orientation stereonets with contours = 0.5-0.8 (equal area projection, lower hemisphere; vertical foliation (black line), mineral lineation L = E - W (black circles)); a) Sample M1, the transition zone of the granite to the dike, stereogram indicates prism <c> slip implying high temperature deformation conditions; b) Sample M4, ribbon-shaped quartz in a recrystallized matrix of quartz. Basal <a> to rhomb <a+c> slip indicate temperatures below greenschist facies; c) Sample M3, elongated quartz aggregates with a sigma fabric (sinistral shear sense) containing undeformed plagioclase. Rhomb <a+c >to basal <a> slip indicate the same temperature conditions as in (b)

the observation of the microstructures in the previous section 4.3.1. The transition zone is characterized by a reduced grain size of the wall rock and a strongly deformed fine-grained matrix (<30µm) with larger components of quartz and feldspar, which show a variation in grain-size from 30 to 200µm (Fig. 4.7a). The larger quartz grains exhibit the same high temperature conditions as observed in the coarse-grained granite, with mainly prism <c> slip activation. The quartz c-axis of the fine-grained matrix could not be determined due to the limited resolution of the Fabric Analyser. The ultramylonite begins beyond a transition zone (sample M2, M4; Fig. 4.3b, 4.4). The quartz c-axis of the recrystallized ground-mass and porphyroclasts form a type I crossed girdle with active basal <a> to rhomb <a+c> slip (Fig. 4.7b), indicating deformation at sub-greenschist facies conditions (300 - 400 °C). Sample M3 (Fig. 4.7b), which is from a section closer to the center of the dike shows a similar trend in the recrystallized matrix. The c-axis distribution of the quartz is characterized by prominent near-X and -Z maxima, with active rhomb <a+c> to basal <a> slip (Fig. 4.7c). These slip systems in quartz imply the same greenschist facies conditions during deformation as in thin section M2-M4.

4.4 Hafafit mylonite shear zone - an example from Egypt

The studied area is an outcrop in the south of Wadi Hafafit, on the granitic gneiss-amphibolite boundary. Abd El-Naby et al., (2008) described three different groups of amphibolites, the study area belongs to the third group with mainly plagioclase, amphibole, quartz and ilmenite (Hafafit Unit).

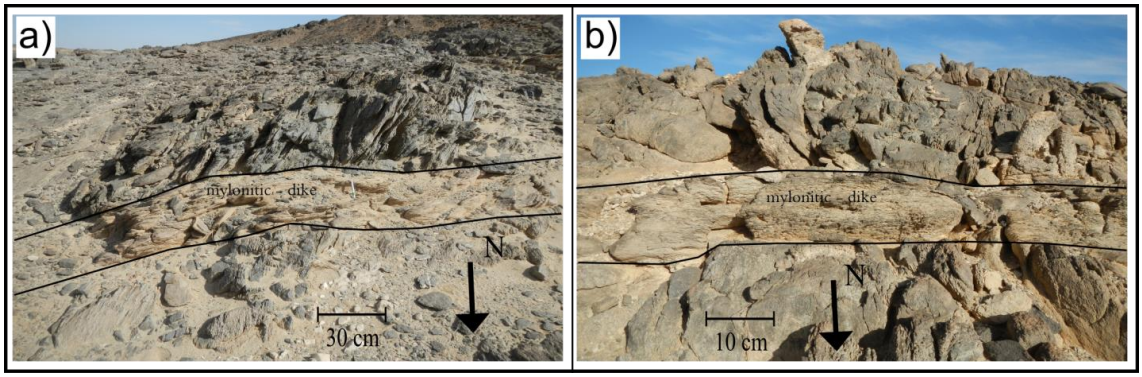

Figure 4.8 Wadi Hafafit mylonite; a-b) Mylonitised granite dike shows a sharp boundary to the wall rock. The amphibolite host rock shows no effect from the deformation in the granite dykes

The amphibolites contain a number of NW-SE and NE-SW-trending dikes with granitic composition, which have been strongly deformed to mylonite. The strain gradient is sharp to the wall rock (amphibolites), where the older foliation (with a steep dip) is cut by a strongly mylonitic foliation in the horizontally-dipping dikes, nearly at right angles to the foliation in the wall rock (Fig. 4.8a, b). The wall rock shows no evidence of deformation, and the transition from the undeformed rock to the high-strain zone is a millimeter-scale sharp boundary. The older foliation of the amphibolites shows no effect from deformation within the dikes.

4.4.1 Microscale observations

We describe the microstructures in the thin sections of the Hafafit mylonite in Egypt, starting with the wall rock (amphibolite, HF7, HF8) and moving on to the inner part of the mylonized dike (HF9-HF10). The wall rock (sample HF7) is characterized by an amphibolite facies paragenesis, with quartz, feldspar and amphibole as the dominant minerals. The coarse-grained matrix of quartz and feldspars show typical curved boundaries with lobate - cuspate fabrics, typical of grain boundary migration recrystallization at high-grade conditions > 600 °C (Fig. 4.9a, b).

The next thin section (HF8) also belongs to the wall rock, but was sampled closer to the transition zone to the mylonized dike. The microstructures indicates similar conditions, with well-developed lobate fabrics of feldspar (Fig. 4.9b). In addition, the quartz aggregates indicate a chessboard extinction fabric within the GBM-recrystallization, indicating a high-temperature sub-grain formation at ~630 °C (Stipp et al., 2002). In comparison to the previous thin section, the quartz boundaries on a few of the grains exhibit a weak bulging recrystallization together with a more strongly-developed undulose extinction, which overprint the pre-existing lobate fabrics. The feldspar crystals show no evidence of overprinting, therefore the second deformation phase can be determined as having occurred at a temperature of ~300 °C. Thin section HF9 is part of the mylonized dike behind the transition zone. The grain-size is clearly smaller at ~100µm for the feldspar and the quartz aggregates. Quartz and feldspar reveal an older deformation phase with classical lobate fabrics (GBM-recrystallization), strongly overprinted by bulging to subgrain rotation recrystallization. In the higher strain parts of the sample C-type shear band cleavage (C/S fabric) occurs with a sinistral shear sense, where the S-planes are

formed by elongated grains and parallel subgrains of quartz (Fig. 4.9c). The strongly deformed elongated quartz aggregates are part of a pre-existing high-grade structure (GBM-recrystallization), which is overprinted by a medium-grade deformation phase shown by subgrain rotation recrystallization.

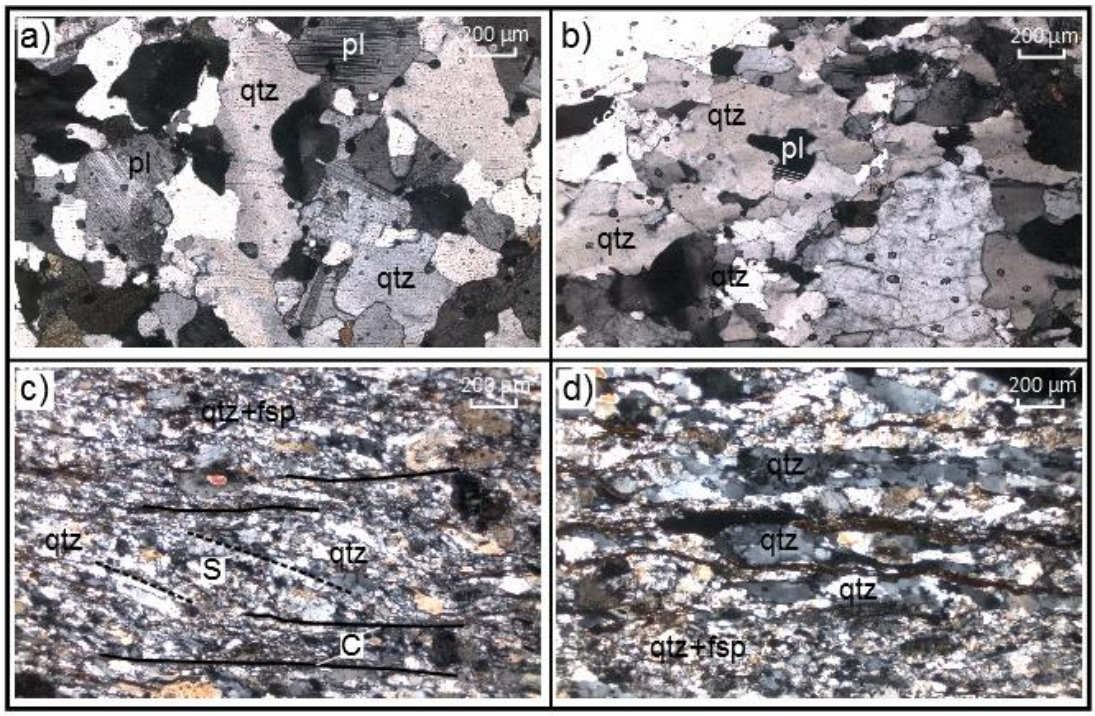

Figure 4.9 Micrographs of the Wadi Hafafit deformation structures; a) Lobate fabrics of the quartz boundaries, indicating a deformation phase under a high-grade condition by GBM-recrystallization (wall rock, HF8); b) Similar high temperature fabrics, shown by a lobate fabric of plagioclase in quartz in the center, quartz grains indicate a overprinting by undulose extinction; c) Mylonite zone with C-type shear band cleavage, where the S-planes are elongated quartz aggregates, sinistral shear sense; d) Quartz ribbon structures with bulging to subgrain rotation recrystallization as the main mechanism, indicating a low to medium grade conditions of the deformation

The center of the mylonized dike (sample HF10) exhibits a similar strong low- to medium-grade deformation, but differs from sample HF9 by elongated quartz aggregates, which start to form ribbon-shaped fabrics of quartz (Fig. 4.9d). The irregular grain boundaries of the quartz ribbons are due to an older GBM-recrystallization, which is overprinted by subgrain rotation recrystallization.

4.4.2 Quartz crystallographic preferred orientation in Wadi Hafafit

A quartz crystallographically-preferred orientation analysis was executed on four thin sections from the Wadi Hafafit location. Two of the samples are from the amphibolite wall rock and two belong to the mylonized dike.

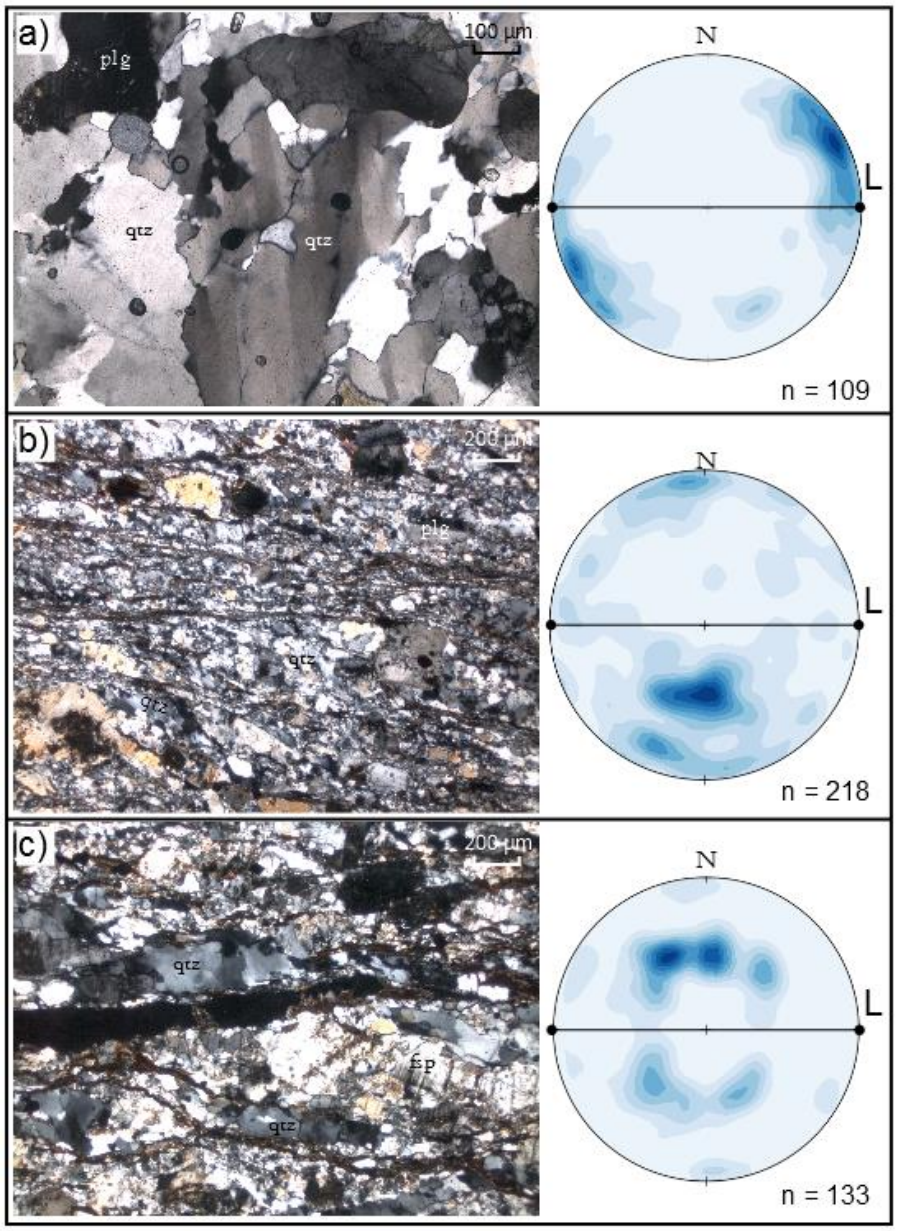

Figure 4.10 Photomicrographs of the mylonite in Wadi Hafafit and associated quartz c-axis orientation patterns, stereonets with contours = 0.5-0.9. Equal area projection, lower hemisphere; vertical foliation (black line), mineral lineation L = E-W (black circles)); a) Sample HF8 from the wall rock amphibolite with GBM- recrystallization, chessboard subgrain fabrics of quartz and evidence for active prism <c> slip; b) C-type shear band cleavage with elongated quartz aggregates (sinistral shear sense) with active rhomb <a+c> to basal <a> slip ; c) Ribbon-shaped quartz aggregates with a c-axis orientation maxima around the Y-axis, indicating weak prism <c> and rhomb <a> slip activity

The quartz c-axis patterns of samples HF7 and HF8 (wall rock) indicate mainly prism <c> slip activity (Fig. 4.9a) with a distinct maximum close to the lineation (L), characteristic of high-temperature deformation (~700 °C). In addition, the distribution of the measurement shows a weak maximum for basal <a> slip activity. The combination of active prism<c> slip, together with basal <a> is typical for high-temperature quartz subgrain deformation in which a chessboard subgrain fabric is formed (Blumenfeld et al, 1986; Mainprice et al., 1986; Kruhl, 1986). The high-temperature trend is confirmed in the microstructures by the presence of typical GBM-recrystallization features (Fig. 4.10a; Stipp et al., 2002). The transition to the mylonized dike (HF9) is characterized by a change of the quartz c-axis orientation in comparison to the previous samples (HF7, HF8), the maxima is more close to Y-axis (Fig. 10b), indicating a rhomb <a+c> ± basal <a> slip activity. The temperature of the deformation can be classified from low to medium grade condition (~400 – 500 °C). Sample HF10 is part of the center of the dike, and shows quartz c-axis maxima in a small circle around the Y-axis (Fig. 4.10c). This distribution indicates weak rhomb <a> ± prism <c> slip activity, characteristic for medium to high-grade conditions of deformation (~500 °C).

4.5 Discussion

4.5.1 Lithology driven shear zones - Wadi Filk

The field geometry of the paired mylonite zone of Wadi Filk was originally interpreted as two mylonite zones that nucleated spontaneously in the host granite and grew parallel because of a uniform stress field in the granite. The rhyolite between the shear zones has a similar field aspect as the main granite, although it is slightly finer grained. The chemical composition of the rock outside and between the shear zones is almost identical. Only the presence of undeformed fine-grained rhyolite pockets in the margins of the shear zones show, that the fine-grained rhyolite margins acted as a nucleation site for ductile mylonitization. The contact between the undeformed external granite and the mylonites is not everywhere tectonic; in many sites, an apparently intrusive contact exists between undeformed granite and undeformed fine-grained rhyolite. The fine-grained mylonite can therefore be explained as the mylonitised rhyolithic edges of a planar intrusion into the host granite. The granitic rock of Wadi filk belongs to the Yutum suite dated at appr. 608

Ma (Jarrar et al., 2003). During this time period, the collision of West and East Gondwana led to an E-W shortening with a northwards escape tectonic (Burke and Sengör, 1986; Stern, 1994; Abdelsalam and Stern, 1996). The rhyolithic dike in the granite trends NW-SE. From the microstructures and crystallographic preferred orientation we suggest the following scenario: the calk-alkaline granitic rock of Wadi Filk underwent a first deformation phase under a high temperature conditions, forming lobate grain boundaries of quartz to feldspar aggregates (GBM-recrystallization) in combination with a strong

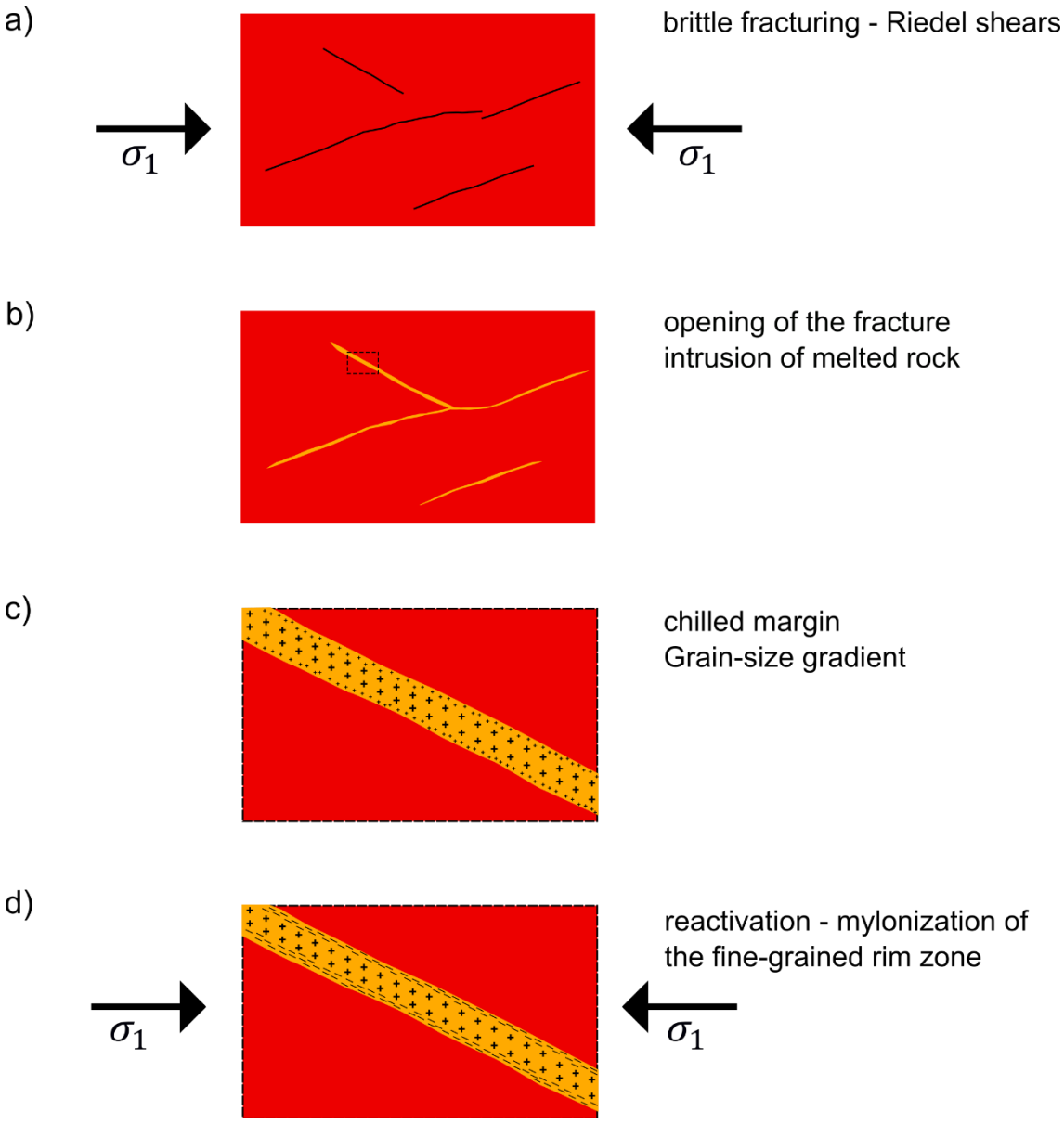

Figure 4.11 Development of the paired shear zones in Wadi Filk. a) brittle fracturing in a simple shear regime (Riedel shearing); b) Intrusion of the rhyolithic melt in the cataclastic zone; c) Enlarged from (b) - The low temperature of the granite wall rock led to a chilled margin effect of the rim zone and development of a smaller grain-size; d) enlarged from (b) - Reactivation of the fine-grained rim zone and overprinting by a ductile shear zone under greenschist facies conditions

crystallographic preferred orientation of the quartz c-axes (mainly prism <c> slip). The dikes in the granite may have opened as extensional fractures, which could be explained by two different orientation of the minimum principal stress axis (σ_3) and therefore a change of the stress direction during the development of the dike. Alternatively, the dike could form in simple shear deformation with an E-W oriented maximum compressive stress, where Riedel shears developed with synthetic (R) and antithetic (R') geometry and with a NW-SE and SW-NE trend (Fig. 4.11a). The relatively straight trend of the boundary zones, the angular grain fragments with a variation in the grain-size and the generally reduced grain-size of the transition zone in the granite indicate an initial a cataclastic event of Riedel shearing generating a brittle fracture (Fig. 4.4). At a later stage, the rhyolithic melt with an equal chemical composition to the surrounded granite intruded into the brittle fracture (Fig. 4.11b). A similar emplacement of a dike into a Riedel shear structure is reported in Xu et al., (2013) for an example from central Mexico. The crystallographic preferred orientation of quartz aggregates along the contact, with a grain-size of 30 to 150µm, indicates mainly active prism <c> slip characteristic of high temperature deformation. These quartz grains are part of the really fined grained transition zone, and suggest the theory of a cataclastic behavior, where the add-on rhyolithic intrusion contains fragments of the quartz feldspar grains from the wall rock (Fig. 4.12a). The grain-size to the margin of the dike is obvious smaller in comparison to the central part, which can be interpreted as a chilled margin of the rhyolithic intrusion (Fig. 4.11c). Studies on polymineralic rocks (quartzo-feldspatic composition) has shown, that feldspar defines the strength of the rock during the deformation under greenschist facies condition (Jordan, 1988; Tullis, 1990). The fine-grained quartzo - feldspathic ground-mass of the rim zones of the rhyolithic dike implied therefore as a mechanical anisotropy in comparison to the surrounded coarsed grained granite. The orientation angle of the Wadi Filk rhyolithic dike at 45° to N is an ideal orientation to initiate a shear zone in a simple shear regime for an E-W σ_1-direction. Finally the ductile shear zones localized on both margins of the dike (Fig. 4.11d). The microstructures and the CPO data exhibit a dominant deformation under low to medium grade conditions by typical bulging or subgrain rotation recrystallization of quartz porphyclasts and of the ground-mass, whereas feldspar aggregates show brittle fabrics and twinning and undulose extinction. Sigmoids of elongated quartz aggregates in the ultramylonite zones indicate a sinistral shear sense, which agrees with orientation of the shear-plane in an E-W shortening regime (Fig. 4.6d, 4.12b). The development of

syntectonic diagonal veins of spessartine grains in the ultramylonite imply an opening of the extensional fractures vertical to N-S and agree with the interpreted σ_1-direction (Fig. 4.12d). Spessartine is a typical indicator for low temperature condition (Theye et al., 1996) and agrees with the interpretation of the microstructure. The presence of elongated sigma objects, a core-mantle structures and ribbon-shaped quartz bands in the ultramylonite indicate a concentration of high strain-rate along the rim zones. The shear strain decreases continuously to the more coarse-grained center of the dike, which represent a larger grain-size similar to the surrounded rocks. This example shows the strong dependence of shear zone localization to pre-existing lithology.

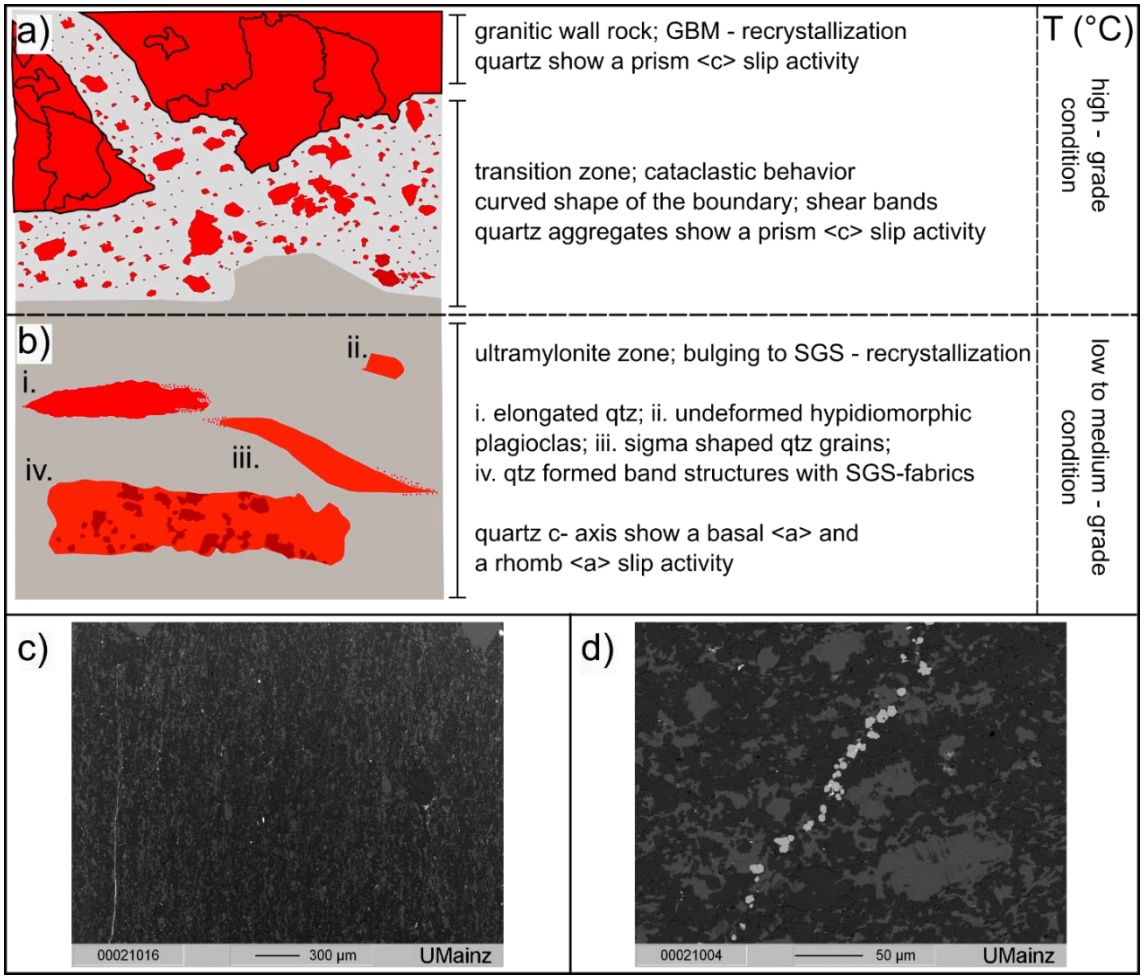

Figure 4.12 Micro-graphical overview of the Wadi Filk; a) The granite to the transition zone and a metamorphic grade of the deformation; b) Overview of shear fabrics in the ultramylonite zone with a description of the metamorphic grade of the deformation c) Ultramylonite ground-mass with oriented, elongated recrystallized quartz grains (grey color), the larger grey colored grains are plagioclase, the dark colored mineral are mainly K-feldspar; d) Diagonal trending vein of spessartine grains, with 45° degree to the shear direction

The similarities in the grade of deformation of the shear zones on both rims and the equal distribution of the strain-fabrics within the shear planes to the center of the dike suggest a simultaneously development of these paired shear zones. In fact, the orientation of the ductile shear zones together with deformation under greenschist facies conditions and the sinistral shear sense show close association to large-scale shear zones of the Najd shear zone system in the Arabian-Nubian Shield (Stern, 1994). Most of the shear zones in the Najd fault system show evidence of a ductile deformation under similar conditions.

4.5.2 A new setting to nucleate paired shear zones

Ductile shear zones are clearly defined zones of high strain in a less deformed host rock (Ramsay, 1980), but natural examples differ in their characteristics of length, width and strain-rate. In contrast to these variations, the shear zones show similarities in their nucleation mechanisms. Shear zones can occur as single structures or in a system with different shear zone branches, as described for homogeneous plutonic rocks by Ramsay and Graham (1970). Such shear zones are characterized by a high strain core with a foliation at a small angle to the shear zone plane, grading to a weak foliation at ~45° to the incipient shear zone plane in the low strain margin (Ramsay, 1980; Ramsay and Huber, 1983). A different situation occurs in the case of reactivation of a pre-existing structure such as a dike by a ductile shear zone. This leads to a sharp strain contrast to the wall rock, as observed on both field examples described above (Fig. 4.2, Fig. 4.8). In either case the wall rock is undeformed, whereas a strong mylonised foliation developed within the dike. If an older foliation is present in the wall rock, this may lie at a high-angle to the newly formed second foliation, separated by the sharp boundary of the dike. A similar structure of a dike-related shear zone with a strong strain-gradient to the wall rock was reported by Christiansen and Pollard (1997) in the Sierra Nevada, where a shear zone localized in a fine grained aplite dike. This structure shows similarity with the Hafafit example by localization of a single shear zone within the dike, as a result of the finer grain-size and different rock composition of the dike with respect to the wall rock. Another field example is described from the Tauern Window (Eastern Alps) where a lamprophyre dike exhibits a similar structure, reported by Pennacchioni and Mancktelow (2007). The paired shear zones from Jordan (Wadi Filk) are different in comparison to other published structures. In our example, the rock composition of the dike and the sur-

rounding rock is equal, but the grain-size difference of the rims initiated two simultaneously active shear zones unlike the structure of Christiansen and Pollard (1997). Similar features of paired shear zones were presented by Mancktelow and Pennacchioni (2005) in metagranidioirits from the Tauern Window (Eastern Alps). They proposed the development of initial brittle fractures, where fluids interact to form a bleached halo on both sides of the vein or dike. These rheological weaker zones on both rims of the haloes were reactivated by a ductile shear zone. These published structures also differ from our example in that the shear zones developed in the neighbor rock along the halos, whereas the localization of the Wadi Filk shear zones is restricted to the rims of the dike and shows a sharp contrast of strain to the undeformed granitic wall rock. A further similar structure is reported by Pennacchioni and Mancktelow (2007) in aplite and lamprophyre dikes at the same location of the Trauern Window. They described aplite dikes with localized shear zones on the boundaries to granodiorite, where the central part of the dike shows less deformation (nearly undeformed). This example looks fairly similar to our field observation of Wadi Filk, but the difference is that the surrounded granodiorite shows evidence of shearing along the boundaries. The pre-existing foliation of the granodiorite (wall rock) changed orientation and trend into the shear direction, whereas the granitic wall rock of the Wadi Filk shows no evidence of deformation. The newly presented structure of Wadi Filk is a new type of a lithology driven nucleation to form paired ductile shear zones. The evolution of such a paired structure is similar to the described theories for reactivation of pre-existing structures associated with shear zones (Christiansen and Pollard 1997; Mancktelow and Pennacchioni, 2005). The presence of this kind of grain-size based structure is a potential source of error for the interpretation of paired shear zones in the field. The ultramylonites show identical chemical composition with the surrounded rocks. The fine grain-size in the mylonites can therefore easily be mis-interpreted as a product of recrystallization, which nevertheless played an important role during deformation. However, the shear zone localization is determined by the location and orientation of the pre-existing intrusive structure and therefore accommodated to the trend of the dike, which exerts an influence on the geometry of the shear zone.

4.6 Conclusions

The development of two parallel ductile shear zones formed in greenschist facies was geometrically influenced by a pre-existing structure. A continuously established background strain produced a network of Riedel shear zones in a semi-brittle regime, where cataclastic zones were traced and replaced by younger syntectonic intrusions. The smaller grain-size, in the chilled margin along the boundaries of the dike, led to a mechanical anisotropic contrast to the chemistry identical surrounded granitic rock. In a later stage of deformation, the increase of deformation reactivated the pre-existing structure and formed paired shear zones. The grain-size difference is the key to develop such a lithology driven shear zone, whereas the wall rock behind the transition zone showed no evidences of deformation. The shear zone localization is characterized by a sharp contrast of high strain along the margins of the dike and a near undeformed wall rock. Similar structures are observed in other regions, whereby these structures differ by the number of the shear localization or that further rheological properties e.g. a different rock composition played a further role in the development of the shear zones. Furthermore the Wadi Filk mylonites show that even the edge areas of the Arabian-Nubian Shield were influenced by a E-W shortening, which formed by a continuously background strain a shear zone.

4.7 References

Abd El-Naby, H., Frisch, W. and Siebel, W., 2008. Tectonometamorphic evolution of the Wadi Hafafit Culmination (central Eastern Desert, Egypt). Implication for Neoproterozoic core complex exhumation in NE Africa: Geologica Acta, 6, 293-312.

Abdelsalam, M.G., and Stern, R.J., 1996. Sutures and shear zones in the Arabian-Nubian Shield: J. African Earth Sciences, V. 23, No. 3, p. 289-310.

Arbaret, L., and Burg, J. P., 2003. Complex flow in lowest crustal, anastomosing mylonites: strain gradients in a Kohistan gabbro, northern Pakistan. Journal of Geophysical Research-Solid Earth 108, art. no. 2467.

Bell, T.H., and Etheridge, M.A., 1976. Deformation and recrystallization of quartz in a mylonite zone, central Australia. Tectonophysics 32 (3-4), 235-267.

Blumenfeld, P., Mainprice, D. and Bouchez, J. L., 1986. C-slip in quartz from subsoildus deformed granite. Tectonophysics, 127, 97-115.

Brook, M., Ibrahim, K. M., and McCourt, W. J., 1990. New geochronological data from The Arabian Shield area of southwest Jordan. In: Proceedings of the 3rd Jordanian Geological. Conference, Amman, Jordan, pp. 361-394.

Burg, J. P., and Laurent, Ph., 1978. Strain analysis of a shear zone in a granodiorite. Tectonophysics 47, 15-42.

Burke, K., and Sengör, C., 1986. Tectonic escape in the evolution of the continental crust, in Reflection Seismology: The Continental Crust, (ed. M. Barazangi, L. Brown), Geodyn. Ser. 14, pp. 41-53. Washington, DC: Am. Geophys. Union.

Cobbold, P. R., 1977a. Description and origin of banded deformation structures. I. Regional strain, local perturbations, and deformation bands. Canadian Journal of Earth Sciences 14, 1721-1731.

Cobbold, P. R., 1977b. Description and origin of banded deformation structures. II. Rheology and the growth of banded perturbations. Canadian Journal of Earth Sciences 14, 2510-2523.

Coward, M. P., 1976. Strain within ductile shear zones. Tectonophysics 34, 181-197.

Christiansen, P.P., and Pollard, D.D., 1997. Nucleation, growth and structural development of mylonitic shear zones in granitic rocks. Journal of Structural Geology 19, 1159-1172.

Fusseis, F., Handy, M.R., and Schrank, C., 2006. Networking of shear zones at the brittle-to-viscous transition (Cap de Creus, NE Spain). Journal of Structural Geology 28, 1228-1243.

Guermani, A., and Pennacchioni, G., 1998. Brittle precursors of plastic deformation in a granite: an example from the Mont Blanc massif (Helvetic, western Alps). Journal of Structural Geology 20, 135-148.

Gueydan, F., Leroy, Y. M., Jolivet, L., and Agard, P., 2003. Analysis of continental midcrustal strain localization induced by reaction-softening and microfracturing. J. Geophys. Res. 108 (B2), 2064. http://dx.doi.org/10.1029/2001JB000611.

Gueydan, F., J. Précigout, and L. G. J. Montési (2014), Strain weakening enables continental plate tectonics, Tectonophysics, Volume 631, p. 189-196.

Hobbs, B.E., Means, W.D., and Williams, P.F., 1976. An Outline of Structural Geology. John Wiley and Sons, 278-280.

Ingles, J., Lamouroux, C., Soula, J. -C., Guerrero, N., and Debat, P., 1999. Nucleation of ductile shear zones in a granodiorite under greenschist facies conditions, Ne´ouvielle massif, Pyrenees, France. Journal of Structural Geology 21, 555-576.

Jarrar, G., 1985. Late Proterozoic crustal evolution of the Arabian Nubian Shield in the Wadi Araba area, SW-Jordan. Geol J. B61, 3-87.

Jarrar, G., 2001. The youngest Neoproterozoic Mafic Dike Suite in the Arabian Shield mildly alkaline dolerites from South Jordan-their geochemistry and petrogenesis. Geol. Mag.138, 309-323.

Jarrar, G., Wachendorf, H., and Zachmann, D., 1993. A Pan-African pluton intruding the Saramuj Conglomerate, South-west Jordan. Geol. Rundsch. 82, 121-135.

Jarrar, G., Stern, R.J., Saffarini, G., and Al-Zubi, H., 2003. Late- and post-orogenic Neoproterozoic intrusions of Jordan: implications for crustal growth in the northernmost segment of the East African Orogen. Precambrian Research, 123, 295-320.

Jordan, P., 1988. The rheology of polymineralic rocks-an approach. Geologische Rundschau 71, 2855294.

Kronenberg, A. K., Segall, P., and Wolf, G. H., 1990. Hydrolytic weakening and penetrative deformation within a natural shear zone. Geophysical Monograph, 56, 2136.

Kruhl, J. H., 1986. Textures and c-axis orientations of deformed quartz crystals from porphyric dikes of the Alpine ‘Root Zone’ (Western Alps). Geologisch. Rundsch. 75, 601-623.

Lister, G. S., and Dornsiepen, U. F., 1982. Fabric transitions in the Saxony granulite terrain. Journal of Structural Geology 4, 81±92.

Mainprice, D., Bouchez, J. L., Blumenfeld, P., and Tubia, J. M., 1986. Dominant c-slip innaturally deformed quartz: implications for dramatic plastic softening at high temperature. Geology 14, 819-822.

Mancktelow, N.S., 2002. Finite-element modelling of shear zone development in viscoelastic materials and its implications for localisation of partial melting. Journal of Structural Geology 24, 1045-1053.

Mancktelow, N.S., 2006. How ductile are ductile shear zones? Geology 34, 345-348.

Mancktelow, N. S., and Pennacchioni, G., 2005. The control of precursor brittle fracture and fluid rock interaction on the development of single and paired ductile shear zones. Journal of Structural Geology 27, 645-661.

Meyer S. E., Kaus, B. J. P., and Passchier, C. W., in review. Numerical models of branching brittle and ductile shear zones. Geochemistry Geophysics Geosystems.

Passchier, C. W., 1986. Flow in natural shear zones-the consequences of spinning flow regimes. Earth and Planetary Science Letters 11, 70-80.

Passchier, C. W., Hoek, J.D., Bekendam, R.F. and de Boorder, H., 1990. Ductile reactiation of Proterozoic brittle fault rocks; an example from the Vestfold Hills, East Antarctica. Precambrian Research 47: 3-16.

Passchier, C.W., and Trouw, R. A. J., 2005. Microtectonics, second ed. Springer, Berlin.

Pennacchioni, G., 2005. Control of the geometry of precursor brittle structures on the type of ductile shear zone in the Adamello tonalites, Southern Alps (Italy). Journal of Structural Geology 27, 627-644.

Pennacchioni, G., and Mancktelow, N. S., 2007. Nucleation and initial growth of a shear zone network within compositionally and structurally heterogeneous granitoids under amphibolite facies conditions. Journal of Structural Geology 29, 1757-1780. Doi: 10.1016/j.jsg.2007.06.002.

Peternell, M., Kohlmann, F., Wilson, C. J. L., Seiler, C., and Gleadow, A. J. W., 2009. A new approach to crystallographic orientation measurement for apatite fission track analysis: effects of crystal morphology and implications for automation. Chem. Geol. 265, 527-539.

Peternell, M., Hasalová, P., Wilson, C.J.L., Piazolo, S., and Schulmann, K., 2010. Eval uating quartz crystallographic preferred orientations and the role of deformation partitioning using EBSD and fabric analyser techniques. Journal of Structural Geology 32, 803-817.

Poirier, J. P., 1980. Shear localization and shear instability in materials in the ductile field. Journal of Structural Geology 2, 135-142.

Ramsay, J. G., 1980. Shear zone geometry: a review. Journal of Structural Geology 2, 83399.

Ramsay, J. G., and Graham, R.H., 1970. Strain variation in shear belts. Canadian Journal of Earth Sciences 7, 786-813.

Ramsay, J. G., and Allison, I., 1979. Structural analysis of shear zones in an alpinised Hercynian granite (Maggia Lappen, Pennine Zone, Central Alps). Schweizerische Mineralogische und Petrographische Mitteilungen 59, 251-279.

Ramsay, J. G., and Huber, M. I., 1983. The Techniques of Modern Structural Geology. Strain Analysis, Volume 1. Academic Press, London.

Rudnicki, J. W, 1977. The inception of faulting in a rock mass with a weakened zone. Journal of Geophysical Research, 82 (5), 844-854.

Segall, P. and Pollard, D. D., 1983. Nucleation and growth of strike slip faults in granite. Journal of Geophysical Research 88: doi: 10.1029/JB088iB01p00555. issn: 0148-0227.

Segall, P., and Simpson, C., 1986. Nucleation of ductile shear zones on dilatants fractures. Geology 14, 56-59.

Sibson, R. H., 1977. Fault rocks and fault mechanisms. Journal of the Geological Society of London 33, 191-213.

Simpson, C., 1983a. Strain and shape fabric variations associated with ductile shear zones. Journal of Structural Geology 5, 61-72.

Stern, R.J., 1994. Arc assembly and continental collision in the Neoproterozoic East African orogen: Implications for the consolidation of Gondwana: Annu Rev of Earth and Planet Sci, V. 22, p. 319-351.

Stern, R.J., and Johnson, P., 2010. Continental lithosphere of the Arabian Plate: A geologic, petrologic, and geophysical synthesis: Earth Science Reviews, 101, 29-67.

Stipp, M., Holger, S., Heilbronner, R., and Schmid, S. F., 2002. Dynamic recrystallization of quartz: correlation between natural and experimental conditions: Geological Society London Special Publications 200: 171-190.

Takagi, H., Goto, K., and Shigematsu, N., 2000. Ultramylonite bands derived from cataclasite and pseudotachylyte in granites, northeast Japan. Journal of Structural Geology 22, 1325-1340.

Theye, T., Schreyer, W., and Fransolet, A. -M., 1996. Low-temperature, low-pressure metamorphism of Mn-rich rocks in the Lienne Syncline, Venn-Stavelot Massif (Belgian Ardennes), and the role of Carpholite. Journal of Petrology. 37, no.3:767-783. 761.

Thielmann, M., and Kaus, B. J. P. 2012. Shear heating induced lithospheric localization: does it result in subduction? Earth and Planetary Science Letters. Vol. 359-360. p. 1-13. doi:10.1016/j.epsl.2012.10.002.

Tullis, J., Snoke, A.W. and Todd, V.R., 1982. Significance and petrogenesis of mylonitic rocks. Penrose Conference Report. Geology, 10: 227-230.

Tullis, J., Dell' Angelo, L., and Yund, R. A., 1990. Ductile shear zones from brittle pre cursors in feldspathic rocks: the role of dynamic recrystallization. In: Duba, A., Durham, W., Handin, J., Wang, H. (Eds.), The Brittle-Ductile Transition: The Heard volume. American Geophysical Union Monograph, vol. 56, pp. 67-82.

White, S. H., Burrows, S. E., Carreras, J., Shaw, N. D. and Humphreys, F. J., I 980. On mylonites in ductile shear zones. Journal of Structural Geology 2, 1755187.

Wilson, C. J. L., Russell-Head, D. S., Kunze, K., and Viola, G., 2007. The analysis of quartz caxis fabrics using a modified optical microscope. J. Microsc. 227, 30-41.

Wilson, C. J. L., and Peternell, M., 2012. Ice deformed in compression and simple shear: control of temperature and initial fabric. J. Glaciol. 58, 11-22.

Xu, S. -S, Nieto-Samaniego, A. F., and Alaniz-Álvarez, S. A., 2013. Emplacement of pyroclastic dykes in Riedel shear fractures: An example from the Sierra de San Miguelito, central Mexico. Journal of Volcanology and Geothermal Research, Vol. 250, p. 1-8.

5. Conclusion

This chapter provides a general conclusion of the previous chapters of the thesis. Based on the questions outlined in the introduction, the conclusion mainly deals with the interaction of strike-slip shear zones and the significance of such structures with regards to geodynamic processes in the crust. The second section of the conclusion treats the variation in geometries of complex shear zones as related to the rheological properties of the material. In the following section a new development in the nucleation of paired ductile shear zones is described which constitutes an approach to numerical experiments in the theory of the initiation of shear localization. Finally, a short suggestion for future work is presented for field-work based studies and for the numerical modeling of strike-slip shear zones.

5.1 Interaction of crustal-scale strike-slip shear zones and their effect on the kinematics

Strike-slip shear zones can generate jog structures with extensional basins or thrusts (e.g. in the Central Pyrenees; van den Eeckhout and Zwart, 1988; Vissers, 1992), but this study shows that they can also develop core complexes. The existing theories to explain these structures such as the Qazaz Complex (Chapter 2) are based on involvement of bends or the linkage of two parallel propagated shear strands to form left-stepping bridge structures by extension (e.g. Burchfiel and Stewart, 1966; Aydin and Nur, 1982). According to these theories the strike-slip shear zones are horizontally-acting structures extending the crust, but the Qazaz shear zones (Chapter 2) show an active contribution to the exhumation of the lower crust, implying a vertical component: a crustal shortening regime generates crustal-scale strike-slip shear zones with a dominant sub-horizontal slip motion, and the interconnection to the detachment leads to a transfer of that mechanical motion to a vertical upwards movement.

Core complexes along strike-slip shear zones can be expected to differ from the "classical" examples of metamorphic core complexes (e.g. Wernicke, 1981; Davis et al., 1986; Le Pourhiet et al., 2012). The fundamental distinction between the Qazaz Complex and other (Chapter 2) is the absence of crustal extensional in the process. The observations made by Denèle et al. (2007) postulated the development of a metamorphic core complex

related to a transpressional regime. This model shows similarities to the structure of the Qazaz Complex described in Chapter 2, but with the difference that the exhumation have a more complex history and no permanent link to the crustal-scale strike-slip shear zones.

Interaction of strike-slip shear zones and the activity of the shear strands can vary during deformation, and forms a more complex kinematic setup. The field example (Chapter 2) shows that the simultaneous activity of the interconnected strike-slip shear zones have influenced the junction zone by internal folding processes. At a later stage, a new shear zone developed, which led to deactivation of the neighboring shear strand and initiated a change in the kinematics. This observation indicates that interconnection to a more complex geometric structure can influence the activity of shear strands, as suggested by the numerical models of Mancktelow (2002).

5.2 Effect of rheological parameters on the development of shear zone networks (Chapter 3)

Studies on simulations of lithospheric extension and on strain localization at lithospheric scales have indicated that strain-softening has a significant influence on the nucleation of shear zones, e.g. reported by Huismans and Beaumont (2003) and Gueydan et al. (2014). Our numerical experiments show that the development of antithetic shear strands (R') in a brittle regime is strictly associated to a decrease in the friction angle to a specific value during deformation, whereas the systemic changes of cohesion show no evidence of Riedel shear zone evolution (Chapter 3). In addition, the implementation of different ratios of decreasing friction angle to critical strain shows an effect on the activity (strain-rate) of the interconnecting anti- and synthetic shear strands. The similarity between simulated and natural examples suggests that the assumptions made in the numerical models are realistic and confirm the theories of weakening of the frictional strength within a brittle shear zone (Zoback, 2000; Collettini et al., 2009, Faulkner et al., 2010).

Deviating orientations of the shear strands in a Riedel shear network have been theoretically explained by a rotational component of the shear planes with respect to the imposed shear direction, with a reactivation event occurring at a later stage of the deformation. Alternatively, a multiple deformation phase took place and therefore also a change of the bulk stress (Bell, 1986; Ham and Bell, 2004; Katz et al., 2004). The numerical simulations show how the complex geometry of interacting shear zones influence the internal kinematic patterns (Chapter 3). The simultaneous activity of the branched shear

strands affects the material between the shear zones by locally changing the orientation of the maximum compressive stress (σ_1), whereby new shear planes form with a different orientation to the bulk stress.

Previous numerical experiments have shown similar results to the brittle simulations, in that the rheology of the material, e.g. strain-softening (e.g. Mancktelow, 2002; Mancktelow, 2006; Montési, 2007), is essential in the nucleation of ductile shear zones, but our simulations show that this factor also play an important role in the development of different geometries of branched shear zones. The propagation of branched ductile shear zones in a strain-intensive narrowed zone (constricted) or in a wider zone (dispersed) in the numerical model is related to specific values of material strain-weakening (Chapter 3). Estimations made by Mehl and Hirth (2008) of the reduction of the viscosity along the shear localization by strain-softening in comparison to the host rock, can be supported by our numerical models. In addition, the development of constricted shear zones only occurred with an obvious reduction of the effective viscosity to a special strain-ratio.

Lozenges are well-studied domains associated with shear zones (e.g. Choukroune and Gapais, 1983; Carreras, 2001; Ponce et al., 2013). Previous studies have shown different ways in which lozenges form; e.g. by linkage of parallel shear strands (e.g. Pollard and Aydin, 1988; Pennacchioni, 2005; Mann, 2007). The numerical models show that the propagating of parallel stepping shear zones linkage to antithetic shear strands play an essential role in the development of lozenges in dispersed shear zones (Chapter 3). In addition, the anastomosing pattern of synthetic and antithetic shear strands combined with an internal variation of the strain-rate induces an inhomogeneous flow perturbation in the imposed shear direction. As a result, the complex kinematics within the shear zone produce shear-related folds and an internal movement of the lozenges to the imposed shear direction.

5.3 Lithology constitutes an important factor in shear zone nucleation (Chapter 4)

Ductile shear zone nucleation can theoretically occur in homogeneous rocks, but in numerical experiments and in nature, recorded examples nucleate along pre-existing structures e.g. dikes or veins (Christiansen and Pollard, 1997; Mancktelow and Pennacchioni, 2005). The Wadi Filk shear zones (Chapter 4) show the complexity of the system

by way of development of paired ductile shear zones by semi-brittle deformation together with an additional effect of the lithology. The strain concentration of the mylonitic shear zones along the chilled margin of the dike with a sharp gradient of highly to undeformed rock shows the efficiency of the nucleated site controlled by the grain-size.

The investigations of the field example in Chapter 4 show that ductile shear zones have a tendency to nucleate along pre-existing structures, which can form simple geometries e.g. single or paired shear zones. In addition, the propagation of these shear zones is constrained by the orientation of the anisotropic domains. Pennacchioni and Mancktelow (2007) describe similar structures in other locations and relate the influence of such pre-existing structures to the nucleation of ductile shear zones. The importance of such structures in forming branched or anastomosed shear zone networks is shown in the model of a strike-slip core complex (Chapter 2). Similar structures of linkage of shear strands to a network related to pre-existing structures are reported by Fusseis et al. (2006). Branched shear zones can also be generated by a linkage of two parallel propagated shear strands as an extensional bridge zone, as shown in the field example where the northern Qazaz shear zones are interconnected (Meyer et al., 2014).

In terms of shear zone nucleation, the numerical model used in Chapter 3 demonstrates the effect of heterogeneities in the material leading to localized shear zones, where, similar to the field example, there exists a tendency towards nucleation of ductile shear zones arising from variations in rheology. The investigation of the rheological properties of the material shows that the dependency of the strain-softening on critical strain ratio is one important factor that controls the nucleation and therefore propagation of the shear zones to a more complex pattern of branched or anastomosed shear localization (Chapter 3).

In summary, field observations (Chapter 2, 4) exhibit the influence of heterogeneities of the host material during the propagation of ductile shear zones, which lead to a change in the interacting of strike-slip shear zones by generating a more complex geodynamic mechanics. The strike-slip core complex may have an important local effect on the crustal strength, which can influence the nucleation and the propagation of new shear zones in the crust (Chapter 3).

5.4 Suggestions for future research

The study of branched and anastomosing shear zones is a first step in understanding complex small- and large-scale structures. Field work and numerical modeling have generated the following questions.

Field work: The newly described strike-slip linked core complex is an efficient manner of lower crust exhumation. Coincidentally this structure would locally change the thermal profile and affect the crustal strength in that locality (Chapter 2). The two-dimensional numerical experiments show how the rheology plays an essential role in the development of shear zones (Chapter 3). New numerical modeling is therefore needed, with a modification to local rheological parameters in order to study the three-dimensional effect of the exhumation of the lower crust in the Qazaz complex.

A strike-slip linked core complex is a powerful tool in exhuming the lower crust in a collision zone, shown by the large vertical and lateral slip motion (Chapter 2). To understand the role of such a structure in the geodynamic processes, however, we need more information about the time period in which the strike-slip linked core complex was active. Therefore the study has to be extended to field work on similar examples in the Arabian-Nubian Shield (e.g. Kirsh gneiss Complex, Hafafit Complex) and subsequently in other regions on Earth (e.g. Northern Pyrenean Zone, Oceanic strike-slip faults).

Another question arises with regards to the development of the detachment: It is clear that the structure was reactivated at a later stage and formed a conjoined structure with the strike-slip shear zones. In the study we have interpreted the detachment as a discontinuity of the material (Chapter 2). It would be interesting to establish how the detachment was oriented to the strike-slip shear zones before it was connected. It is possible that the structure rotated from its initial position towards the bulk shear direction. Field work with a structural analysis of the overlying Thalbah group would help to reconstruct the particulars of the evolution of the detachment and to understand in detail how such a structure were reactivated.

A general problem of doing a field work-based study, (also related to the previous questions), is the time-intensive collection of structural data. The reconstruction of the tectonic history is based mostly on structures from kilometer- to centimeter-scales, which makes it impossible to find all related structures for the modification of the existing work. Using a drone (quadrocopter) will increase the efficiency and scope of the field work. A

standard drone can reach high altitudes to provide an overview of the field area, furthermore hundreds of meters can be scouted and recorded allowing local data interpretation - improving the organization of the daily field work plans. Image-processing programs can be used to evaluate structures from the collected pictures, linked to a geographic coordinate system. Automated evaluation of digital pictures would help geologists to improve field work in future.

Numerical experiments: The results of the numerical simulations show that strain-softening plays an essential role in the evolution of different geometries of shear zone networks. Strain-weakening is implemented in the codes as being linearly related to the strain, and the propagation of a shear zone is characterized by a similar strain-softening along the shear plane (Chapter 3). The study on natural shear zones indicates a stronger influence of heterogeneities, e.g. local fluid interactions lead to mineral exchanges which would have an effect on the weakening of the material. Simulations of the upper crust with a Mohr Coulomb plasticity shows high and low pressure zones, associated with the geometries of the shear zones (Chapter 3). Fluids intrude to the low-pressure zones, which can lead to fluid-rock interaction by mineral alteration, thereby locally changing the material strength. Numerical experiments could be modified to simulate these mineral alterations by imposing a controlled ratio onto the original rock properties and therefore a change in the local strain-softening.

Furthermore, the simulations used fixed boundary conditions and a permanent overall strain-rate (Chapter 3). A change of the bulk stress in a later stage of the numerical modeling could simulate a second deformation event, to get an insight how the orientation of pre-existing shear zones towards the previous bulk stress will be affected by the reactivation.

A final point to be mentioned is the interaction of the strike-slip shear zones in three dimensions. Simulations (Chapter 3) report propagation of strike-slip shear zones in either brittle or ductile regimes, but natural crustal-scale shear zones are continuous structures from the lower to the upper crust, and they confirm brittle as well as ductile rheological plasticity. The question is how the geometries of the brittle and ductile shear localization interact by forming a continuous structure in the crust. The numerical simulations (Chapter 3) showed that geometries differed in different orientation of the shear zones with respect to the bulk stress in either brittle or ductile regimes. The combination of three dimensional models can therefore show how the propagation of the crustal-scale shear zones will be influenced in the pure brittle or ductile regimes.

5.5 References

Aydin, A., and Nur, A., 1982. Evolution of pull-apart basins and their scale independence. Tectonics 1, 91-105.

Bell, T.H., 1986. Foliation development and refraction in metamorphic rocks: reactivation of earlier foliations and decrenulation due to shifting patterns of deformation partitioning. Journal of Metamorphic Geology 4, 421-444.

Burchfiel, B. C., and Stewart, J. H., 1966. "Pull-apart" origin of the central segment of Death Valley, California. Geological Society of America Bulletin 77, 439-442.

Carreras, J., 2001. Zooming on northern Cap de Creus shear zones. Journal of Structural Geology 23, 1457-1486.

Choukroune, P., and Gapais, D., 1983. Strain pattern in the Aar granite (Central Alps): orthogneiss developed by bulk inhomogeneous flattening. Journal of Structural Geology 5, 411-418.

Christiansen, P. P., and Pollard, D. D., 1997. Nucleation, growth and structural development of mylonitic shear zones in granitic rock. Journal of Structural Geology 19, 1159-1172.

Collettini, C., Niemeijer, A., Viti, C., and Marone, C., 2009. Fault zone fabric and fault weakness. Nature 462, 907-910. http://dx.doi.org/10.1038/nature08585.

Davis, G. A., Lister, G. S., and Reynolds, S. J., 1986. Structural evolution of the Whipple and South Mountains shear zones, southwestern United States. Geology 14, 7-10.

Denèle, Y., Olivier, P., Gleizes, G. and Barbey, P., 2007. The Hospitalet gneiss dome (Pyrenees) revisited: lateral flow during Variscan transpression in the middle crust, Terra Nova, 19, 6, 445-453.

van den Eeckhout, B., and Zwart, H. J., 1988. Hercynian crustal-scale extensional shear zone in the Pyrenees. Geology, 16(2), 135-138.

Faulkner, D. R., C. A. L. Jackson, R. J. Lunn, R. W. Schlische, Z. K. Shipton, C. A. J. Wibberley, and M. O. Withjack, M. O., 2010. A review of recent developments concerning the structure, mechanics and fluid flow properties of fault zones, J. Struct. Geol., 32, 1557–1575, doi:10.1016/j.jsg.2010.06.009.

Fusseis, F., and Handy, M. R., 2006. Grain-scale processes and inferred stress drops during the formation of shear zone networks at the brittle-to-viscous transition (BVT), Geophys. Res. Abstr., 8, 07323.

Gueydan, F., Précigout, J, and Montesi, L. G., 2014. Strain weakening enables continental plate tectonics, Tectonophysics, 631, 189-196.

Ham, A.P., and Bell, T. H., 2004. Recycling of foliations during folding. Journal of Structural Geology 26, 1989-2009.

Huismans, R. S., and Beaumont, C., 2003. Symmetric and assymetric lithospheric extension: Relative effects of frictional-plastic and viscous strain softening, J. Geophys. Res., 108(B10), 2496, doi:10.1029/2002JB002026.

Katz, Y., Weinberger, R., and Aydin, A., 2004. Geometry and kinematic evolution of Riedel shear structures, Capitol Reef National Park, Utah. Journal of Structural Geology 26, 491-501.

Mancktelow, N. S., 2002. Finite-element modelling of shear zone development in viscoelastic materials and its implications for localization of partial melts. Journal of Structural Geology 24, 1045-1053.

Mancktelow, N. S., 2006. How ductile are ductile shear zones? Geology, 34 (5), 345-348.

Mancktelow, N. S., and Pennacchioni, G., 2005. The control of precursor brittle fracture and fluid-rock interaction on the development of single and paired ductile shear zones. Journal of Structural Geology, 27 (4), 645-661.

Mann, P., 2007. Global catalogue, classification and tectonic origins of restraining- and releasing bends on active and ancient strike-slip fault systems. In: Cunningham, W. D., Mann, P. (Eds.) Tectonics of Strike-slip Restraining and Releasing Bends. Geological Society, London, Special Publications, 290, 367-385.

Mehl, L., and G. Hirth, 2008. Plagioclase preferred orientation in layered mylonites: Evaluation of flow laws for the lower crust, J. Geophys. Res., 113, B05202, Doi: 10.1029/2007JB005075.

Meyer, S. E., Passchier, C., Abu-Alam, T., and Stüwe, K., 2014. A strike-slip core complex from the Najd fault system, Arabian shield. Terra Nova, 26 (5), 387-394.

Montési, L. G. J., 2007. A constitutive model for layer development in shear zones near the brittle-ductile transition. Geophys. Res. Lett. 34.

Pennacchioni, G., 2005. Control of the geometry of precursor brittle structures on the type of ductile shear zone in the Adamello tonalites, Southern Alps (Italy). Journal of Structural Geology 27, 627-644.

Pennacchioni, G., and Mancktelow, N. S., 2007. Nucleation and initial growth of a shear zone network within compositionally and structurally heterogeneous granitoids under amphibolite facies conditions. Journal of Structural Geology, 29(11), 1757-1780.

Pollard, D. D., and Aydin, A. A., 1988. Progress in understanding jointing over the past century. Geological Society of America Bulletin 100, 1181-1204.

Ponce, C., Druguet, E., and Carreras, J., 2013. Development of shear zone-related lozenges in foliated rocks. Journal of Structural Geology 50: 176-186.

Le Pourhiet, L., Huet, B., May, D. A., Labrousse, L., and Jolivet, L., 2012. Kinematic interpretation of the 3D shapes of metamorphic core complexes. Geochemistry, Geophysics, Geosystems, 13, 9 1-17, doi: 10.1029/2012GC004271.

Vissers, R. L. M., 1992. Variscan extension in the Pyrenees. Tectonics, 11, 1369-1384.

Wernicke, B., 1981. Low-angle normal faults in the Basin and Range Province: Nappe tectonics in an extending orogen: Nature, 291, 645-648.

Zoback, M. D., 2000. Strength of the San Andreas, Nature, 405, 31–32, doi: 10.1038/35011181.

6. Appendix

The appendix contains the reference rock properties of the simulations together with Quicktime movies of the numerical experiments.

6.1 Appendix A:

Tab. A1 Reference rock properties

Parameters	**Upper crust** Burg and Schmalholz, 2008	**Lower crust** Burg and Schmalholz, 2008	**Anomaly** (Granite)
fixed parameters			
initial viscosity	$1.2768 * 10^{21}$ Pa s	$3.0484 * 10^{21}$ Pa s	$7.4893 * 10^{20}$ Pa s
initial temperature	300 °C	500 °C	
lithostatic pressure	264.9 MPa	530 MPa	
overall strain-rate	10^{-14} 1/s	10^{-14} 1/s	
elastic parameters			
elastic shear modulus	10^{10} Pa	10^{10} Pa	10^{10} Pa
Mohr Coulomb plasticity			
initial friction angle	30 °	–	30 °
end friction angle	10 °	–	10 °
initial cohesion	35 MPa	–	25 MPa
end cohesion	1 MPa	–	25 MPa
critical shear strain	0-0.6		0.1-1.5
power-law rheology			
initial factor	–	1	1
end factor	–	0.01	0.1
critical shear strain	–	0-0.6	0.1-1.5
stress exponent	–	3	3.2

6.2 Appendix B: DVD-ROM

A DVD-ROM is attached to this thesis. It is separated in brittle and ductile shear zone simulations, furthermore an insight into the drone-technology is shown by a short movie.